NAVAL POSTGRADUATE SCHOOL

Monterey, California

AD-A257 334

DTIC
ELECTE
NOV 2 3 1992
S   D
A

THESIS

TEMPERATURE DISTRIBUTION
AND THERMALLY INDUCED STRESSES
IN ELECTRONIC PACKAGES

by

Andrei Sapsai Jr.

September, 1992

Thesis Advisor: David Salinas

Approved for public release; distribution is unlimited

92-29892

REPORT DOCUMENTATION PAGE

1a. REPORT SECURITY CLASSIFICATION Unclassified		1b. RESTRICTIVE MARKINGS		
2a. SECURITY CLASSIFICATION AUTHORITY		3. DISTRIBUTION/AVAILABILITY OF REPORT Approved for public release; distribution is unlimited.		
2b. DECLASSIFICATION/DOWNGRADING SCHEDULE				
4. PERFORMING ORGANIZATION REPORT NUMBER(S)		5. MONITORING ORGANIZATION REPORT NUMBER(S)		
6a. NAME OF PERFORMING ORGANIZATION Naval Postgraduate School	6b. OFFICE SYMBOL (If applicable) 34	7a. NAME OF MONITORING ORGANIZATION Naval Postgraduate School		
6c. ADDRESS (City, State, and ZIP Code) Monterey, CA 93943-5000		7b. ADDRESS (City, State, and ZIP Code) Monterey, CA 93943-5000		
8a. NAME OF FUNDING/SPONSORING ORGANIZATION	8b. OFFICE SYMBOL (If applicable)	9. PROCUREMENT INSTRUMENT IDENTIFICATION NUMBER		
8c. ADDRESS (City, State, and ZIP Code)		10. SOURCE OF FUNDING NUMBERS		

		Program Element No.	Project No.	Task No.	Work Unit Accession Number

11. TITLE (Include Security Classification)

TEMPERATURE DISTRIBUTION AND THERMALLY INDUCED STRESSES IN ELECTRONIC PACKAGES

12. PERSONAL AUTHOR(S)   Andrei Sapsai Jr.

13a. TYPE OF REPORT Master's Thesis	13b. TIME COVERED From To	14. DATE OF REPORT (year, month, day) September, 1992	15. PAGE COUNT 104

16. SUPPLEMENTARY NOTATION

The views expressed in this thesis are those of the author and do not reflect the official policy or position of the Department of Defense or the U.S. Government.

17. COSATI CODES			18. SUBJECT TERMS (continue on reverse if necessary and identify by block number)
FIELD	GROUP	SUBGROUP	thermoelastic stresses, tri-material package

19. ABSTRACT (continue on reverse if necessary and identify by block number)

This investigation is concerned with the steady state temperature and thermally induced stress distributions in electronic packages due to heat generated by the chip. Finite Element codes were employed to solve for the distribution of temperature and stresses within the package. Four parametric studies were undertaken to determine their effects on system behavior. The material study considered two chip and two solder materials and four substrate materials. Convective heat transfer was varied from 200 $W/m^{**}2C$ through 500 $W/m^{**}2C$. In the geometric study, chip height to overall height was varied. The effect of package encapsulation was studied. Results are presented for both temperature and stress distributions at the solder interfaces.

20. DISTRIBUTION/AVAILABILITY OF ABSTRACT [X] UNCLASSIFIED/UNLIMITED [ ] SAME AS REPORT [ ] DTIC USERS	21. ABSTRACT SECURITY CLASSIFICATION Unclassified	
22a. NAME OF RESPONSIBLE INDIVIDUAL Salinas, David	22b. TELEPHONE (Include Area code) (408) 646-3426	22c. OFFICE SYMBOL ME/Sa

DD FORM 1473, 84 MAR   83 APR edition may be used until exhausted   SECURITY CLASSIFICATION OF THIS PAGE
All other editions are obsolete   Unclassified

i

Temperature Distribution
And Thermally Induced Stresses
In Electronic Packages

by

Andrei Sapsai Jr.
Lieutenant, United States Navy
B.S., Trenton State College, 1984

Submitted in partial fulfillment
of the requirements for the degree of

MASTER OF SCIENCE IN MECHANICAL ENGINEERING
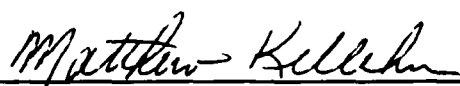
from the

NAVAL POSTGRADUATE SCHOOL
September, 1992

Author: _____
Andrei Sapsai Jr.

Approved by: _____
David Salinas, Thesis Advisor

_____
Matthew D. Kelleher, Chairman
Department of Mechanical Engineering

ABSTRACT

This investigation is concerned with the steady state temperature and thermally induced stress distributions in electronic packages due to heat generated by the chip. Finite Element codes were employed to solve for the distribution of temperature and stresses within the package. Four parametric studies were undertaken to determine their effects on system behavior. The material study considered two chip and two solder materials and four substrate materials. Convective heat transfer was varied from 200 $W/m^2{}^\circ C$ through 500 $W/m^2{}^\circ C$. In the geometric study, chip height to overall height was varied. The effect of package encapsulation was studied. Results are presented for both temperature and stress distributions at the solder interfaces.

TABLE OF CONTENTS

I. INTRODUCTION

The trend in packaging of electronic components is to place more power in an ever decreasing space. Computers that occupied an entire room 20 years ago, now occupy a small corner of that room. With the size of chips decreasing, the volumetric power generation (q''') is of the order of MW/m^3 in magnitude.

This can lead to high temperature operation of the chips with a resulting degradation in performance and or failure. The military has set the maximum temperature of a semiconductor junction to between 100 and 110 °C [Ref. 1].

This investigation deals with the steady state temperature distribution and resulting thermally induced stresses in a tri-material electronic package as shown in Figure 1.1, dimensions not shown to scale. The package consists of a semi-conductor (chip) attached to a substrate material by a solder joint. The chip is a source of thermal energy. The package is exposed to a convective environment on all sides.
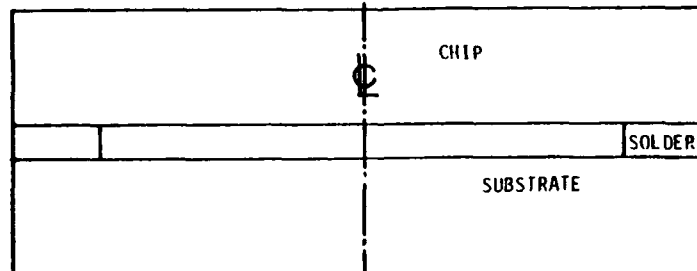
Figure 1.1 Tri-material electronic package

1

With the increase in volumetric power generation the overall temperature of the package is increased. The stresses in the package arise from two sources, (a) thermal strains (ϵ_T) caused by temperature gradients within a material and (b) differences in the materials mechanical properties, coefficient of thermal expansion (α) and stiffness (E). At material interfaces, displacement continuity requires expansion or contraction accommodations between materials. There are two such interfaces where this will occur, at the chip/solder interface, and at the solder/substrate interface.

A. BACKGROUND

Thermal stresses of bi-material assemblies were investigated by Timoshenko in a 1925 paper [Ref. 2], where a bi-metallic thermostat assembly was subjected to a uniform temperature field. Timoshenko obtained analytical expressions for the bending stresses through the cross section of the bimetallic strip. He also noted that the 'distribution of shearing stresses along the bearing surface cannot be determined in an elementary way, that they are of a local type concentrated near the ends of the strip', and that the shearing stresses can be of the same magnitude of the bending stresses. He mentions, in passing, the existence of 'local' normal stresses between the assembly interfaces but says nothing of their magnitude. Goland and Reissner [Ref. 3] determined the shear and peeling stresses at the interface

2

of a cemented lap joint, where the peeling stress tends to pull the materials apart.

In a comprehensive review of the subject of tri-material assemblies, Suhir [Ref. 4] took the analysis one step further by investigating the stresses in a tri-material system due to a thermal environment. His model is based on an assembly fabricated at elevated temperatures and subsequently cooled. Specific restrictions were placed on the tri-material assembly in a uniform temperature field. He obtained analytical solutions of the problem. For the present study the general tri-material problem is solved numerically. In particular the tri-material system is that of an electronic package.

B. PROBLEM DEFINITION

The problem was partitioned into two parts, a thermal analysis, whereby the heat conduction equation was solved, and a thermal stress analysis whereby the stresses produced by the thermal field were obtained. Both problems were solved numerically by the Finite Element Method (FEM). For the numerical analysis, symmetry is invoked along the centerline of the system as shown in Figure 1.1. The steady state thermal study focuses on the effects material properties, geometric configuration, convective cooling, and encapsulation have on temperature distribution in an electronic package. Once the temperature field is known the data is input into a program that assigns temperatures to another FEM mesh which is

3

used in the stress analysis. The stresses examined include bending stress at the centerline of the package (σ_b), the bending (σ_{bu}), normal (σ_{ou}), and shear (τ_u), stresses along the chip/solder interface, and the bending (σ_{bl}), normal (σ_{ol}), and shear (τ_l) stresses at the solder/substrate interface.

II. FEM DEVELOPMENT OF THERMAL PROBLEM

A. PROBLEM STATEMENT AND ASSUMPTIONS

As noted in the introduction, the purposes of this investigation are to (a) determine the variation of temperature in the electronic package and (b) determine the stresses associated with these temperatures. The results here are the steady state results.

The steady state thermal study focuses on effects that certain key parameters have on system behavior. They include, the effects total power (P) in the chip, material combinations, convective cooling, geometric configuration and encapsulation have on the temperature distribution in the electronic system.

Finite element codes were used to solve for the temperature distribution and stresses of the electronic package. In order to limit the mathematical complexity of the problem the following approximations and specific assumptions for FEM program HEATSTEADY in Appendix A. are made as follows:

- The thermal contact resistances due to 'imperfect' contact at the solder interfaces are negligible.

- The thermal conductivity and coefficient of thermal expansion (k and α) are considered constant over the range of temperatures encountered in the study.

5

- Because the temperatures are not very large radiation heat transfer between the package and the surrounding enclosure is negligible.

- The convection heat transfer coefficient (h) is constant over the entire edge upon which it acts.

All of these assumptions are reasonable within the scope of this study. Once the temperature distribution of the package is obtained the position and temperature of all the Global nodal points are entered into program Filter in Appendix B. to obtain temperatures that correspond to FEM program Weld in Appendix C. to determine the stresses developed in the package. The development of program WELD is discussed in Chapter III.

B. FEM FORMULATION OF THERMAL PROBLEM

The Galerkin FEM is an approximation method which transforms a linear partial differential equation into a system of linear algebraic equations. Using the two-dimensional heat equation [Ref. 5]:

$$\nabla \cdot (k \nabla T) + q''' = 0 \qquad (2.1)$$

and boundary conditions

$$Cauchy: \qquad -k\frac{\partial T}{\partial n} = h(T - T_\infty) \qquad (2.2)$$

$$Nuemann: \qquad \frac{\partial T}{\partial n} = 0 \qquad (2.3)$$

6

where the ∇ operator denotes $i\frac{\partial}{\partial x} + j\frac{\partial}{\partial y}$, and thus

$$\nabla \cdot (k\nabla T) = k\nabla^2 T = k\left[\frac{\partial^2 T}{\partial x^2} + \frac{\partial^2 T}{\partial y^2}\right] \qquad (2.4)$$

where k is the thermal conductivity, T is the temperature, and q''' is the volumetric heat generation. The temperature distribution can be determined at system nodal points of the electronic package. For this method, a linear triangular shape function (N_i) which possesses the Kronecker Delta property (equation 2.5):

$$N_i(nodej) = \delta_{ij} \quad \begin{array}{l} if\ i = j \quad then\ N_i = 1 \\ if\ i \neq j \quad then\ N_i = 0 \end{array} \qquad (2.5)$$

is used. The linear shape functions maintain function continuity throughout the domain.

Heat flux continuity at material interfaces is built into the FEM formulation. The thermal FEM grid and boundary conditions are given in Figure 2.1 and Figure 2.2 respectively.

7
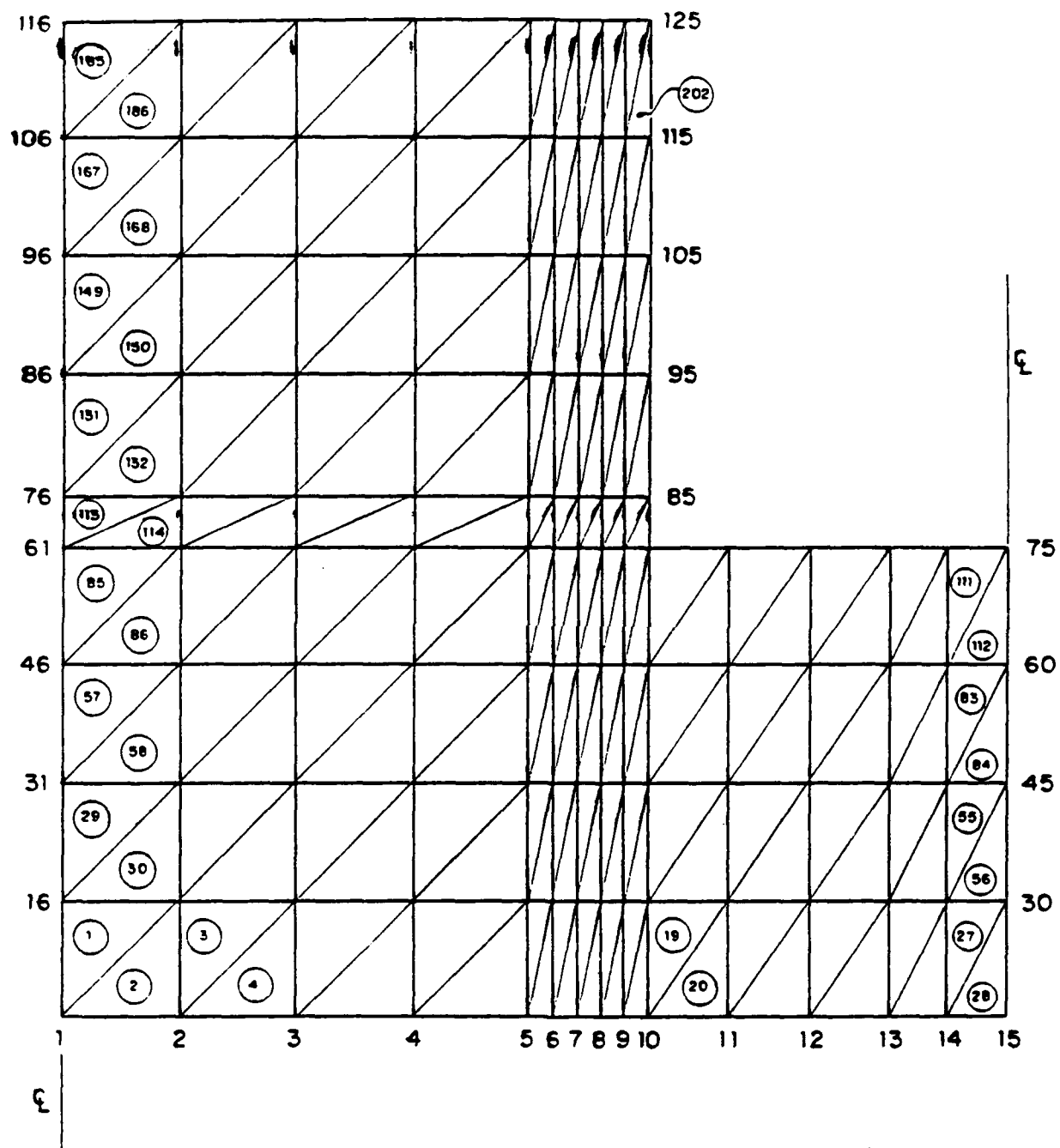
Figure 2.1 FEM thermal grid

A

B

F

C

D

E
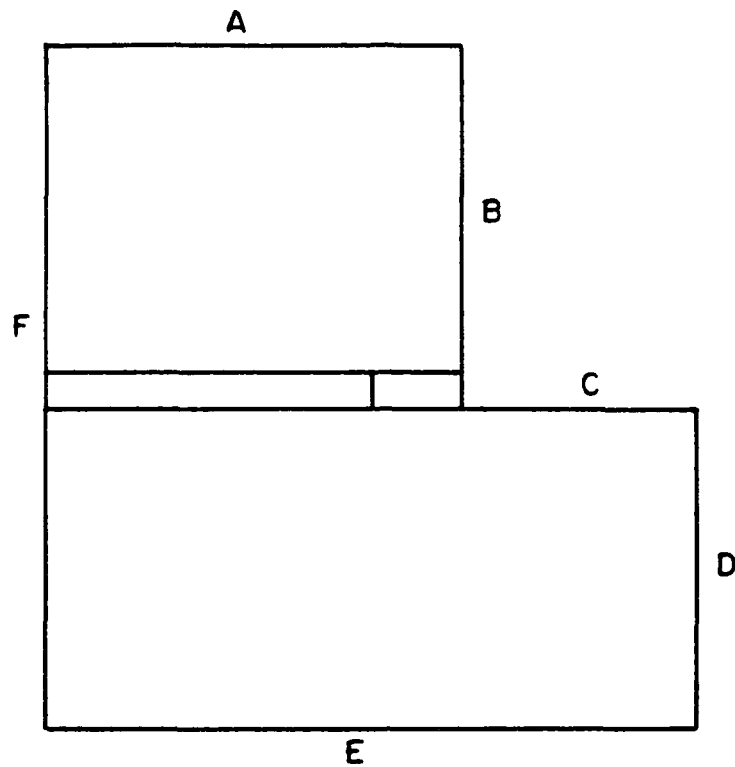
B DRY   BOUNDARY CONDITION

A	$-k \dfrac{\partial T}{\partial y} = h (T - T_\infty)$
B	$-k \dfrac{\partial T}{\partial x} = h (T - T_\infty)$
C	$-k \dfrac{\partial T}{\partial y} = h (T - T_\infty)$
D	$\dfrac{\partial T}{\partial x} = 0$
E	$-k \dfrac{\partial T}{\partial y} = h (T - T_\infty)$
F	$\dfrac{\partial T}{\partial x} = 0$

BOUNDARY CONDITIONS FOR
THERMAL PROBLEM

Figure 2.2 FEM thermal problem boundary conditions

9

An approximate solution, t, for temperature, $T(x,y)$, is formed as follows:

$$T \approx \tilde{t} = \{N\}^T \{\tilde{T}\} \qquad (2.6)$$

where T is the exact solution of the heat equation in continuous space, t is the approximate solution in discrete space, $\{N\}^T$ is the transpose of a column vector of the triangular linear shape functions, and $\{T\}$ is the vector of nodal temperatures.

After the approximation is formulated, the next step is to form the Residual, R, as follows:

$$R = \mathscr{L}(t) - q'''(s) \qquad (2.7)$$

where q''' is the heat generation term and $\mathscr{L}$ denotes the differential operator which in the case of the heat equation is defined by:

$$\mathscr{L}(t) = \nabla \cdot (k \nabla t) \qquad (2.8)$$

With this substitution, the residual becomes:

$$R = [\nabla \cdot (k \nabla (\{N\}^T \{T\}))] - q'''(s) \qquad (2.9)$$

From the residual, the Galerkin Equations are formed:

$$\int_D \{N\}(R) \, ds = \{0\} \qquad (2.10)$$

10

where D denotes surface integration and where {0} is the null vector. Further substitution for R into the Galerkin vector equation results in:

$$\int_D \{N\} \left[\nabla \cdot (k \nabla (\{N\}^T \{T\})) \right] ds - \int_D \{N\} q'''(s) \, ds = \{0\} \qquad \textbf{(2.11)}$$

To solve the Galerkin Equation, Green's Theorem is evoked which yields:

$$\oint_B \{N\} (k \nabla T) \, dB - \int_D \left[\nabla \{N\} (k \nabla (\{N\}^T \{T\})) \right] ds + \int_D \{N\} q''' ds = \{0\}$$

where B subscript on the integral denotes evaluation of these integrals around the boundary of domain D of the electronic package. When integrated the boundary integral and the heat generation integral form the "force" vector {F}. The middle integral *forms* the [A] matrix. Thus the heat conduction differential equation becomes,

$$[A] \{T\} = \{F\} \qquad \textbf{(2.13)}$$

where {T} contains the vector of nodal temperatures.

C. THERMAL PROGRAM DESCRIPTION AND VALIDATION

The main thermal program, HEAT.FOR, a VAX Fortran 77 Code for the FEM thermal analysis is contained in Appendix A. The program begins by reading in a data file DATA3.DAT. This input data is then processed through several subroutines that perform the FEM analysis.

11

1. Subroutine Input Description

The following information is supplied to the Input subroutine from a data file.

Input file form: NCOL1,NCOL2,NROW,
XPOS,YPOS,DIVX,DIVY,
THERCON,GEN,QTPR,
DIVSUB,DIVXAIR,DIVYAIR,
NBCLOW,NBCUP,NBCVERT,NBCSUB,TAMB,
HLOW,HUP,HVERT,HSUB

Parameter	Description
NCOL1	The number of columns of substrate in the FEM grid.
NCOL2	The number of columns of chip in the FEM grid.
NROW	The number of rows in the FEM grid.
XPOS	Starting position for new grid density along X axis.
YPOS	Starting position for new grid density along Y axis.
DIVX	Spacing of grid density along X axis.
DIVY	Spacing of grid density along Y axis.
THERCON	Thermal conductivity (k).
GEN	0 = no heat generation term 1 = heat generation term
QTPR	Amount of volumetric heat generation (q''').
DIVSUB	Number of rows in FEM grid composed of substrate.
DIVXAIR	Number of columns in FEM grid composed of air.
DIVYAIR	Number of rows in FEM grid composed of air.
NBCLOW	0 = insulated boundary at the bottom of substrate. 1 = convective boundary at the bottom of substrate.
NBCUP	0 = insulated boundary at the top of chip. 1 = convective boundary at the top of chip.

12

NBCVERT	0 = insulated boundary on the side of the chip.
	1 = convective boundary on the side of the chip.
NBCSUB	0 = insulated boundary on top of the substrate.
	1 = convective boundary on top of the substrate.
HLOW	Convection coefficient corresponding to NBCLOW.
HUP	Convection coefficient corresponding to NBCUP.
HVERT	Convection coefficient corresponding to NBCVERT.
HSUB	Convection coefficient corresponding to NBCSUB.

2. Subroutine Grid Description

Subroutine GRID takes the input information and constructs a grid of horizontal and vertical lines on a geometry as shown in Figure 2.1. This grid will be used to form the triangular elements used in the thermal FEM analysis. This subroutine allows the user to generate a variety of meshes and/or refinements and permits validation of grid independence very quickly.

To optimize computer time the subroutine is able to generate different grid meshes with a variety of spacing options as shown in Figure 2.3. Fine meshes are used at convective boundaries and material interfaces. A coarse mesh is used within a material away from boundaries. The subroutine allows the user to independently vary the mesh density both horizontally and vertically for up to nine different densities in either direction. The number of mesh densities can be increased by simply adding a number of "IF THEN" statements at the top of the program (line 34).

13
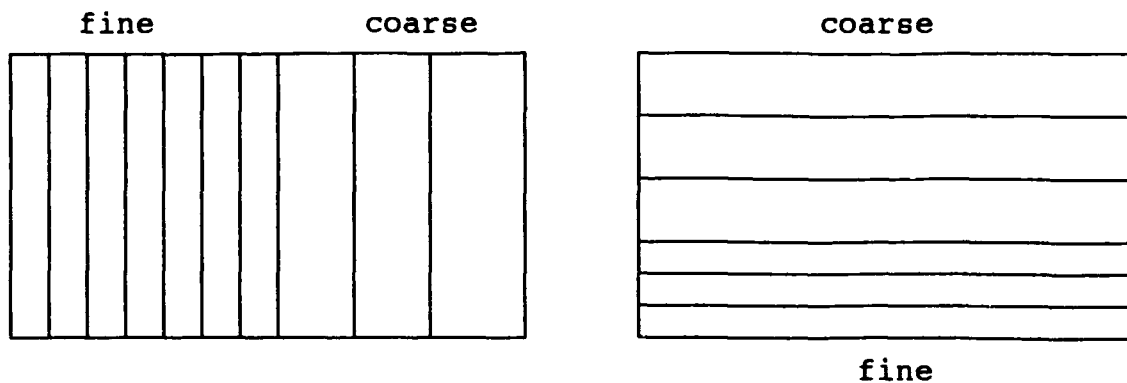
Figure 2.3 Fine and coarse vertical mesh and fine and coarse horizontal mesh

Local nodal points are assigned to each element, one at each corner, counterclockwise as shown in Figure 2.4.
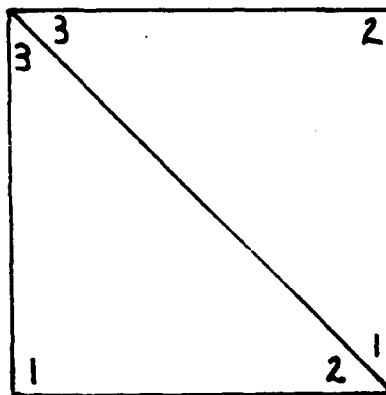
Figure 2.4 Triangular element numbering

Next the subroutine generates a correspondence table which identifies the correspondence between local nodal points and global nodal points. Next, each triangular element is identified with a specific material and assigned a thermal conductivity (k) and whether or not it will have a volumetric heat generation term (q'''). Lastly boundaries are assigned according to Figure 2.2.

14

3. Subroutine Heatmat, Heatmod and Lsarg Description

Subroutine HEATMAT constructs the global matrix [A] and the heat generation vector {F} according to the correspondence table made in subroutine GRID.

Subroutine HEATMOD is not used in this program but can be used to modify the global matrix [A] for a Dirichlet boundary. HEATMOD replaces the Galerkin equation for the specific nodal points with the specified temperatures. LSARG is an equation solver provided by the IMSL Library used to solve equation 2.13.

4. Subroutine Output Description

Subroutine OUTPUT creates data files and performs an energy balance between the thermal energy which is convected at the boundaries and the thermal energy generated by the chip according to:

$$\sum_{i=1}^{4} h_i \left(T_i - T_\infty \right) L_i = q''' A_{chip} \tag{2.14}$$

where h_i and l_i correspond to the convection coefficient and length of each convective boundary, T_i corresponds to the average temperature across the boundary and A_{chip} is the area of the chip. This heat balance is conducted for each case study.

15

D. VALIDATION I. DIRICHLET AND CAUCHY BOUNDARY

A two dimensional body subjected to both Dirichlet and Cauchy boundary conditions was taken from [Ref. 6] and run on program HEAT to validate the programs ability to handle both boundary conditions. The results of program HEAT were identical to Reference 6.

E. VALIDATION II. GRID INDEPENDENCE

In order to ensure that the numerical errors are kept to a minimum the size of the mesh was decreased with incremental steps until there was a less than 1% change in the solution from one grid to the next finest grid (grid independence).

The final mesh chosen has 125 degrees of freedom (DOF) with 202 elements. The mesh which provided less than 1% difference had 161 DOF with 268 elements. The total power of the chip used is P = 40 W. The total power convected for the DOF = 125 grid was P_{conv} = 39.95 W. The total power convected for the DOF = 161 grid was P_{conv} = 39.94 W. The percent difference in total power P from the coarse mesh to the fine mesh is 0.03%.

F. VALIDATION III. ENERGY BALANCE

As mentioned previously, there is an energy balance in subroutine OUTPUT which is given by equation 2.14. This checks program HEAT's ability to correctly handle a generation term. The total power for the majority of case studies was

16

equal to P = 1 W. The average convective power output was q_{conv} = .99785 W for a percent difference of 0.21%.

III. FEM STRESS DEVELOPMENT

The finite element stress formulation utilizes a recently developed element which provides for axial and lateral displacement continuity. The results of the stress code are in good agreement with existing solutions [Ref. 2,4] to problems with uniform temperature fields.

A. FORMULATION OF THE MODEL

A brief description of the FEM formulation for stresses follow. In Figure 3.1, each element has six degrees of freedom; axial displacements at the four corner points, and lateral displacements at the two ends. An advantage of the element is that axial and lateral displacement continuity results.
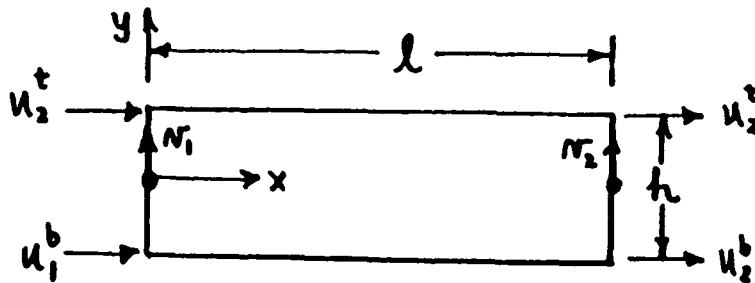
Figure 3.1 A typical element with 6 degrees of freedom

The axial displacement field $u(x,y)$ is assumed to be linear in both the axial and transverse directions. That is,

$$u(x,y) = \sum_{i=1}^{2} N_i(x) \left[H_1(y) u_i^b + H_2(y) u_i^t \right] \qquad (3.1)$$

Superscripts b and t on the nodal displacements refer to bottom and top displacements respectively. The linear shape functions N_i and H_i are given by

$$H_1(y) = \frac{h-y}{h} \qquad H_2 = \frac{y}{h} \qquad N_2(x) = \frac{l-x}{l} \qquad N_2 = \frac{x}{l}$$

The lateral displacement field is given by

$$v(x) = \sum_{i=1}^{2} N_i(x) v_i \qquad (3.2)$$

The strain-displacement relations are,

$$\epsilon_x = \frac{\partial u}{\partial x} = \frac{H_1(y)}{l} \left[u_2^b - u_1^b \right] + \frac{H_2(y)}{l} \left[u_2^t - u_1^t \right] \qquad (3.3)$$

and

$$\gamma_{xy} = \frac{N_1(x)}{h} \left[u_1^t - u_1^b \right] + \frac{N_2(x)}{h} \left[u_2^t - u_2^b \right] + \frac{v_2 - v_1}{l} \qquad (3.4)$$

19

Defining the axial displacement vector as

$$\{\delta_b\}^T = \langle\ u_1^b\quad u_1^t\quad u_2^b\quad u_2^t\ \rangle \qquad (3.5)$$

and the stiffness matrix as

$$[K_B]\ =\ \int_0^l\int_o^h\{B\}E\{B\}^T dy\,dx \qquad (3.6)$$

where the B vector is,

$$\{B\}^T = \langle\ \frac{\partial N_1}{\partial x}H_1\quad \frac{\partial N_1}{\partial x}H_2\quad \frac{\partial N_2}{\partial x}H_1\quad \frac{\partial N_2}{\partial x}H_2\rangle \qquad (3.7)$$

and the force vector due to temperature as,

$$\{F_B\}\ =\ \frac{Eh}{6\,l}\int_0^l\int_0^h\{B\}E\alpha\,\Delta T dy\,dx \qquad (3.8)$$

gives the bending matrix equations as,

$$[K_B]\ \{\delta_B\}\ =\ \{F_B\} \qquad (3.9)$$

Equation (3.9) defines the bending behavior. Behavior due to shear is obtained as follows. Define the row vector of displacement degrees of freedom as

$$\{\delta_s\}^T = \langle u_1^b\quad u_1^t\quad v_1\quad u_2^b\quad u_2^t\quad v_2\rangle \qquad (3.10)$$

The shear stiffness matrix is given by

20

$$[K_s] = \int_0^1 \int_0^h \langle B' \rangle G \langle B' \rangle \, dy \, dx \qquad (3.11)$$

where

$$\langle B' \rangle = \langle N_1 \frac{\partial H_1}{\partial y} \quad N_1 \frac{\partial H_2}{\partial y} \quad \frac{\partial N_1}{\partial x} \quad N_2 \frac{\partial H_1}{\partial y} \quad N_2 \frac{\partial H_2}{\partial y} \quad \frac{\partial N_2}{\partial x} \rangle \quad (3.12)$$

which gives the equations for shear behavior

$$[K_s] \{ \delta_s \} = \{ 0 \} \qquad (3.13)$$

The matrix equations for bending and shear behavior are combined to give the stiffness equations for the system.

B. PRELIMINARY RESULTS

Assessment of the present model was obtained from comparisons with previous analytical models [Ref. 2,4]. Exact agreement for bending stresses was obtained when the present model was applied to a sample bimetallic case solved in [Ref.2]. For a tri-metallic case the present model produced shear stress results in reasonably good agreement with results obtained from [Ref. 4].

IV. STEADY STATE TEMPERATURE ANALYSIS

A. OVERVIEW OF STEADY STATE TEMPERATURE ANALYSIS

The analysis begins with an FEM approximation of the temperature distribution of the tri-material electronic package. First the chip volumetric power generation is examined to determine the effect an increase in q''' has on the chip temperature. Keeping the power of the chip and the level of convective cooling constant, several packaging materials are combined to determine how the temperature distribution varies with the variation in the material thermal conductivities. This is followed by a convection cooling analysis, in which temperatures and temperature gradients are examined for a common electronic package while the convection coefficient h varies. The package geometry is then studied, holding the overall package height equal and varying the chip size as a percentage of overall package height. This is done for the case of constant heat flux, and for the case of constant volumetric heat generation. Lastly the effects of placing a protective coating "encapsulation" on the chip is studied to determine the variation in temperature distribution from a chip which has not been encapsulated.

B. EFFECT OF VOLUMETRIC POWER GENERATION ON TEMPERATURE OF THE CHIP

The heat fluxes of electronic packages is expected to reach nearly 10^6 W/m^2 by the year 2000. This is two magnitudes in power over the chip studied here. The total power output (P) of the chip studied is one watt. This translates to a volumetric power generation (q''') of 20 MW/m^3 for a device 5mm x 5mm x 2mm in dimension or a heat flux (q'') of 4×10^4 W/m^2. The dimensions chosen are of a typical electronic device size.

The temperature results throughout the study can be modified for any power output due to the linearity of the generation term in the heat equation. In Figure 4.1 the temperature of the chip is plotted against chip volumetric power output (q'''). All other quantities must be constant for this to remain true, including boundary conditions and other materials within the package. For the particular geometry studied, temperature (T) as a function of volumetric power output q''' W/m^3 is given by equation 4.1

$$T = m * q''' + T_{\infty} \tag{4.1}$$

where the change in temperature per unit change in volumetric power output is b = 4.65 °C/MW/m^3 and T_{∞} is the ambient temperature of the convective fluid.

23
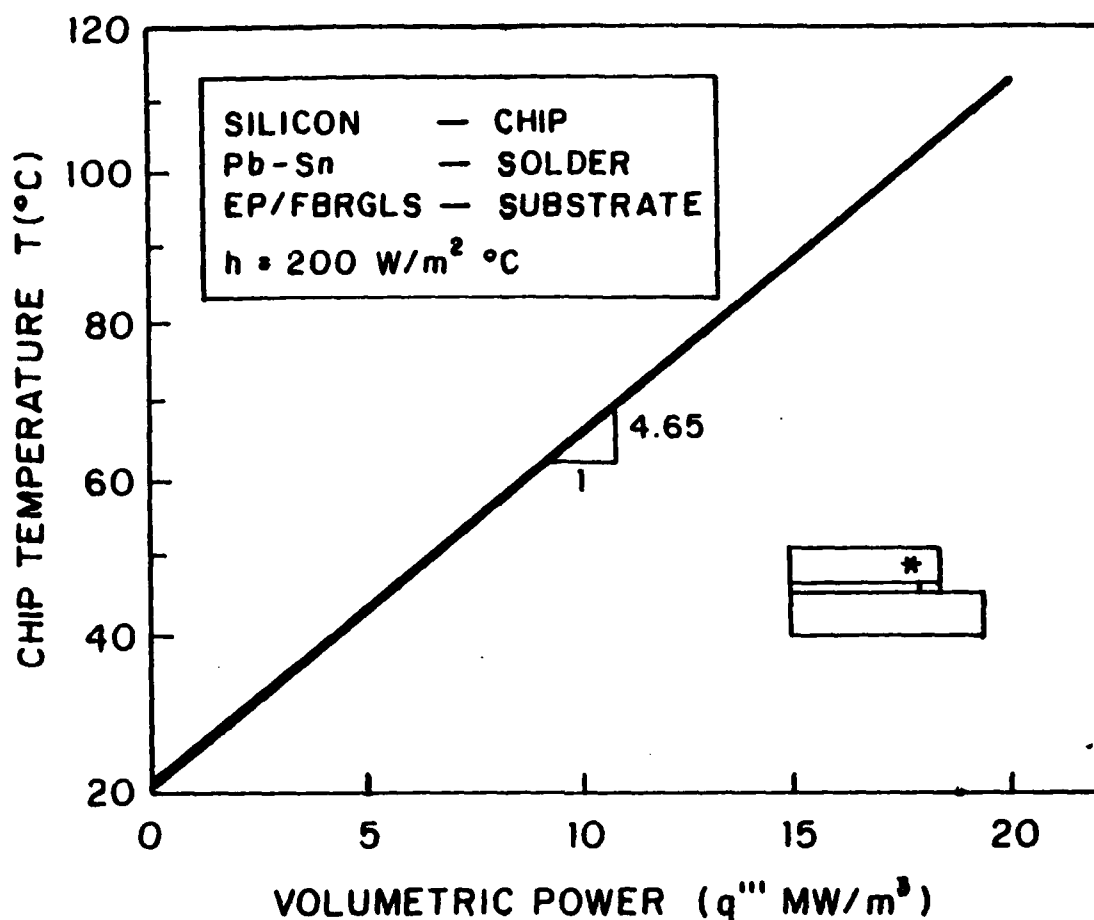
Figure 4.1 Chip temperature as a function of volumetric power

C. EFFECT OF VARIOUS MATERIAL COMBINATIONS

The materials used in this investigation along with their key thermal properties are listed in Table 4.1. The set of materials that comprise the electronic tri-material package focused on for the majority of this study are the silicon chip, a Pb-Sn solder, along with several substrate materials including, Epoxy Fiberglass, Polyimide Fiberglass, Alumina,

24

and Aluminum Nitride. These are the most common materials used in electronic packaging. The other chip and solder materials considered in this study account for large variations in thermal conductivity and/or thermal expansion coefficient (α).

TABLE 4.1 ELECTRONIC PACKAGE MATERIALS AND PROPERTIES

Use	material	k (W/mK)	α $(10^{-7}/^{\circ}C)$
Chip	Silicon	150	27
	Gallium Arsenide	58	57
Substrate	Epoxy Fiberglass	0.16	140 – 180
	Polyimide Fiberglass	0.35	120 – 160
	Alumina	18	60
	Aluminum Nitride	230	33
Solder	Pb(5%)/Sn	63	290
	Au(20%)/Sn	57	159
Air Gap		0.026	–

Throughout the study within this section the following parameters are held constant; volumetric power (q''') of the chip, ambient temperature $T_{\bullet}$ of the convective fluid, and coefficient of convection cooling (h). Figure 4.2 shows the non-dimensional temperature profiles of the package at a non-dimensional distance, $\phi_x = 0.564$. The plotted values of T_n were obtained at the FEM grid nodes. The temperatures which lie along $\phi_x = .564$ were chosen because they pass through the solder joint of the package. Thermal stresses will result not only from temperature gradients within a material, but also from the direct contact of the three different materials within the package which have large differences in their coefficients of thermal expansion (α). In Figure 4.2 the

abscissa is a normalized temperature T_n given by equation 4.2,

$$T_n = \frac{T_i - T_\infty}{T_\infty} \qquad (4.2)$$

where T_i is the FEM grid temperature. The ordinate is the non-dimensional y location ϕ_y that is given by equation 4.3.

$$\phi_y = \frac{y}{H} \qquad (4.3)$$

where H is the total height of the package and y is the FEM grid global nodal location.
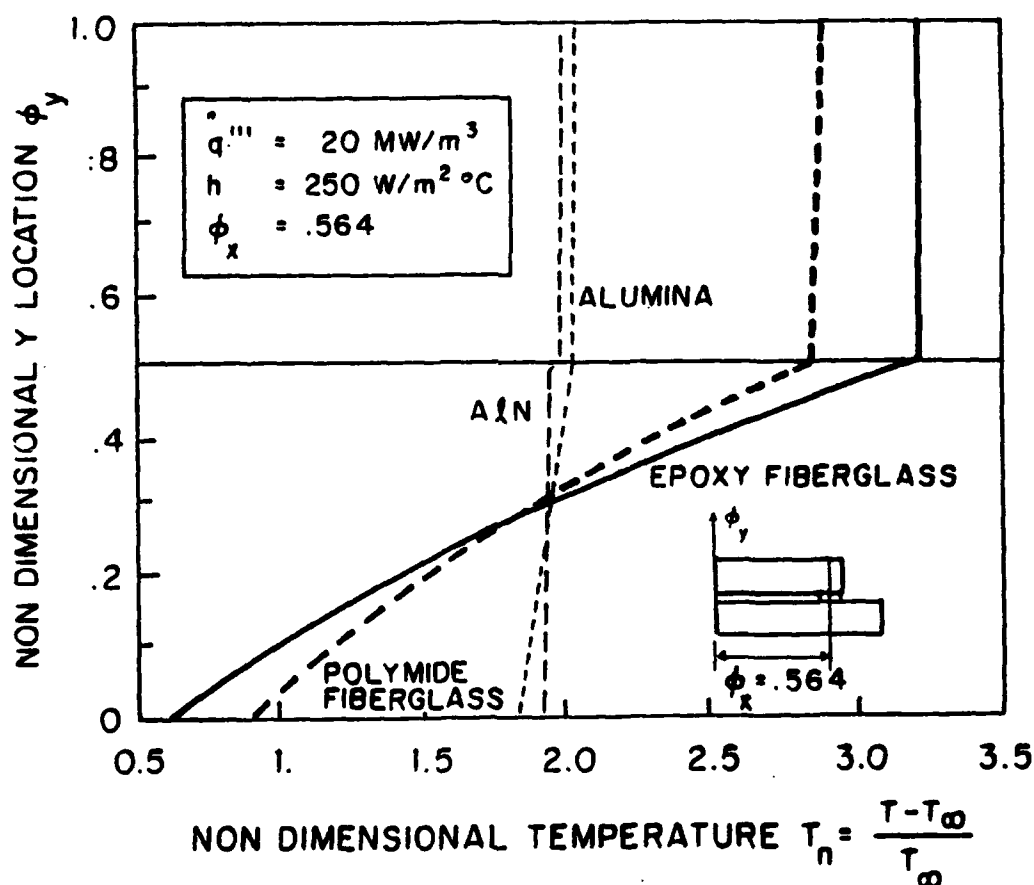
Figure 4.2 Non-dimensional temperature for silicon chip, Pb-Sn solder and various substrates.

All sixteen combinations of materials were analyzed for a temperature profile. There was no significant difference in temperature profile with regard to which chip or solder material was used in the package. For the volumetric power level used in this analysis the difference in thermal conductivity of the Silicon chip (k=150 W/m°C) or Ga/As chip (k=58 W/m°C) does not influence the temperature profile. A study was conducted in which the volumetric power was raised by four times the initial amount. This failed to produce any significant difference in temperature profile or magnitude.

The temperature profiles show that the substrate is the governing material which determines the temperature profile a given electronic package takes on. The following symbology will be used in further analysis. A subscript of 1 refers to the chip, subscript 2 refers to the solder, and subscript 3 refers to the substrate. Low thermal conductivity substrates used in this analysis have ratios of $k_3/k_1 < 0.0025$. High thermal conductivity substrates used in this analysis have a ratio range of $0.10 < k_3/k_1 < 1.6$.

A characteristic of a high k_3/k_1 package is a uniform temperature field throughout all materials in the package. All materials within the package can conduct heat very well. With the low k_3/k_1 substrates a temperature gradient is developed within the substrate in both the X and Y directions. As a result of not being able to conduct the heat effectively through the low conductive substrate, the chip temperature is

increased by approximately 40% over a package with a highly conductive substrate.

The solders have thermal conductivities which are close to the chip thermal conductivity (k_2/k_1 = 0.446) and do not effect the temperature profile. However, the coefficient of thermal expansion α between the two solders chosen vary by 55% thereby influencing the thermal strain profile significantly. The solder joint takes on the chip temperature in all cases because of its ability to conduct the heat generated by the chip.

Thermal strain profiles are presented in Figures 4.3 and 4.4 for the two different solders. In these figures, the
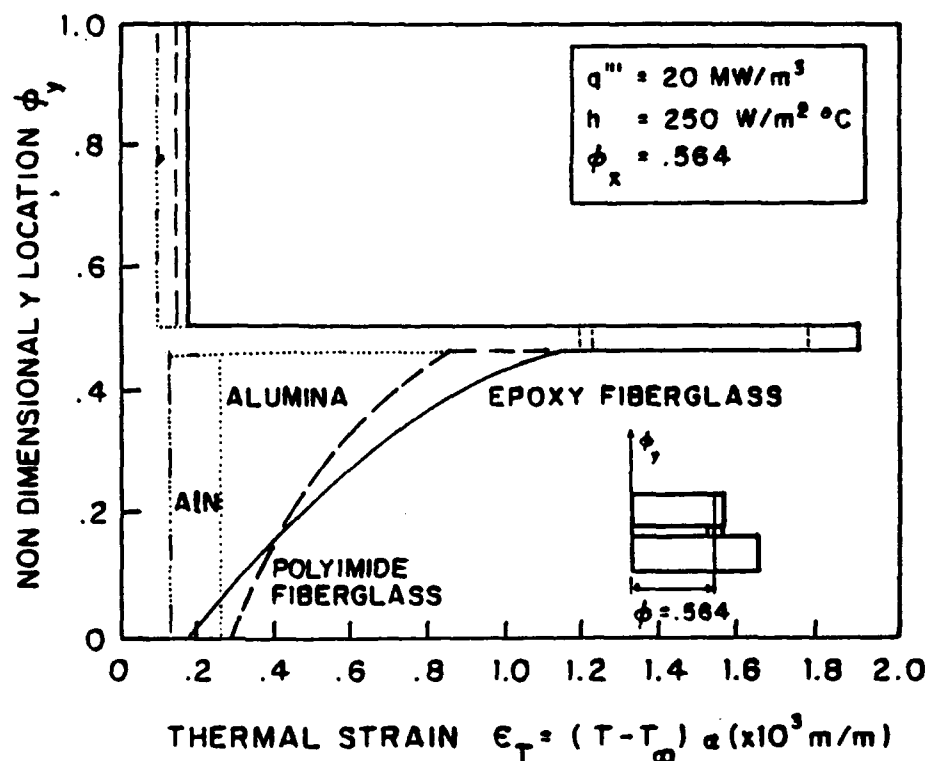
Figure 4.3 Thermal strain profile for silicon chip, Pb-Sn solder and various substrates.

28

abscissa is the difference of the nodal temperature and initial temperature multiplied by the coefficient of thermal expansion α given by

$$\epsilon_T = (T_i - T_\infty) * \alpha \qquad (4.4)$$

and the ordinate is given by equation 4.3.
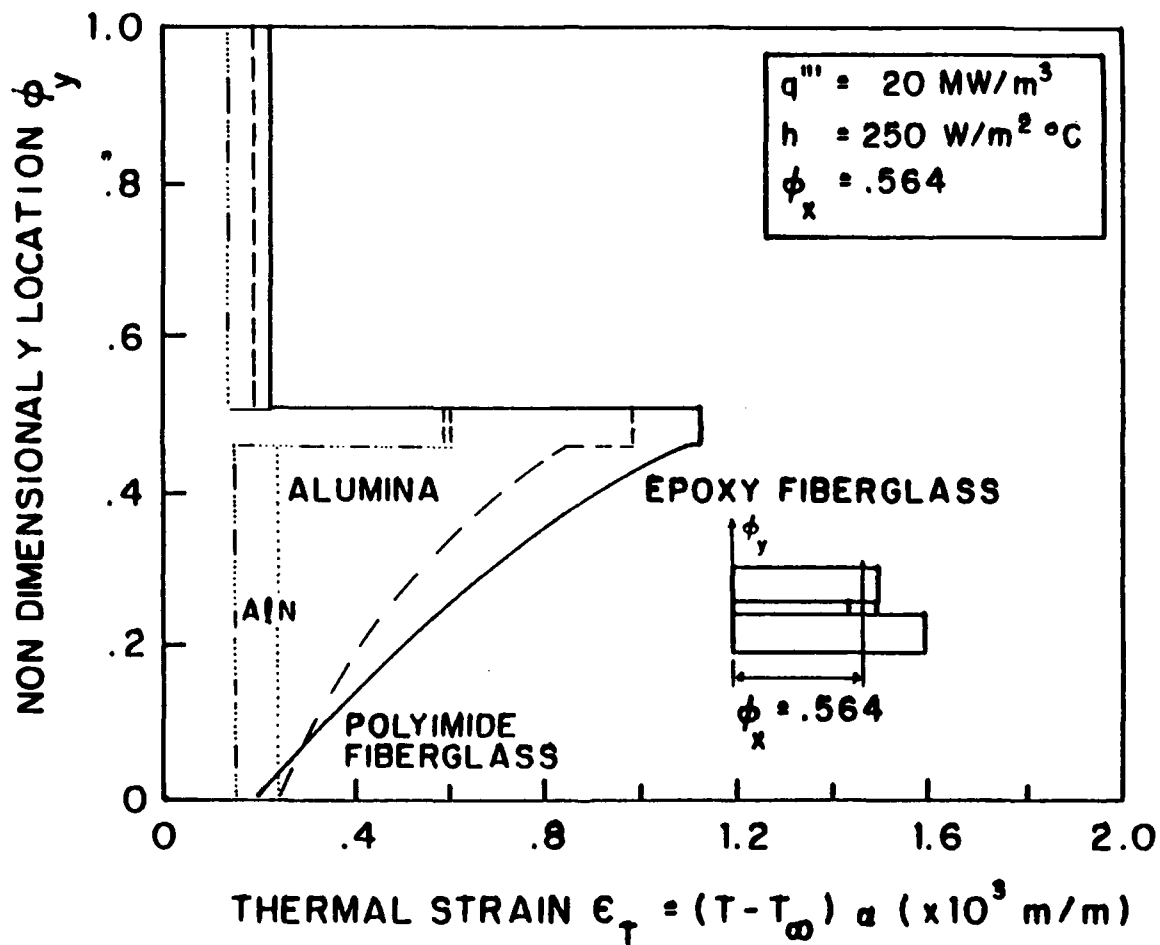
Figure 4.4 Thermal strain profile for silicon chip, Au-Sn solder and various substrates.

1. Low Thermal Conductivity Substrate Packages

Further analysis is conducted by dividing the packages into two groups, low thermal conductivity substrates and high thermal conductivity substrates. The two substrates chosen, Epoxy Fiberglass (k_3/k_1 = 0.00106) and Polyimide Fiberglass (k_3/k_1 = 0.0023), are part of a group of substrates that have k_3 ranging from 0.12 W/m°C to 0.35 W/m°C [Ref. 1]. The temperature achieved throughout the chip for each of the case studies, Figure 4.2, are approximately constant, that is, not dependent on position. The variation in temperature of the chip was limited to less than 1.2% over the entire cross section. The solder achieved the same temperature as the chip due to the solders high thermal conductivity. The variation between the chip temperature and the solder temperature is less then 0.1%.

Within the substrate temperature gradients θ_x and θ_y are developed in both the X and Y directions respectively. Temperature gradients are given by:

$$\frac{\partial T}{\partial x} = \theta_x = \frac{(T_i - T_{i+1})}{(x_i - x_{i+1})} \qquad (4.5)$$

$$\frac{\partial T}{\partial y} = \theta_y = \frac{(T_j - T_{j+1})}{(y_j - y_{j+1})} \qquad (4.6)$$

where T_i and T_j are FEM Global nodal temperatures, x_i and y_j are FEM Global nodal distances in the X and Y directions respectively.

30

These temperature gradients are only found in low thermal conductivity substrates and an explanation for this can be found by examining Fourier's Law, equation 4.7,

$$q'' = -k\frac{\partial T}{\partial X} = -k\,\theta_x \qquad (4.7)$$

where q" is the heat flux in the X direction.

The solder acts as a sort of 'heat funnel' for the chip to transfer its thermal energy to the substrate since the air pocket under the chip acts as an insulator. By examining Fourier's law there are two ways to increase the heat flux q".

First by increasing the thermal conductivity (k) of the material, and secondly by increasing the temperature difference (or temperature potential). The convection heat transfer from the chip surface to the surrounding medium is unable to transfer all the thermal energy in the chip generated by the power source q''' and therefore results in the conduction of heat flux through the solder. When the thermal conductivity of the substrate is low (as in the Fiberglass substrates), the temperature difference through the substrate must become proportionally larger to account for the heat flux out of the chip. For this reason, when the substrate has a high thermal conductivity, the temperature potential need only be very small to conduct the same amount of thermal energy.

In the X direction the gradient is largest at the upper right hand side of the solder/substrate interface. As

Figure 4.5 shows, the gradient Θ_x diminishes by roughly 72%
when only 25% into the substrate. The temperature gradient
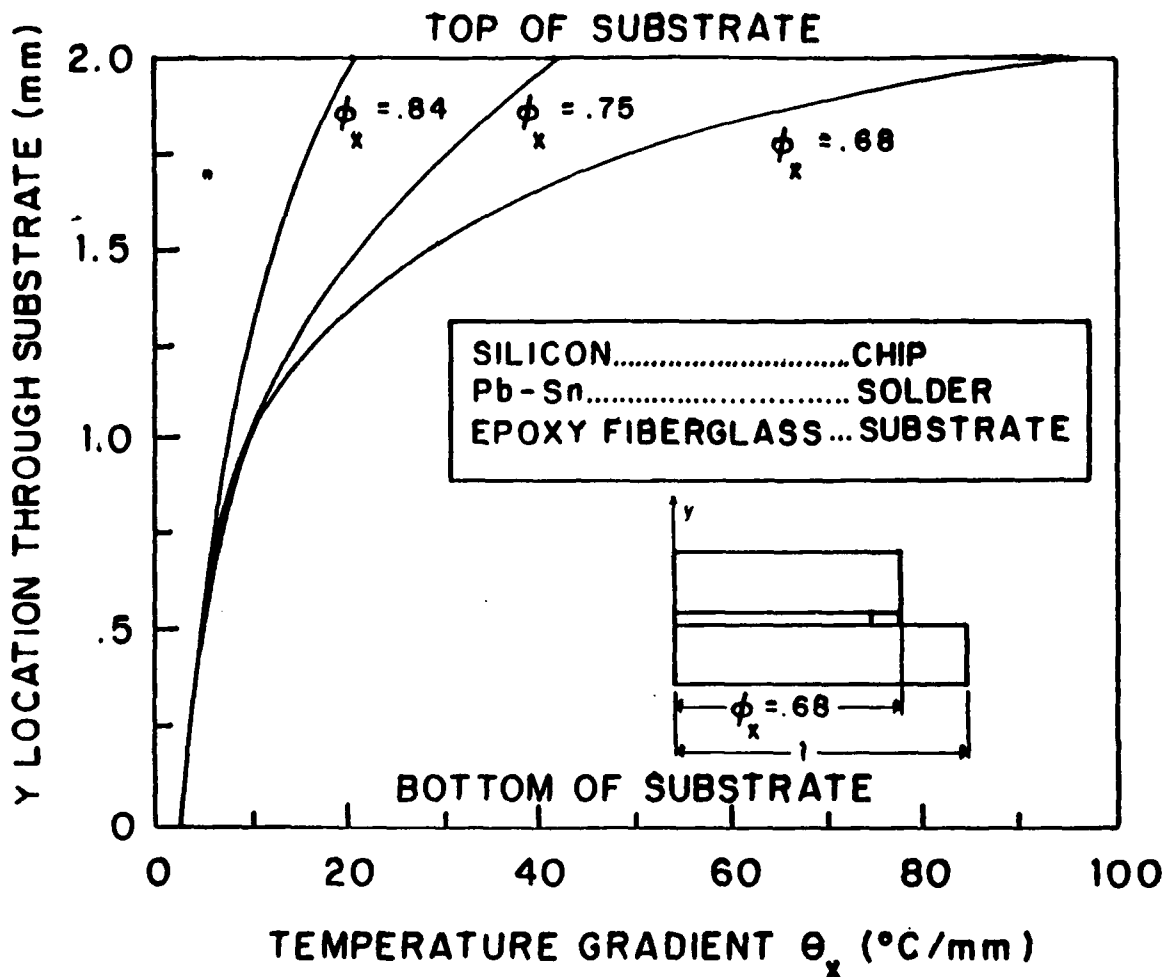
Figure 4.5 Θ_x in epoxy fiberglass substrate

has decreased by 88% when half way through the substrate.
This behavior can be accounted for by the fact the thermal
resistance of the substrate in conduction is greater then the
thermal resistance of the convection surface at the top of the
substrate. Equivalent thermal resistances in conduction and
convection are given by:

$$R_{cond} = \frac{\Delta X}{k\,A} \qquad\qquad \textbf{(4.8)}$$

where Δx is the distance between two points of interest

$$R_{conv} = \frac{1}{h\,A} \qquad\qquad \textbf{(4.9)}$$

and A is the area in which the heat flux is acting.

Taking the area under the solder joint for conduction and the top of the substrate to the right of the solder joint for convection the following equivalent thermal resistances are obtained:

$$R_{cond} = \frac{0.002}{0.16\,(0.00088)\,(1)} \approx 14.2\,^{\circ}C/W \qquad \textbf{(4.10)}$$

$$R_{conv} = \frac{1}{200\,(0.001)\,(1)} = 5\,^{\circ}C/W \qquad \textbf{(4.11)}$$

which shows clearly that the thermal energy has approximately 1/3 less resistance at the convective boundary versus conduction through the substrate.

The gradient in the X direction on the left hand side of the solder joint is only 41% of that on the right, as shown in Figure 4.6. This again is a result of a higher thermal resistance in conduction within the substrate. With the insulated boundary condition imposed in the FEM formulation, the gradient in the X direction at X=0 and X=L is necessarily zero.
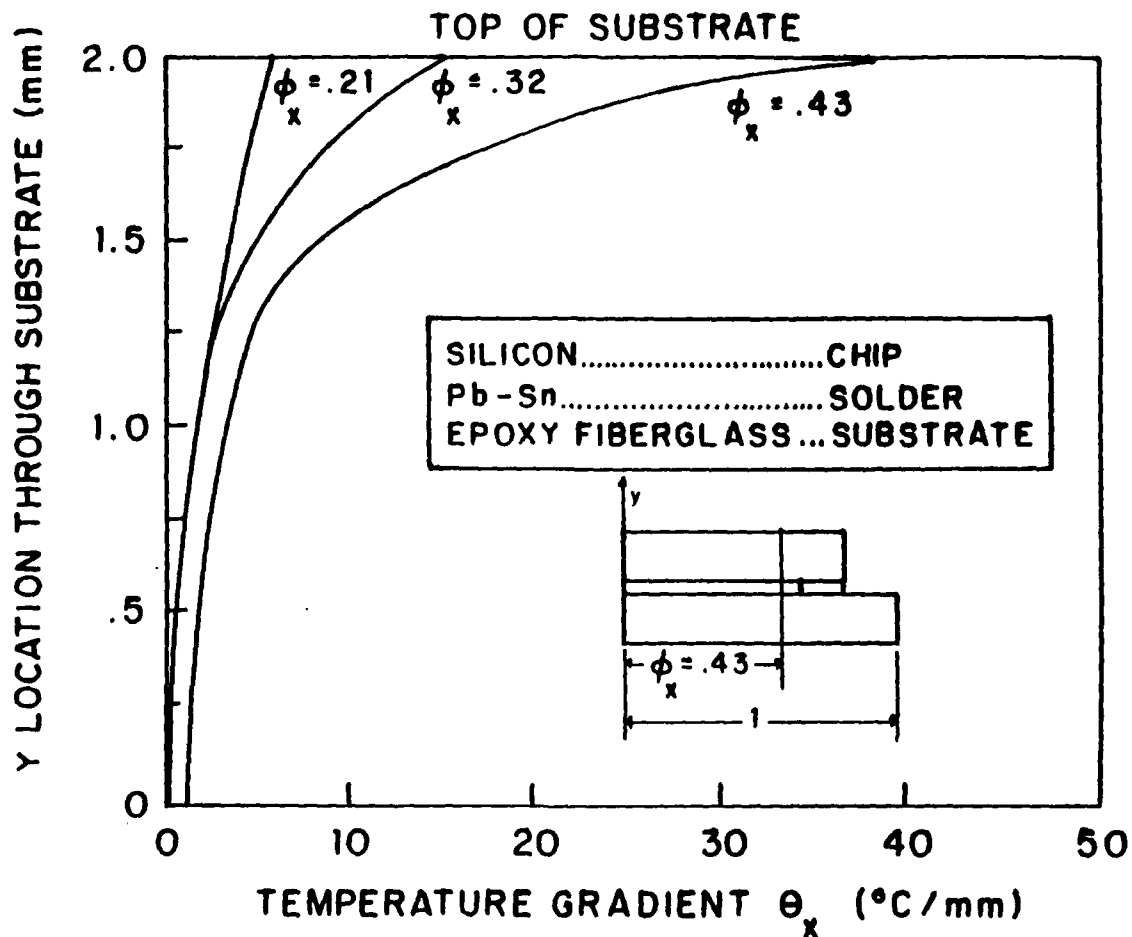
Figure 4.6 θ_x in epoxy fiberglass substrate

The temperature gradient in the Y direction, θ_y, is largest at 49.02 °C/mm at the solder/substrate interface as shown in Figure 4.7. Away from this interface the gradient decreases to approximately 20 °C/mm and remains constant throughout the entire substrate.
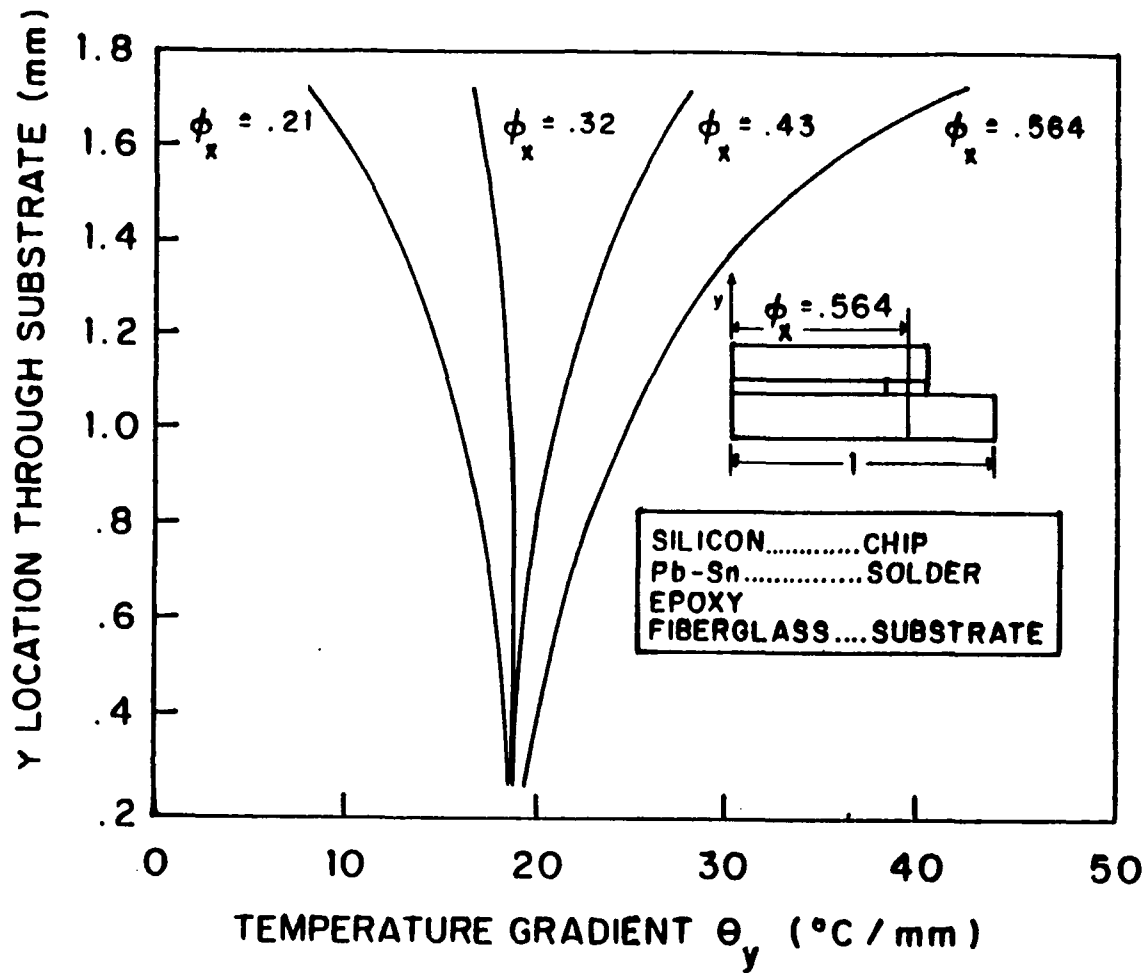
Figure 4.7 θ_y in epoxy fiberglass substrate

The position where the largest temperature gradients in both the X and Y directions are found are shown in Figure 4.8. These are the points where maximum heat fluxes are conducted through the solder/substrate interface.
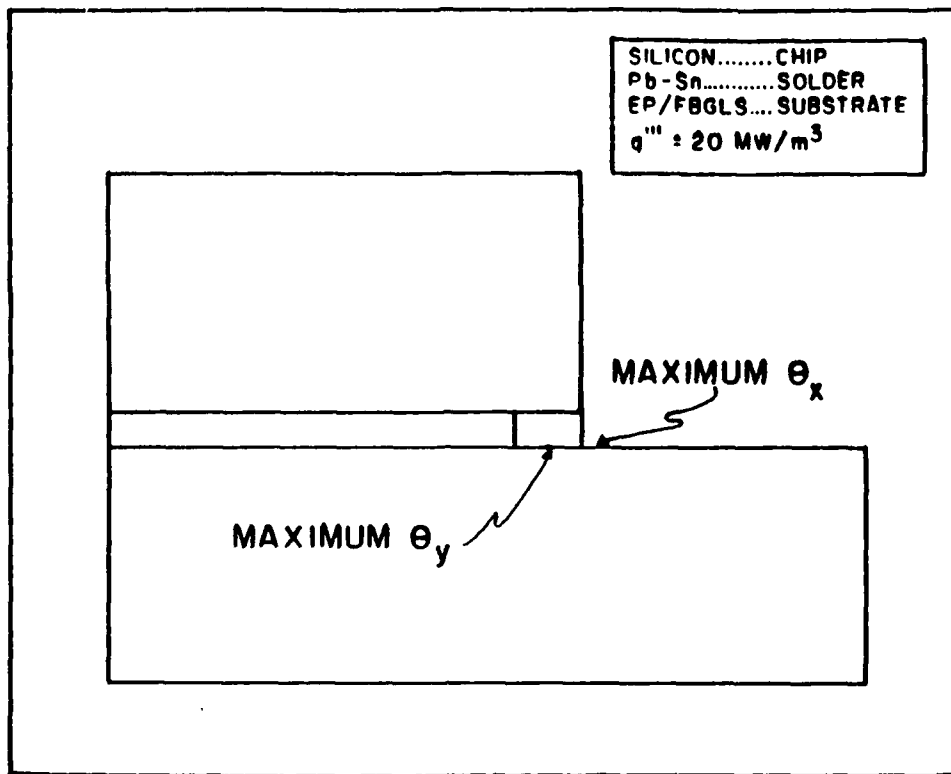
Figure 4.8 Maximum temperature gradients in epoxy fiberglass substrate

2. High Thermal Conductivity Substrate Packages

The two substrates chosen in this range are Alumina k_3 = 18 W/m°C (k_3/k_1 = 0.12) and Aluminum Nitride (AlN) k_3 = 230 W/m°C (k_3/k_1 = 1.53). Referring back to Figure 4.2 the non-dimensional temperature distribution along ϕ_x = .564 for Alumina and AlN graph is approximately a vertical straight line. Therefore there are no temperature gradients anywhere within the package. The reason for no temperature gradients

36

in the substrate is due to the substrate's high thermal conductivity, enabling it to diffuse a large heat flux without developing a temperature gradient, as shown by Fourier's Law of heat conduction, equation 4.7. Figure 4.3 shows the largest shear strains at the solder interface have been reduced by 40% over the low thermal conductivity substrates due to the increased ability of the high thermal conductivity substrates to conduct heat away from the chip thereby lowering the overall temperature of the package and decreasing the thermal expansion.

There is however no appreciable temperature difference between the Alumina and AlN substrate despite the thermal conductivity of the Aluminum Nitride being approximately 13 times as large as the Alumina thermal conductivity. The limiting factor for reduction of temperature of the package has become the convective thermal resistance, which must be lowered in order to lower the package temperature. The conductive thermal resistances of the Alumina and AlN substrate and convective thermal resistance follow:

$$Alumina \quad R_{cond} = \frac{0.002}{18\,(0.00088)\,(1)} \approx 0.13\,°C/W$$

$$AlN \quad R_{cond} = \frac{0.002}{230\,(0.00088)\,(1)} \approx 0.01\,°C/W$$

$$R_{conv} = \frac{1}{200\,(0.001)\,(1)} = 5\,^{\circ}C/W$$

showing that the thermal resistance to heat transfer by convection is 38 and 500 times as large as resistance to heat transfer by conduction in the Alumina and AlN respectively.

D. EFFECT OF CONVECTION HEAT TRANSFER ON SYSTEM BEHAVIOR

This study focuses on the effect of convection cooling on the temperature gradients developed within the low thermal conductivity substrates and the overall temperature decrease of the chip. The electronic packages with high thermal conductivity substrates do not develop any temperature gradients and exhibit an overall decrease in package temperature. The following parameters are held constant; volumetric power output (q''' W/m^3) of the chip, ambient temperature (T_a) of the convective fluid, and the following materials, silicon chip, Lead/Tin solder and Epoxy Fiberglass substrate.

The governing equation for convection cooling is given by:

$$q'' = h\,(T - T_a) \qquad\qquad (4.12)$$

where q'' is the heat flux in W/m^2 and T is the surface temperature. The inverse relation of system temperature to convection coefficient is shown in Figure 4.9. This figure illustrates the need for ever increasing cooling to maintain electronic packages within a temperature tolerance range. An

38

increase in convective cooling from 100 W/m^{2}K to 300 W/m^{2}K results in a reduction of chip temperature of 90 °C. The same increase in convective cooling from 300 W/m^{2}K to 600 W/m^{2}K produces a decrease in chip temperature of only 26 °C.
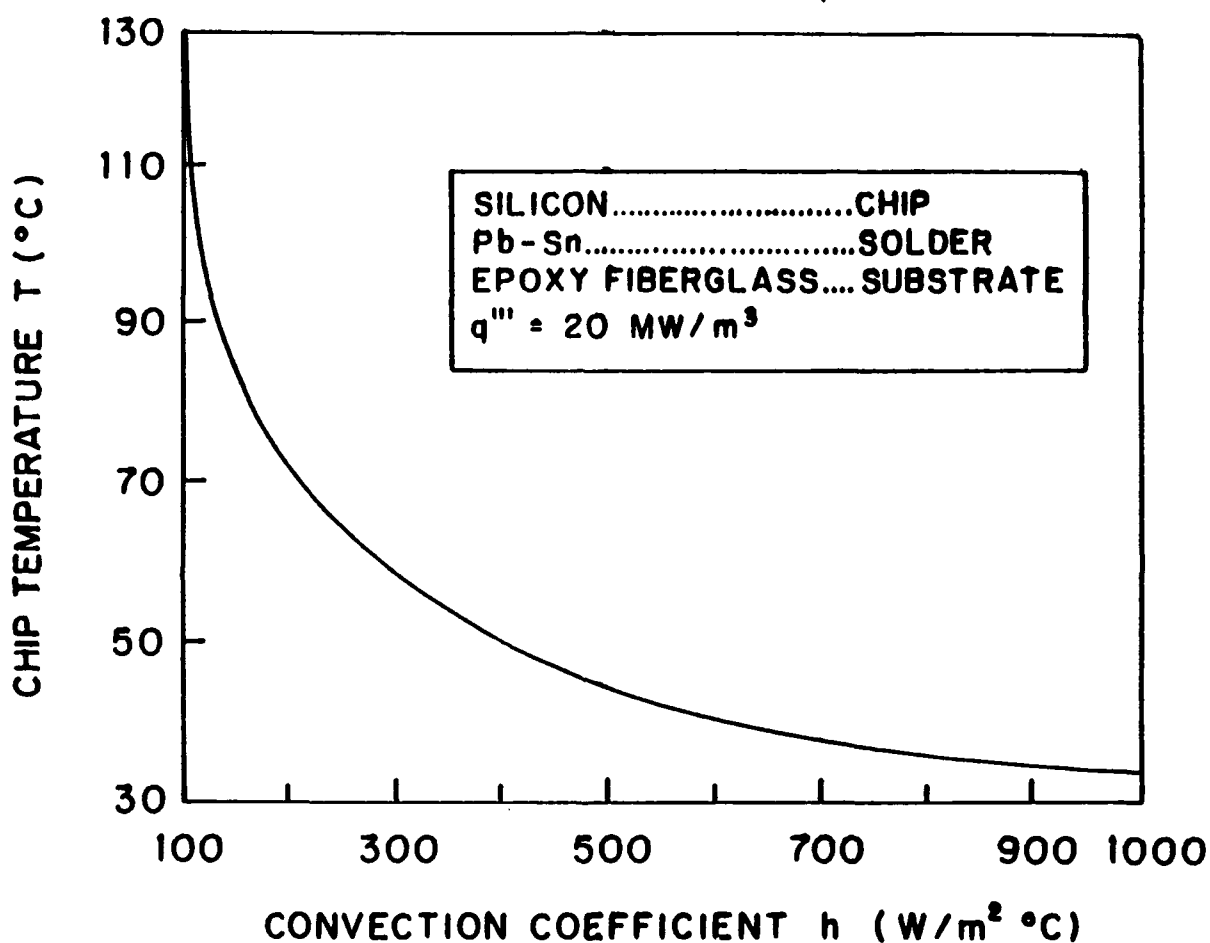
Figure 4.9 Convection coefficient vs. chip temperature

The temperature gradients in both X and Y directions that are developed within the low thermal conductivity substrates are diminished by increasing the convective heat transfer as shown in Figures 4.10 and 4.11.
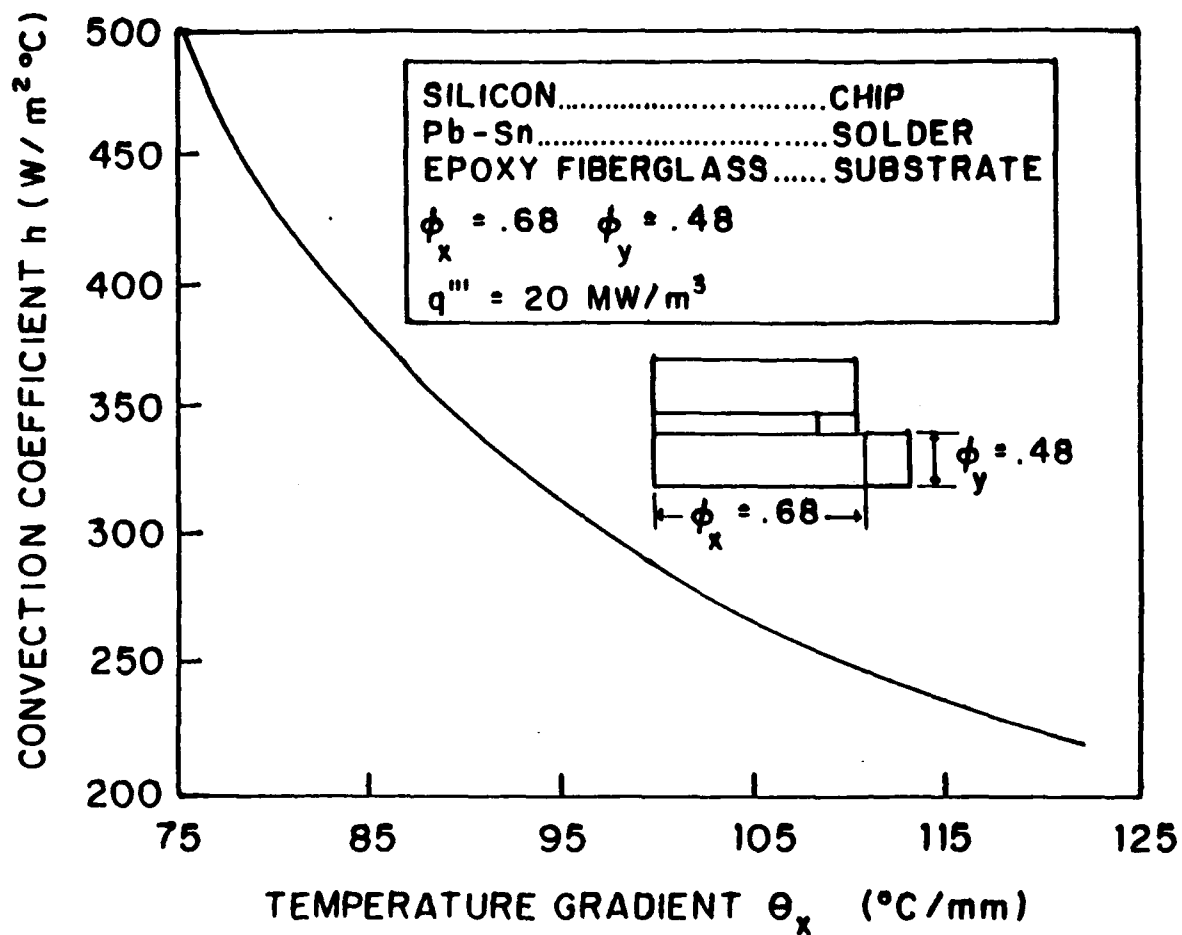
Figure 4.10 θ_x **in epoxy fiberglass substrate vs. convection coefficient**

In the X direction the maximum temperature gradient is decreased by 60% by increasing the convective cooling by 250%. In the Y direction the maximum temperature gradient is decreased by 52% by increasing the convective cooling by 250%.

40
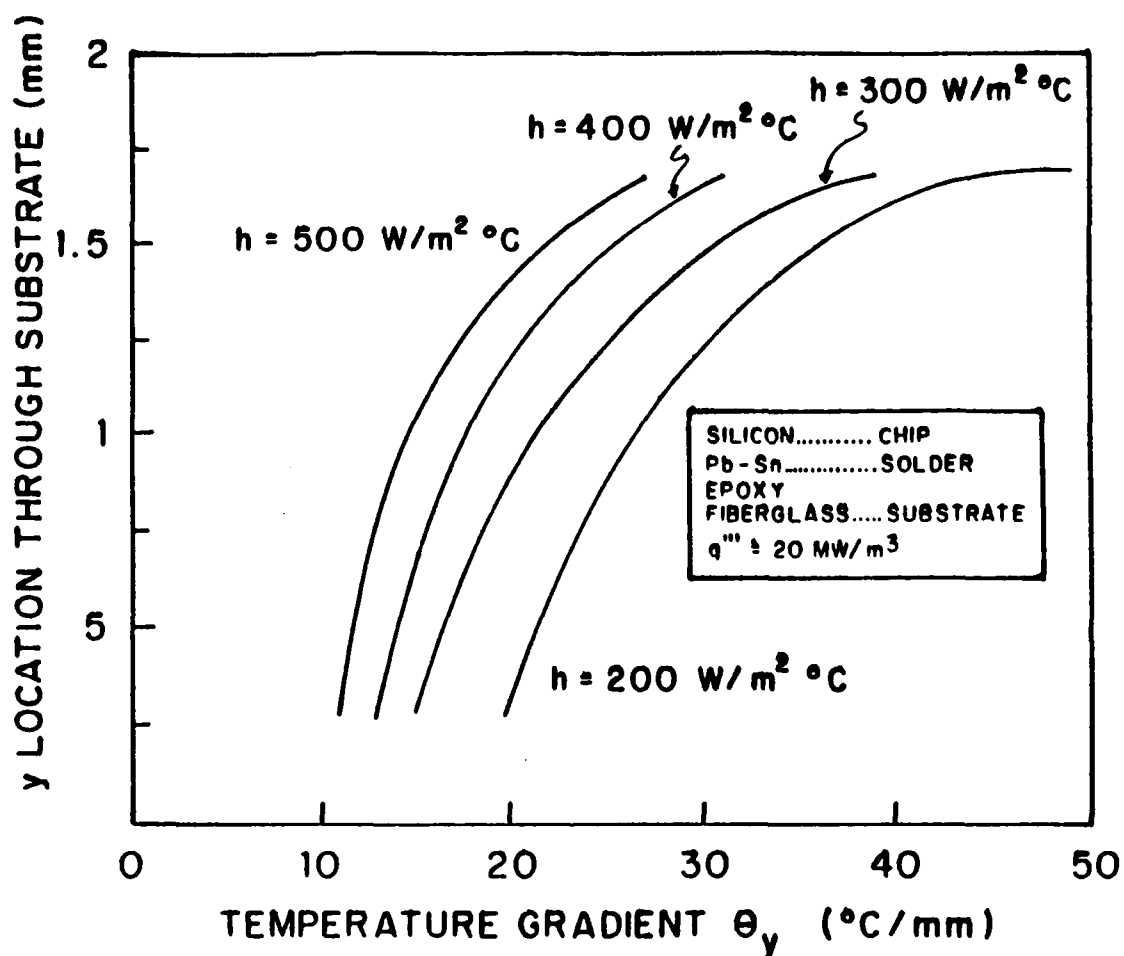
Figure 4.11 θ_y in epoxy fiberglass substrate vs. convection coefficient

E. EFFECT OF GEOMETRY ON SYSTEM BEHAVIOR

The dimensions of the chip and substrate are varied by assuming the chip is a percentage of a fixed overall height and the solder and substrate make up the remaining percentage. We define the non-dimensional term β as the ratio of chip height to overall package height (H) as in equation 4.13,

41

$$\beta = \frac{H_{chip}}{H} \qquad\qquad (4.13)$$

Substrates are approximately kept at a minimum of one half a millimeter [Ref. 1]. The following material combination was selected; a Silicon chip, a Lead/Tin solder and a Epoxy Fiberglass substrate. The following parameters were held constant; convective cooling, ambient temperature, the height of the air/solder interface and the overall height of the package.

First, a study with a constant heat flux (q'') was conducted by varying the volumetric heat generation (q''') to obtain a flux of 4 x 10^4 W/m^2. Next the volumetric heat generation (q''') was constant which resulted in different heat fluxes from the chip.

1. Constant Heat Flux (q'').

The result of maintaining a constant heat flux is a chip that is a highly concentrated heat source when $\beta=0.18$ and a greatly distributed heat source when $\beta=0.81$. In Figure 4.12 the non-dimensional temperature profile is shown for $\beta= 0.18$ to 0.81 at a value of $\phi_x = .564$.

42
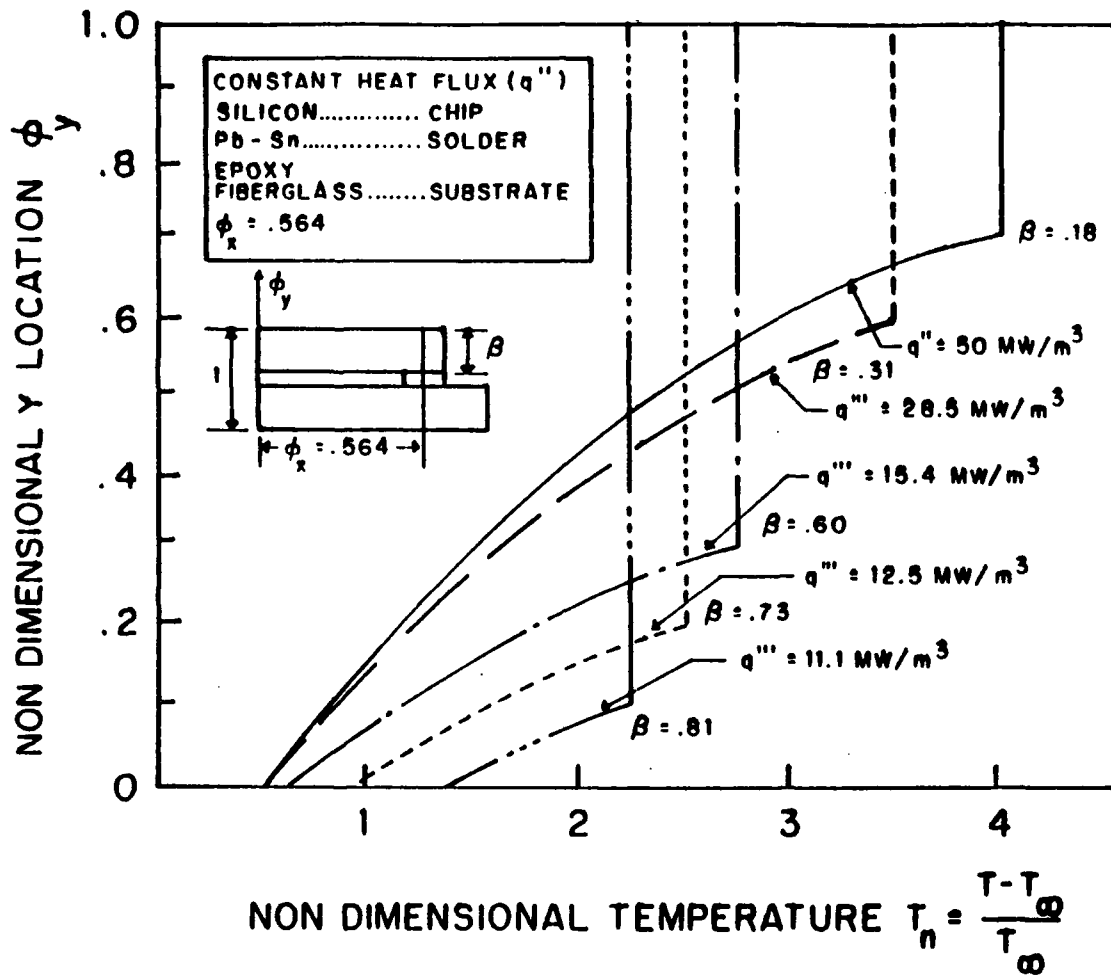
Figure 4.12 Non-dimensional temperature for various size chips constant heat flux

When the chip height results in a value of $\beta=0.18$, the chip is acting as a concentrated heat source with a volumetric heat generation $q''' = 50$ MW/m^3 and the temperature of the chip is greatest. The larger the chip is to the rest of the package the lower the temperature of the overall package is.

A partial explanation for this is the amount of surface area exposed to convective cooling is smaller when $\beta = 0.18$ then when $\beta = 0.81$.

The thermal strain profile is shown if Figure 4.13 for the same value of $\phi_x = .564$. The thermal strain profiles can be explained in much the same way the temperature profiles were. That is, when the chip is smallest the largest expansion of the package occurs.
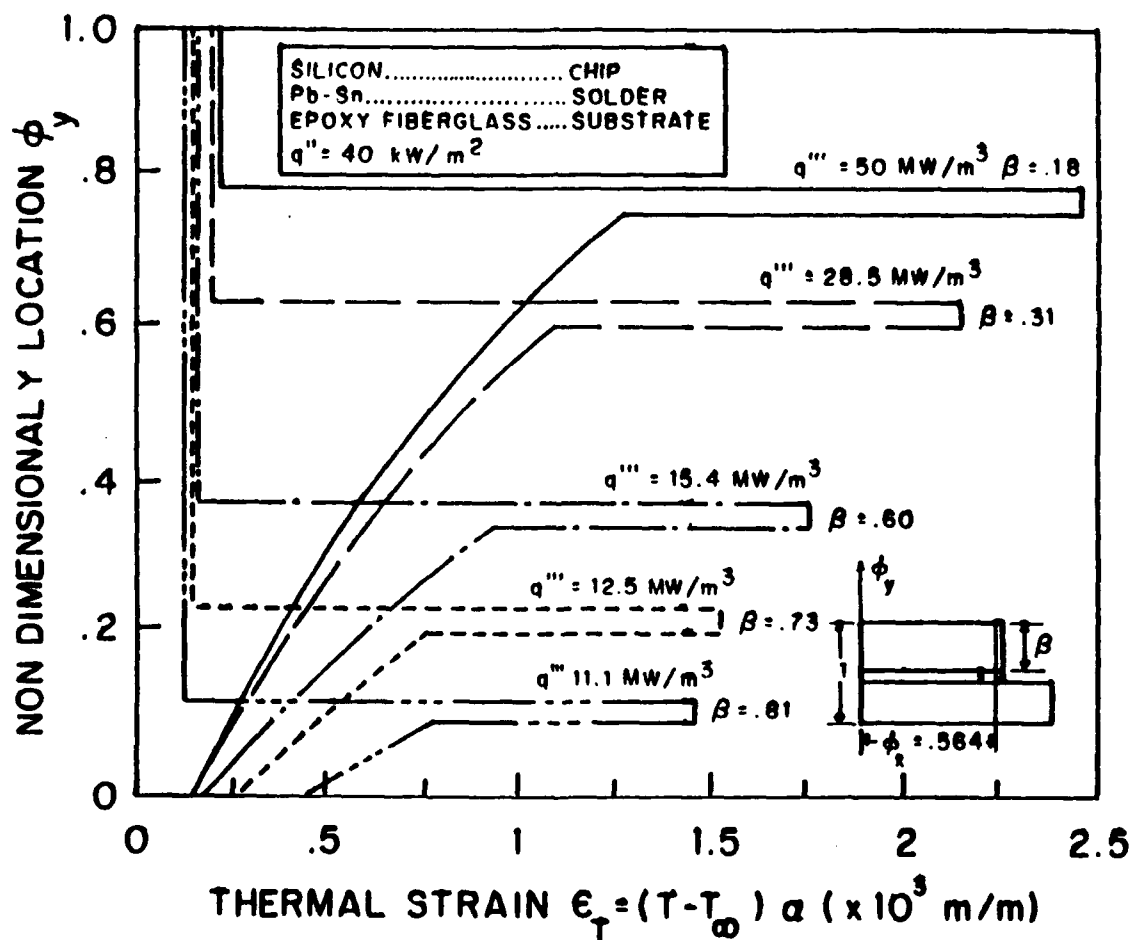
Figure 4.13 Thermal strain profile for various chip heights constant heat flux

The temperature gradient Θ_y is shown in Figure 4.14 for β values of 0.18 through 0.81. Figure 4.14 shows that Θ_y
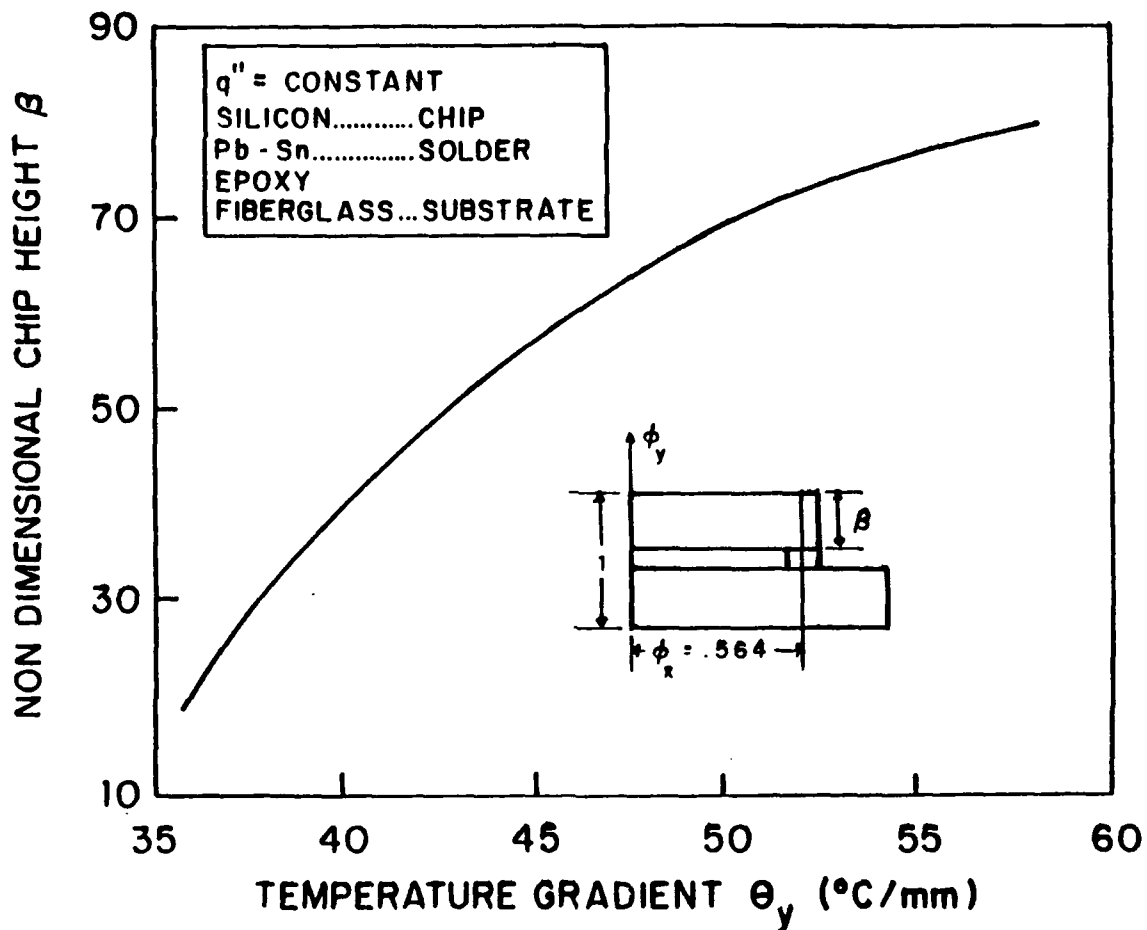
Figure 4.14 Θ_y for various chip heights at constant heat flux increases with an increase in β, from $\Theta_y = 36$ °C/mm at $\beta = .18$ to $\Theta_y = 57$ °C/mm at $\beta = .81$. When $\beta = .18$ the volumetric heat generation q''' is largest at 50 MW/m^3 and provides the least surface area exposed to convection. The thermal resistance for the substrate is attributable to the temperature gradient

developed in the substrate. At $\beta = .18$ the thermal resistance

$$R_{cond}(\beta = .18) = \frac{3.2}{.16 \, (.88) \, 1} \approx 22.7$$

is large, thereby not allowing much heat flux to conduct through the substrate, thereby keeping Θ_y small.

At $\beta = .81$ the thermal resistance

$$R_{cond}(\beta = .81) = \frac{.4}{.16 \, (.88) \, 1} \approx 2.8$$

is very small, allowing for a much larger heat flux to pass through the substrate thereby increasing Θ_y. Figure 4.15 shows the temperature gradient Θ_x at varying
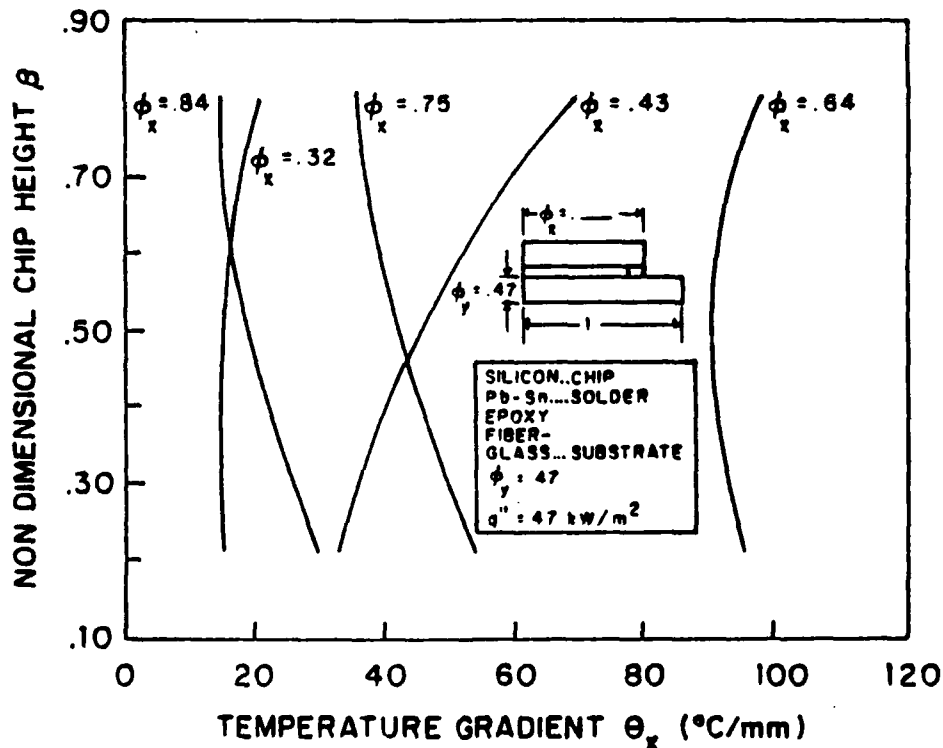
Figure 4.15 Θ_x for various chip heights at constant heat flux

46

positions of ϕ_x for β of 0.18 through 0.81. These gradients are taken at the top of the substrate corresponding to a value of ϕ_y = .47. At ϕ_x = .64 Θ_x is approximately constant at 97 °C/mm for all values of β. This can be attributed to the fact that no matter what thermal energy is generated by the chip it will tend to always flow through the solder and towards the upper right convective portion of the substrate.

In the section of substrate between chips corresponding to ϕ_x = .75 and ϕ_x = .84, Θ_x increases slightly from 31 °C/mm to 52 °C/mm and 14 °C/mm to 27 °C/mm respectively. This can be accounted for by looking at the substrate equivalent thermal resistances. When β = .81 the resistance is small in the Y direction as compared to the X direction as shown by,

$$(R_{cond})_x = \frac{1.5}{.16\,(.4)\,1} \approx 23.4°C/W$$

$$(R_{cond})_y = \frac{.4}{.16\,(.5)\,1} \approx 5°C/W$$

Therefore heat transfer would rather take place in the Y direction instead of the X direction. When β = .18, the thermal resistances are large in the Y direction and small in the X direction that is,

$$R_{cond\,x} = \frac{1.5}{.16\,(3.2)\,1} \approx 3^{\circ}C/W$$

$$R_{cond\,y} = \frac{3.2}{.16\,(.5)\,1} \approx 40^{\circ}C/W$$

This change in thermal resistance now favors heat transfer in the X direction, which accounts for the increase in Θ_x for smaller values of β.

2. Constant Volumetric Heat Generation (q''').

This study shows the effect of using larger power chips in increasing sizes. The heat generation of each chip is proportional to chip volume, that is, heat generation increases with an increase in β. Figure 4.16 is the
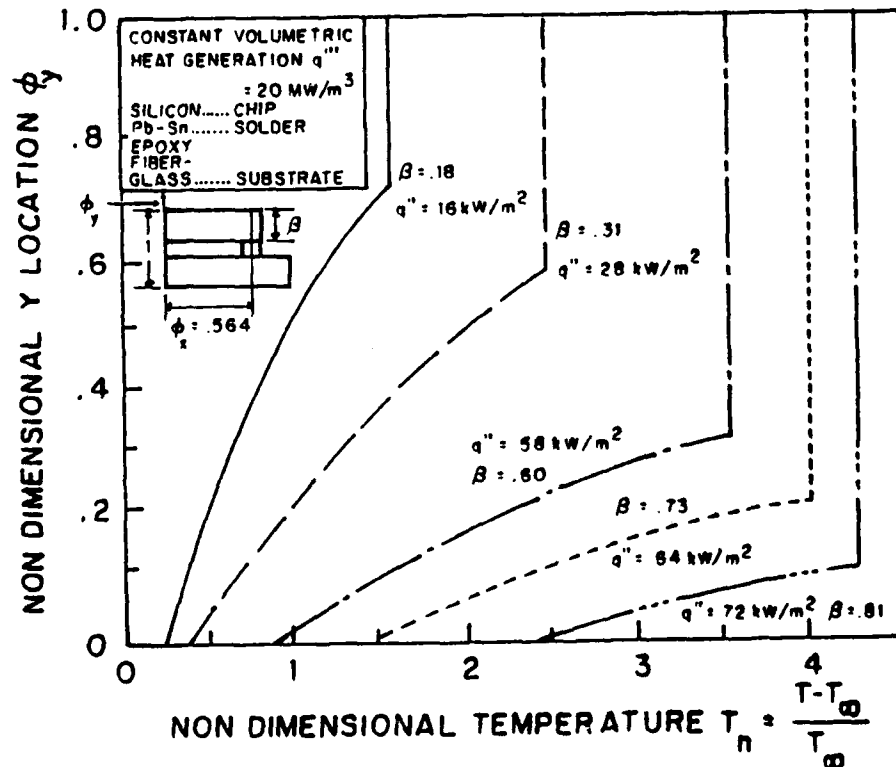
Figure 4.16 Non-dimensional temperature for various size chips constant volumetric power generation

normalized temperature profile for $\beta = 0.18$ to $\beta = 0.81$ at a position of $\phi_x = .564$.

The non dimensional temperature of the package follows the identical relationship as did volumetric heat generation to β. As β increases so does the non-dimensional temperature of the package. If the ratio of heat flux to non-dimensional temperature is examined, the increase in non-dimensional temperature is found to be non-linear. The following ratios q''/T_n are given for various values of β,

β	.18	.31	.60	.73	.81
$\frac{q''}{T_n}$ (w/m^2)	10	11.2	16.1	16.0	16.0

The increase in heat flux $q''(W/m^2)$ from $\beta = .18$ to $\beta = .31$ is 12 KW/m^2 and from $\beta = .6$ to $\beta = .81$ the increase is 14 KW/m^2. Even though the increase in q'' is 2 KW/m^2 more for the later β's the ratio of q''/T_n remains constant. The factors that contribute to this are, an increase in the convection surface area of the chip and a decrease in the conduction thermal resistance of the substrate to allow for a greater heat transfer through the substrate.

Figure 4.17 shows the thermal strain profile at a value of $\phi_x = .564$. The chip does not have a large increase in thermal strain over the range of β's while the solder has a very large increase in thermal strain. This goes back to Table 4.1, where the coefficient of thermal expansion for the Pb-Sn

49

solder is roughly eleven times greater than that of Silicon.
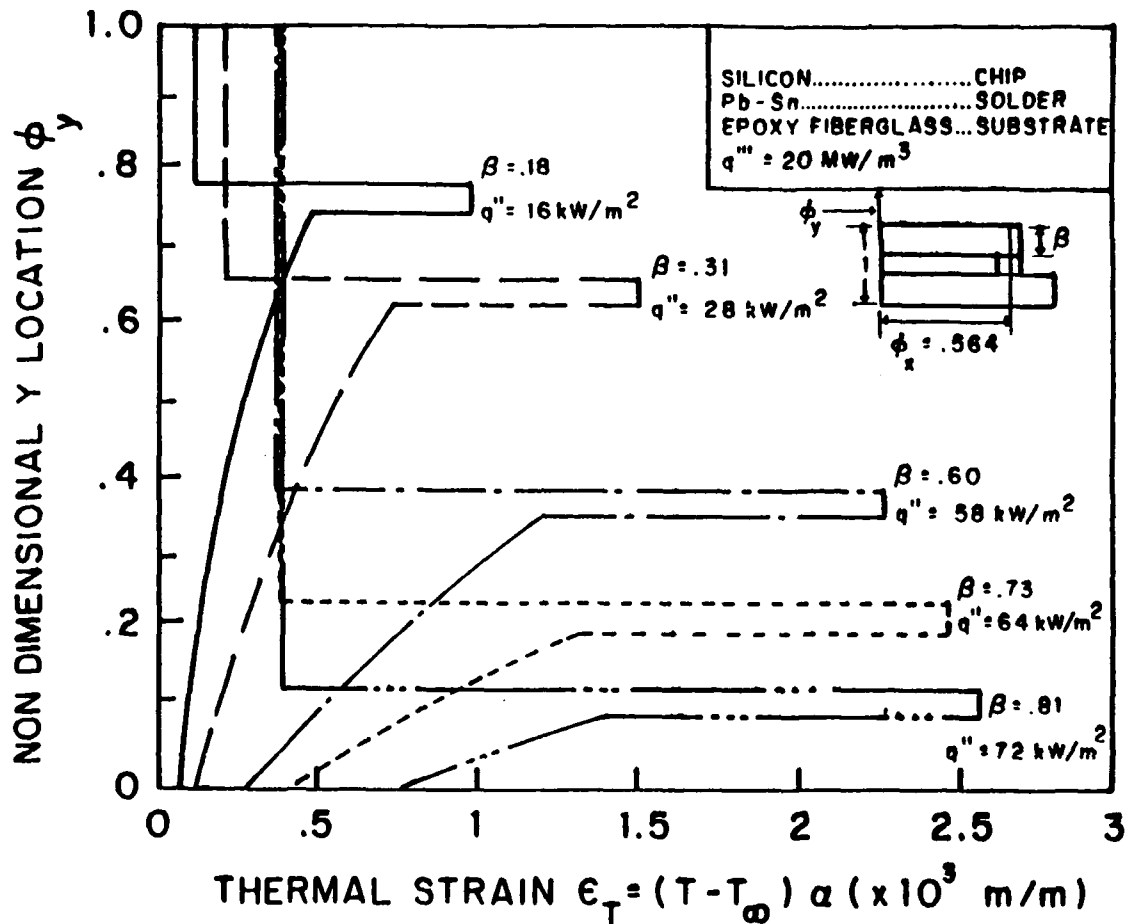
Figure 4.17 Thermal strain profile for various chip heights constant volumetric power

Figure 4.18 shows the variation of the temperature gradient Θ_x at the top of the substrate at various values of ϕ_x. At values of $\phi_x = 0.64$ and $\phi_x = 0.43$ the temperature gradient is largest and this corresponds to either side of the solder joint. At other values of ϕ_x the temperature gradient is diminished greatly. At a value of $\beta = 0.81$ the temperature

gradients are large. They are almost twice as large as encountered in any other analysis. For this large a chip (large q") the convection cooling must be increased significantly to reduce this temperature gradient. For small chip sizes the temperature gradient is very small for any value of ϕ_x.
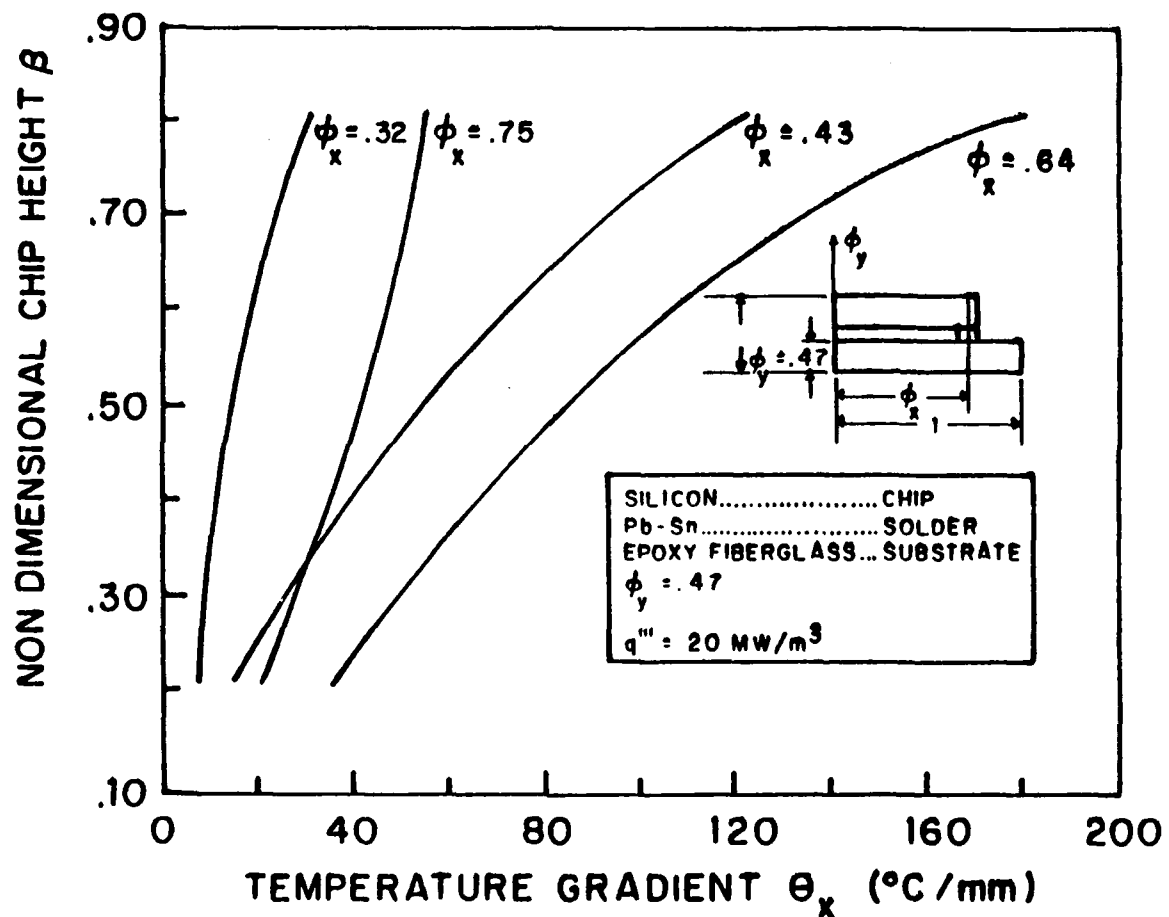
Figure 4.18 θ_x for various chip heights at constant volumetric power

Figure 4.19 shows the variation in Θ_y at the top of the substrate where the largest value of the temperature gradient within the depth of the substrate occurs.

When $\beta = 0.81$ the chip has the greatest heat flux, $q' \approx 72$ KW/m^2 with a correspondingly large Θ_y. When $\beta = 0.18$ the chip has the lowest heat flux, $q' \approx 16$ KW/m^2 and Θ_y is all but non-existent.
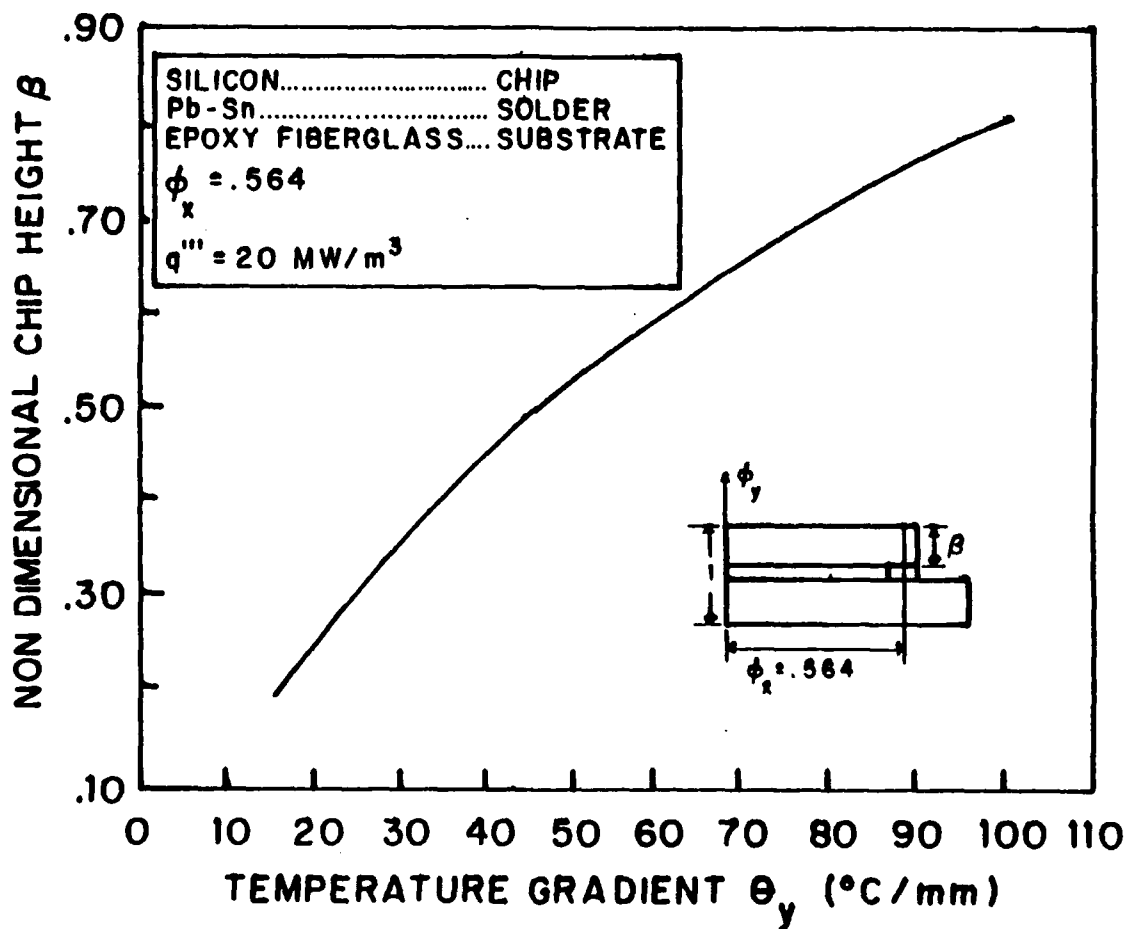
Figure 4.19 Θ_y for various chip heights at constant volumetric power

3. Overview Of Geometric Study

For both the constant heat flux q" (W/m^2) and the constant volumetric heat generation q''' (W/m^3), the temperature gradient in the Y direction at the top of the substrate is greatest when the chip is largest (β = .81). The reasons as given previously are the interaction between the conductive thermal resistance, the convective thermal resistance, and the ratio of volumetric heat generation to available convection area.

If the convective thermal resistance is small as compared to the conductive thermal resistance then the convective mode will dominate the heat transfer process as the heat transfer process is governed by the path of least resistance.

F. EFFECT OF CHIP ENCAPSULATION ON SYSTEM TEMPERATURE

Some electronic packages are protected from moisture and the environment by a protective "encapsulating" coating. For this study the encapsulation material EME-1100-T.[Ref. 1] is 0.1875 mm thick. The effect of encapsulation on the chip temperature and gradients developed within the package is studied.

The following parameters will be held constant, volumetric heat generation (q'''), convection cooling (h), and ambient temperature (T$_a$). These values were the same as in section B for comparison purposes. The materials are a Silicon chip, a

Lead/Tin Solder, with all four substrates, and the encapsulation material. The thermal conductivity of the encapsulation material is k = 0.67 W/m°C. Within the other encapsulation materials the thermal conductivity (k) varied from 0.67 to 1.97 W/m°C.

Figure 4.20 is the non-dimensional temperature profile taken at a value of ϕ_x = 0.564. The entire package experiences less then a 5% temperature change, when low thermal conductivity substrates are used and less then 2% temperature change when high thermal conductivity substrates are used. The encapsulation material causes the surface temperature to decrease by a small amount.
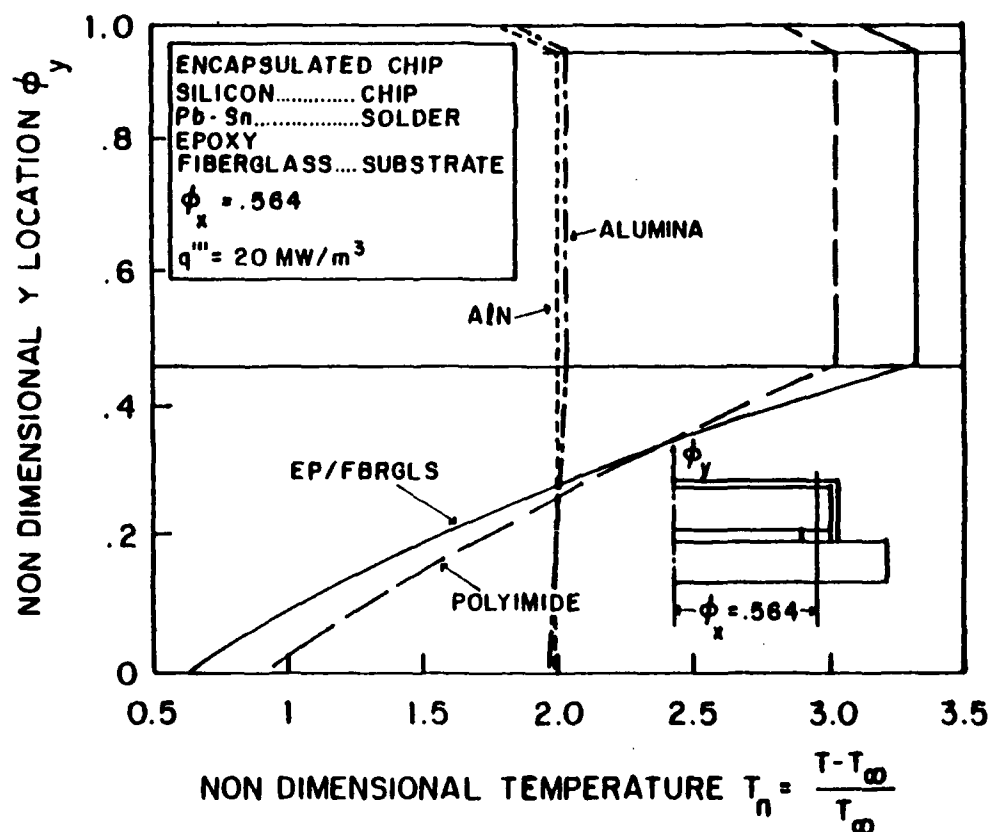
Figure 4.20 Encapsulated chip non-dimensional temperature

Even though the encapsulation material has a low thermal conductivity its overall thermal resistance is low because its less then two tenths of a millimeter thick.

$$R_{cond} = \frac{.1875}{.67\,(2.5)\,1} \approx .11^\circ C/W$$

This is a very low thermal resistance accounting for the small change in temperature profile. Figure 4.21 shows the thermal strain profile for $\phi_x = .564$.
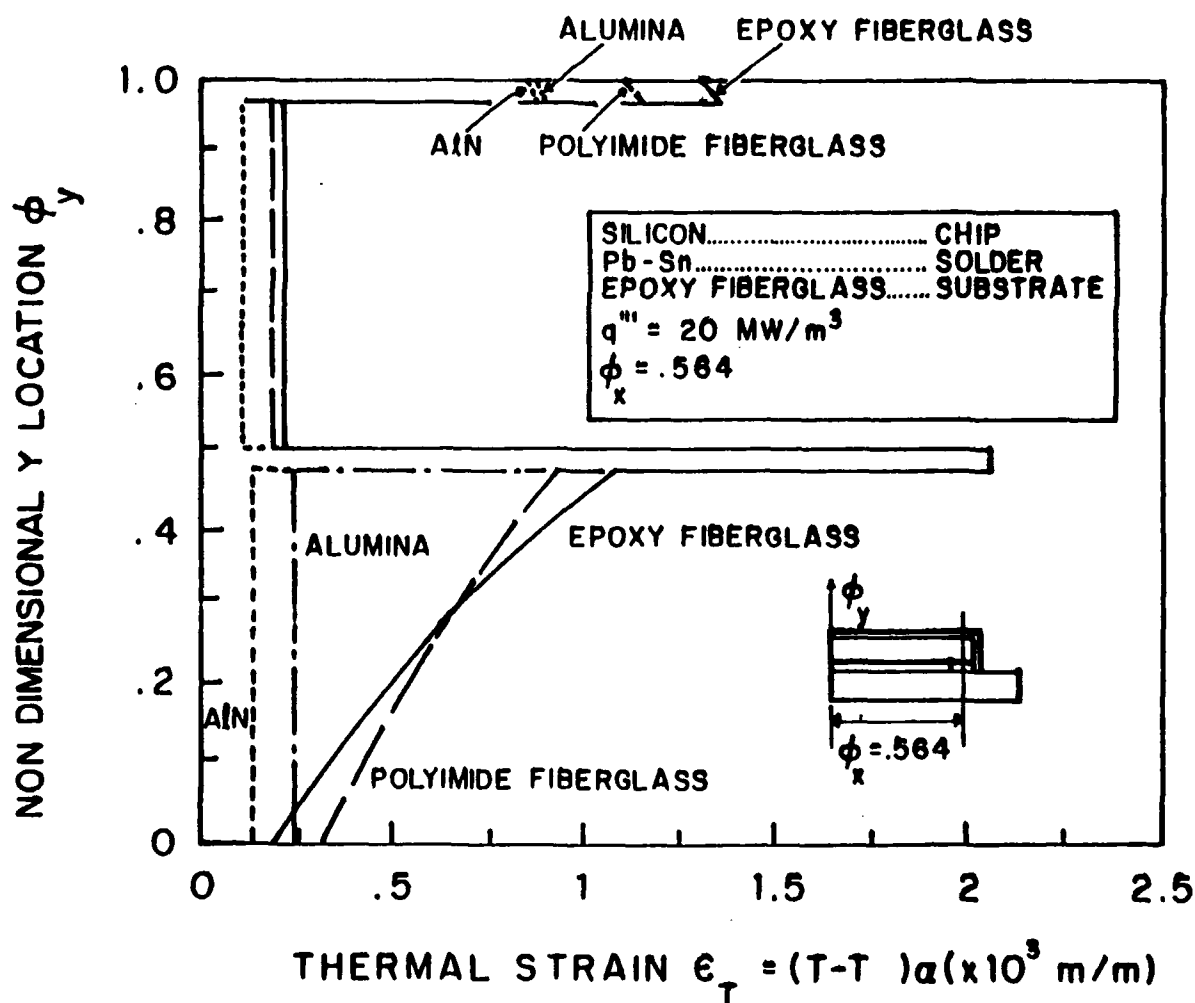
Figure 4.21 Encapsulated chip thermal strain profile

The thermal strain profile has the same negligible increases as the normalized temperature profile had except the encapsulation material has a very large coefficient of thermal expansion (α).

In summary the effect of encapsulation on system temperature and temperature gradients are negligible.

V. STRESS ANALYSIS

A. OVERVIEW OF STRESS ANALYSIS

The stress analysis conducted is based on using different materials in the package and keeping all other factors constant.   A silicon chip material was used for all cases, with two solders Pb–Sn and Au–Sn , and the four substrates Epoxy Fiberglass, Polyimide Fiberglass, Alumina and Aluminum Nitride. These eight sets of material combinations correspond to the thermal strain graphs, shown in Figures 4.3 and 4.4 in Chapter IV.

Figure 4.3 corresponds to the material combinations of a silicon chip, the Pb–Sn solder, and the four substrates listed above. Figure 4.4 corresponds to the material combinations of a silicon chip, the Au–Sn solder, and the four substrates listed above.

The following other factors remain constant, $q''' = 20 \ MW/m^3$ and $h = 250 \ W/m^2 \cdot C$. All stresses given with the exception of the bending stresses at the centerline of the package are along the solder interfaces.   The following stresses are calculated.   First, the bending stresses (σ_b), along the package centerline.   Three stresses are calculated along the solder–chip interface, the upper shear stress (τ_u), an upper bending stress ($\sigma_{b,u}$), and an upper normal stress ($\sigma_{o,u}$).   Three

57

stresses are calculated along the solder-substrate interface, the lower shear stress (τ_l), a lower bending stress ($\sigma_{b,l}$), and a lower normal stress ($\sigma_{o,l}$).

Table 5.1 gives mechanical properties of electronic packaging materials, elastic modulus given in GPa. These properties are used in the calculation of stresses in accordance with the FEM development of chapter three.

TABLE 5.1

Material	Elastic Modulus	Poisson's Ratio
Silicon	13.03	0.3
Pb-Sn	7.4	0.4
Au-Sn	59.2	0.4
EP Fbgls	35.0	0.3
Polyimide	40.0	0.3
Alumina	262.0	0.3
AlN	339.0	0.3

B. STRESS ANALYSIS WITH (Pb-Sn) SOLDER

1. Bending Stress Along Centerline, σ_b

The bending stress at the centerline of the package is the lowest of all stresses presented and is shown in Figure 5.1. The bending stress σ_b, through the chip is of the order of 1 MPa for all four substrates. Through the chip the bending stress is tensile for the low thermal conductivity

substrates (Epoxy and Polyimide Fiberglasses) and compressive for the high thermal conductivity substrates (Alumina and AlN). Through the substrates the bending stresses in the low
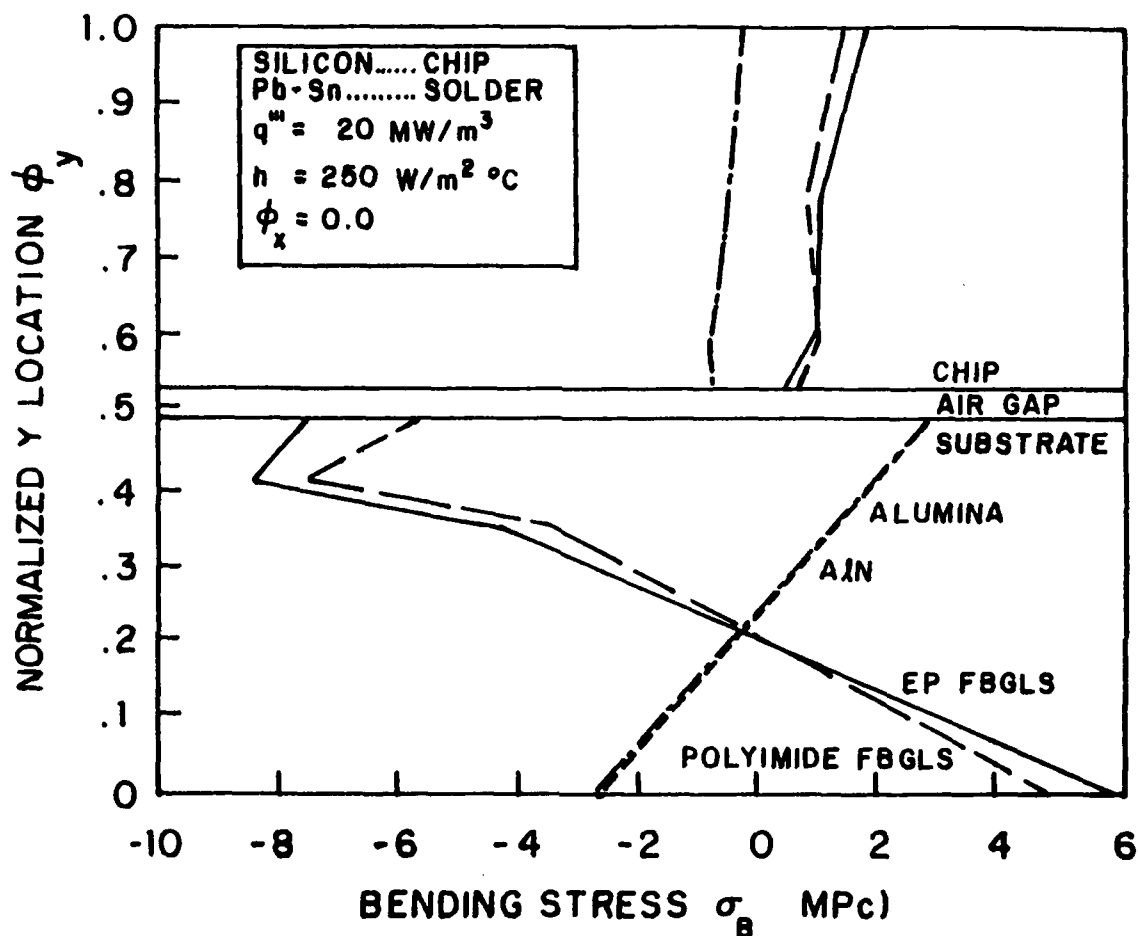
Figure 5.1 Centerline bending stresses σ_b

thermal conductivity substrates is a maximum in compression at the top of the substrate (ϕ_y = .47) at -8 MPa and is a maximum in tension at the bottom of the substrate (ϕ_y = 0) at 6 MPa. The high thermal conductivity substrates have just the opposite results, with a maximum in tension at the top of the

substrate (ϕ_y = .47) at 2.5 Mpa and maximum in compression at the bottom of the substrate (ϕ_y = 0) at -2.5 MPa. Thus the bending stresses in the low thermal conductivity substrates are about twice as large as the bending stresses in the high thermal conductivity substrates. The advantage with respect to bending stresses along the centerline of the chip is with the high thermal conductivity substrates (alumina and AlN).

2. Upper Normal Stress, $\sigma_{o,u}$

The upper normal stress distribution along the chip-solder interface for all the substrates are compressive with a minimum occurring at δ = .05 and maximum occurring at $\delta \approx$ 0.8 as shown in Figure 5.2. For the low thermal conductivity substrates the maximum upper normal stress for Epoxy Fiberglass is -49 MPa, and the maximum for Polyimide Fiberglass is -40 Mpa. Both curves show a decrease in the upper normal stress at the edges of the solder due to the fact that the edges at δ = 0.0 and δ = 1.0 are free surfaces. For the Pb-Sn group of materials the normal stress is the maximum stress examined for the low thermal conductivity substrates.

The upper normal stresses for the high thermal conductivity substrates are about -16 MPa and are within 5% of each other, decreasing in magnitude slightly at the edges of the solder. This shows that the upper normal stresses in the high thermal conductivity substrates are about a third of the upper normal stress in the low thermal conductivity

60

substrates.   We note that the normal stresses are fairly
uniform from δ = .25 to δ = .9.

In contrast to the chip-solder interface, the normal
stresses at the solder-substrate interface (i.e. the lower
normal stresses) are very small on the order of KPa and in
addition are tensile stresses for all substrate combinations.
With respect to $\sigma_{o,u}$ the advantage is again seen with the high
thermal conductivity substrates (alumina and Aln).
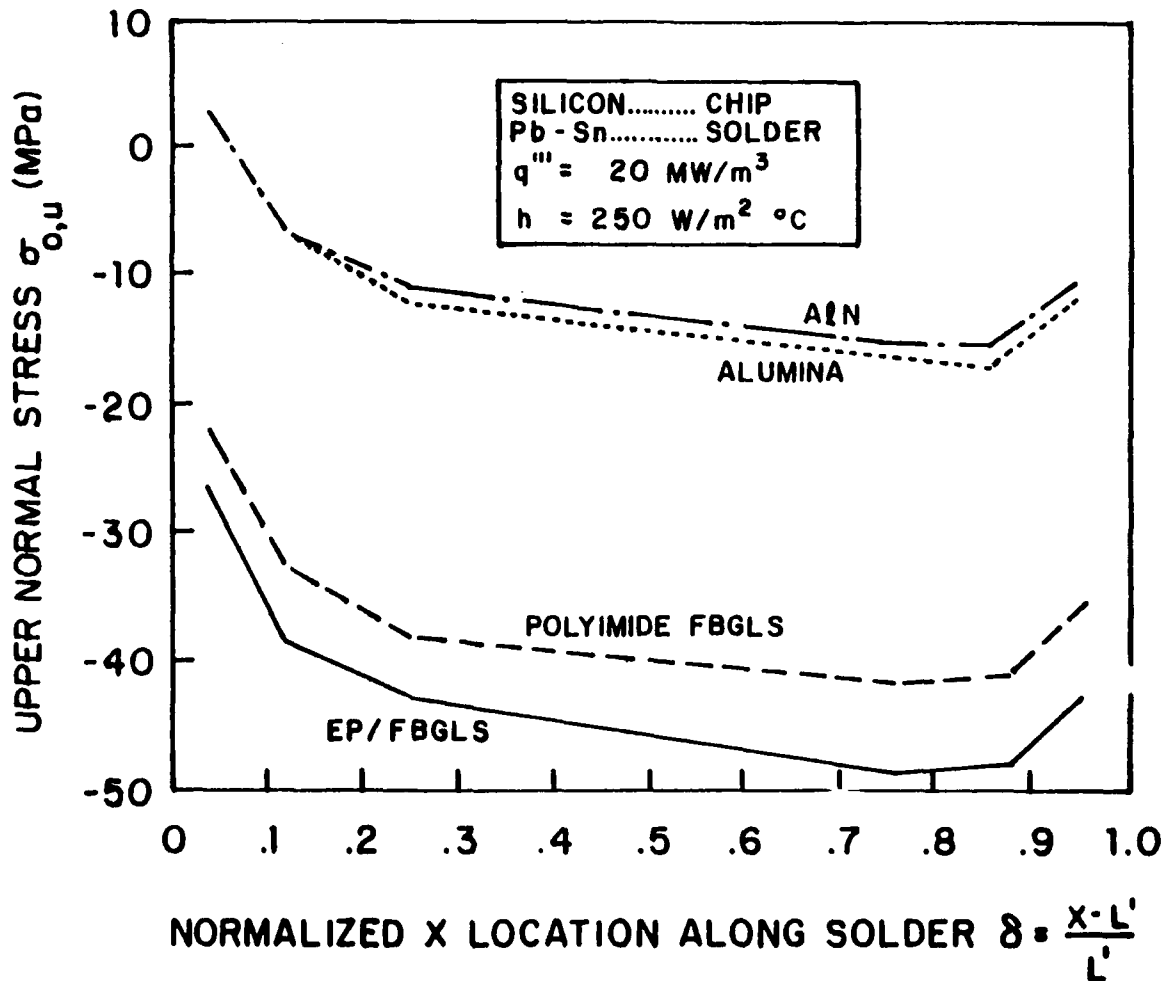
Figure 5.2 Upper normal stresses $\sigma_{o,u}$

3. Upper Bending Stress, $\sigma_{b,u}$

The upper bending stress $\sigma_{b,u}$ along the chip solder interface, is defined as the normal σ_x stress. However, these stresses are presented along the interface, where they are greatest, as a function of δ rather than across the Y direction through the solder. These bending stresses are compressive for all substrate combinations. For the low thermal conductivity substrates the maximum upper bending stresses occur at $\delta = 0.05$ and 0.95 with values of -16 MPa and -15 Mpa respectively. For the high thermal conductivity substrates maximum upper bending stresses occur at $\delta = 0.05$ with -17 Mpa magnitude, and minimums of -8.5 MPa occur at $\delta = 0.8$ as shown in Figure 5.3. Again we note that severe
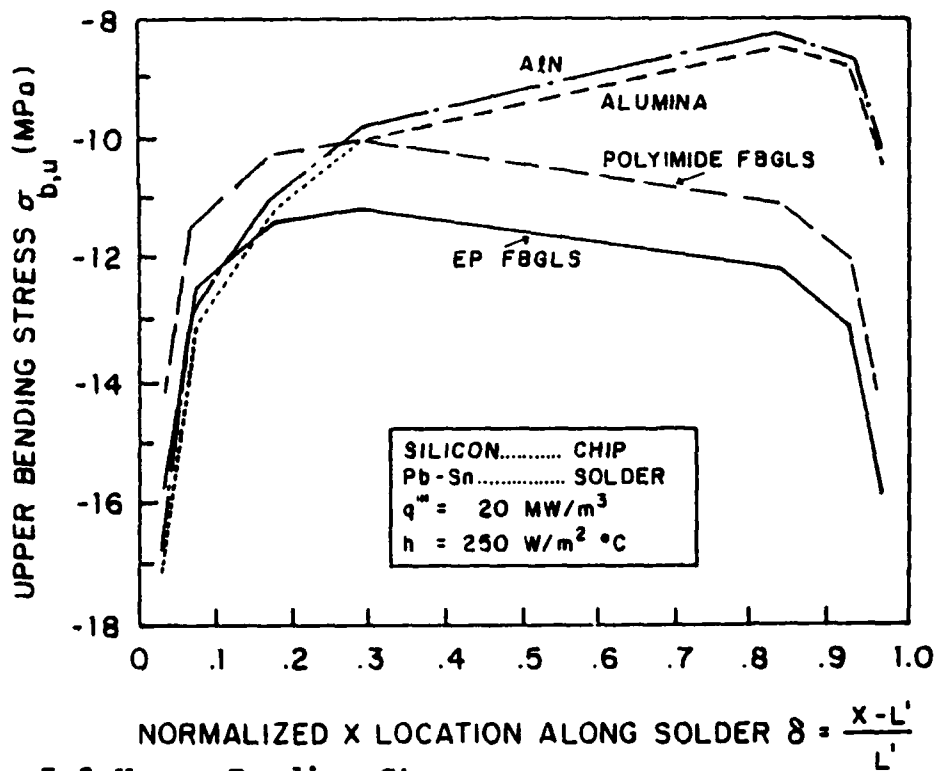
Figure 5.3 Upper Bending Stress $\sigma_{b,u}$

gradients occur close to the free edges, and with fairly uniform stresses along the center of the chip-solder interface. We note these bending stresses fall between the bending stresses at the centerline and normal stresses reported in the previous sections. With respect to these stresses, the advantage (i.e., lower stresses) is obtained for the low thermal conductivity substrates (epoxy and polyimide fiberglasses).

4. Lower Bending Stress $\sigma_{b,l}$

The lower bending stresses are compressive in nature for all substrate combinations as shown in Figure 5.4. For the low thermal conductivity substrates, an immediate decrease from about -18 MPa to about -13 MPa, that is about a 30% change. Thereafter a gradual decrease to about -11 MPa, that is, about 15% change over the remaining domain. The lower bending stress for the high thermal conductivity substrates remains constant over the entire length of the solder joint at -15 MPa.

In comparison with the upper bending stresses the lower bending stresses are greater for the low thermal conductivity substrates. The advantage for the lower bending stresses goes with the high thermal conductivity substrates (alumina and AlN).
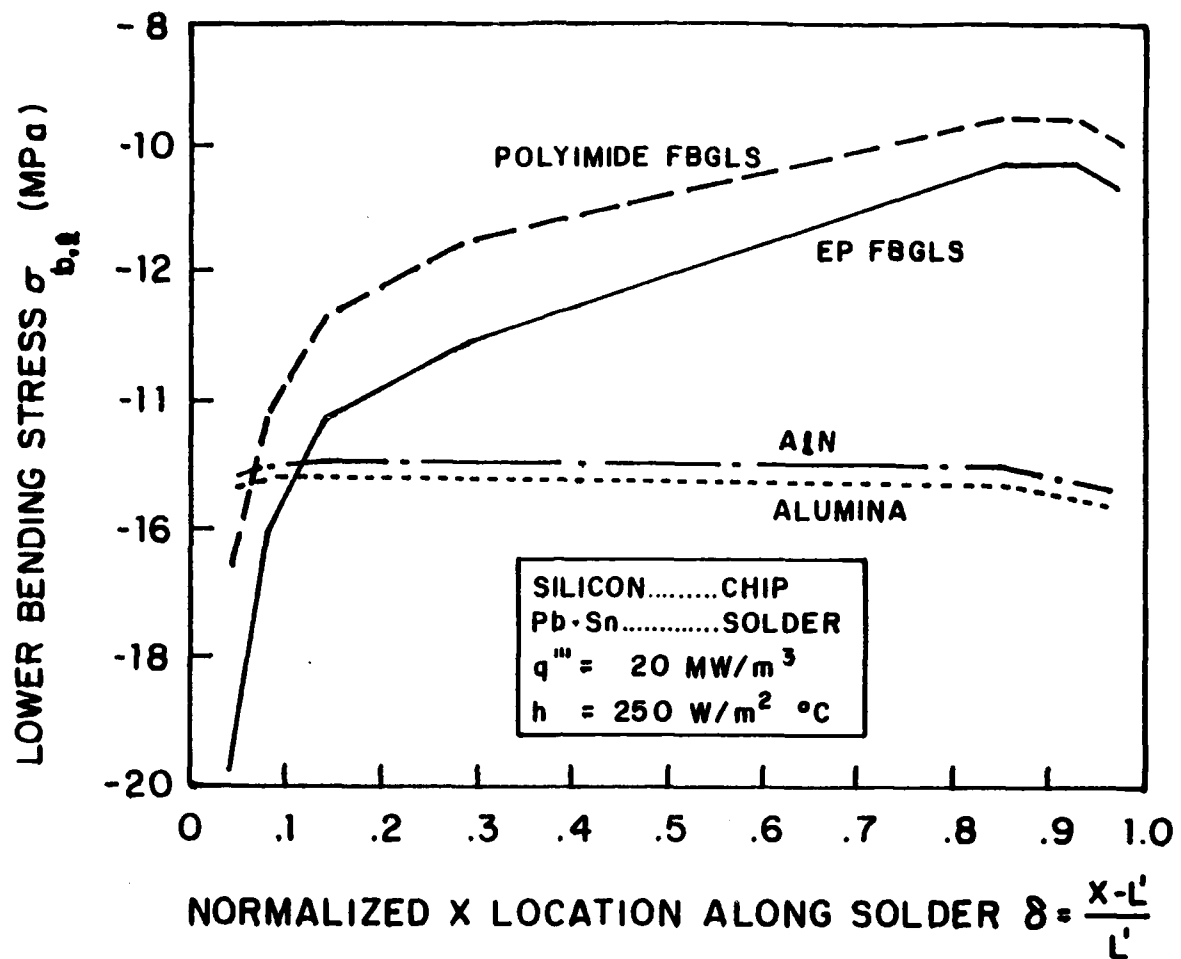
Figure 5.4 Lower bending stress $\sigma_{b,l}$

5. Upper Shear Stress τ_u

The upper shear stresses at the chip/solder interface are positive at δ = .05 and negative at δ = .95 for all substrate combinations as shown in Figure 5.5. For the low thermal conductivity substrates the maximum shear stress is negative and occurs at δ = .95 at −14 MPa and crosses zero stress at δ ≈ .15. For the high thermal conductivity

substrates the maximum shear stress is positive and occurs at $\delta = .05$ at 11 MPa and crosses zero stress at $\delta \approx .8$. The upper shear stresses have large gradients at either edge of the chip-solder interface, but remain fairly constant through the majority of the domain. From $\delta = .2$ through $\delta = .9$ the upper shear stresses are less than 5 MPa in magnitude.

These stresses fall in between the upper bending stresses and the bending stresses at the centerline. With respect to these stresses the advantage goes to the high thermal conductivity substrates (alumina and AlN).
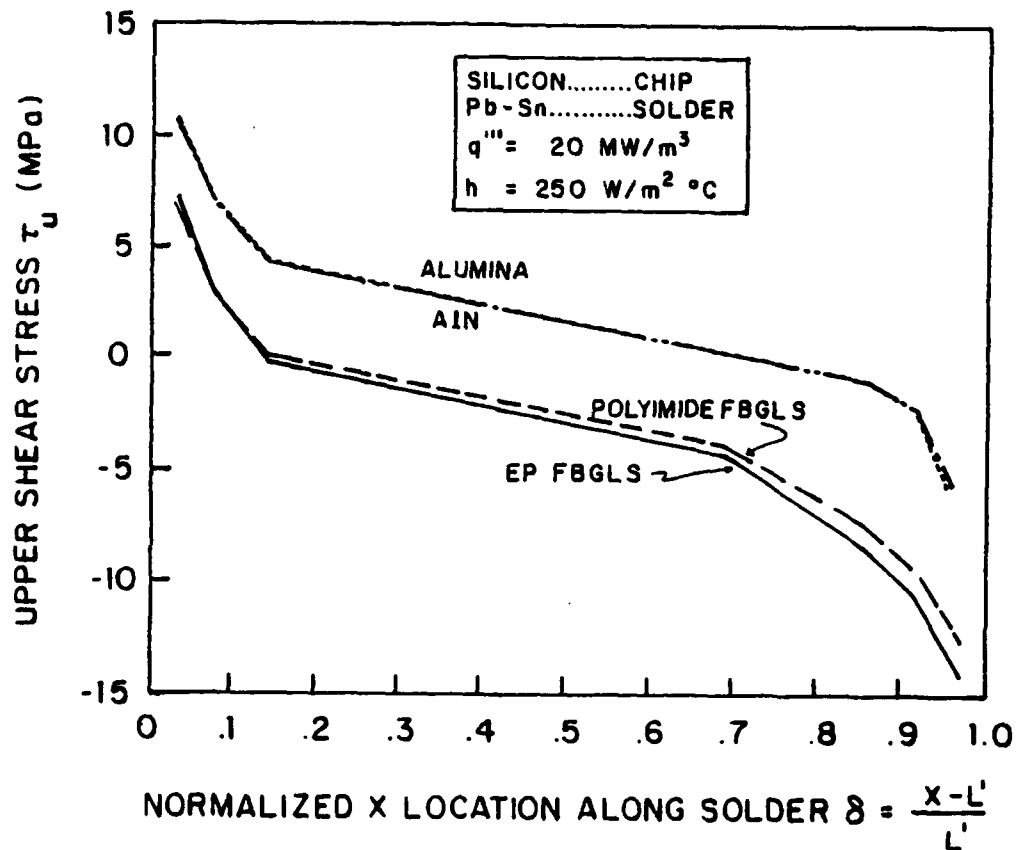
Figure 5.5 Upper shear stress τ_u

65

6. Lower Shear Stress τ_l

The lower shear stresses are opposite in sign from the upper shear stresses, in that the lower shear stresses at the solder/substrate interface are negative at $\delta = .05$ and are positive at $\delta = .95$ for all substrate combinations as shown in Figure 5.6. For the low thermal conductivity substrates the maximum shear stresses occur at $\delta = .05$ at about -16 MPa. This is comparable in magnitude with the upper shear stresses. For the high thermal conductivity substrates the maximum positive shear stress occurs at $\delta = .95$ at 16 MPa while the maximum negative shear stress occurs at $\delta = .05$ at -10 Mpa. This stress at $\delta = .05$ is twice the magnitude as compared to the upper shear stresses. Again we note that steep gradients occur at the edges of the solder-substrate interface and the low thermal conductivity substrates have a gradual decrease over the center of the domain. The τ_l stresses of the low thermal conductivity substrates cross zero at $\delta = .9$. The τ_l stresses for the high thermal conductivity substrates vary linearly with δ between $\delta = .2$ and .9. These τ_l stresses range from -5 MPa at $\delta = .15$ to 10 Mpa at $\delta = .9$ crossing zero stress at $\delta = .45$. We note these lower shear stresses are comparable in magnitude to the upper shear stresses. With respect to these stresses, there is no clear advantage for either set of substrates.
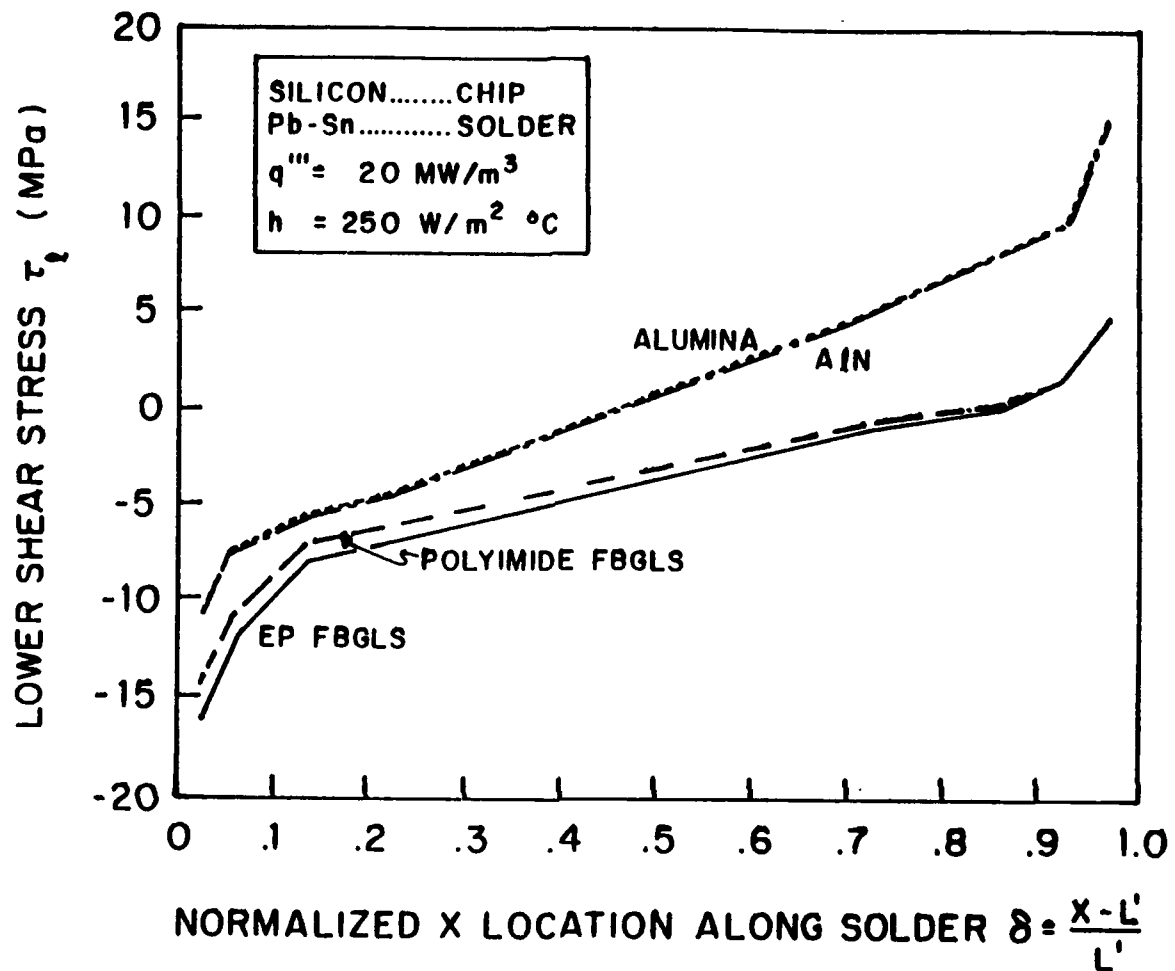
Figure 5.6 Lower shear stress τ_l

C. STRESS ANALYSIS WITH (Au–Sn) SOLDER

1. Bending Stress Along Centerline, σ_b

The bending stress at the centerline of the package remains the lowest of all stresses presented as shown in Figure 5.7. The bending stresses at the centerline ($\phi_x = 0.0$) for the packages with Au-Sn solder are identical to those with Pb-Sn solder. The centerline bending stress is independent of

which solder is used. With respect to these stresses, the advantage is obtained by the high thermal conductivity substrates (alumina and AlN).
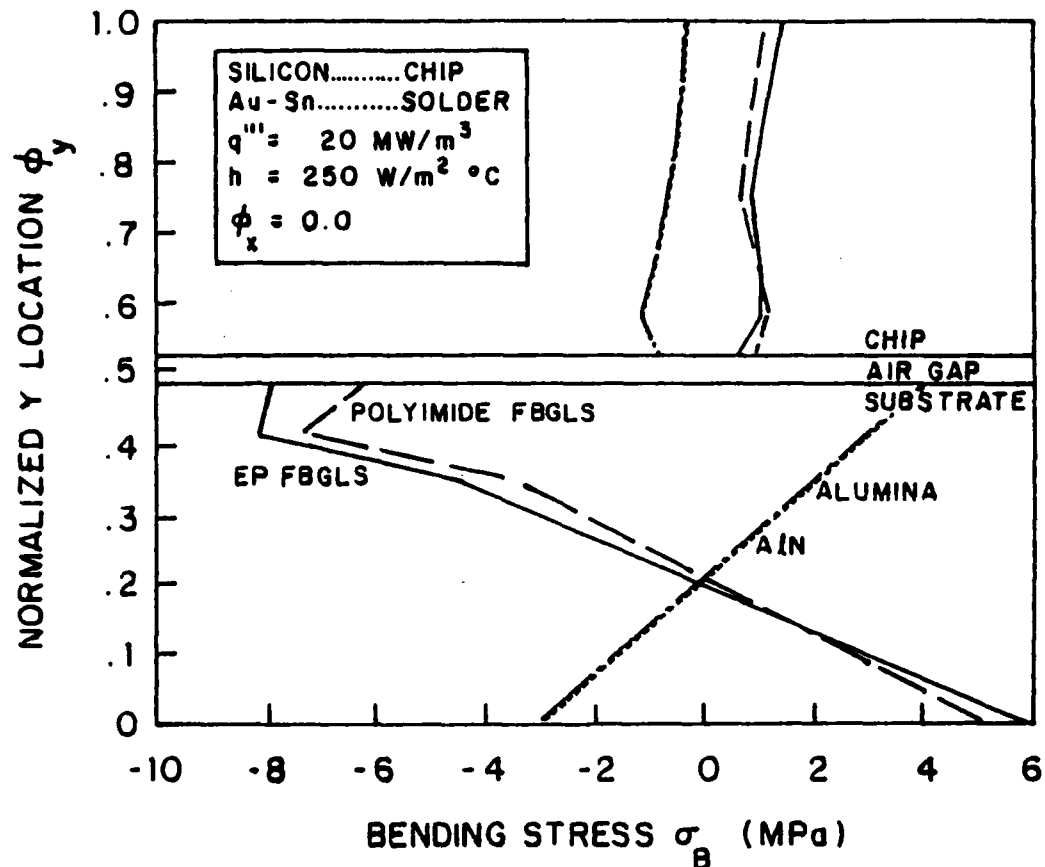
Figure 5.7 Centerline bending stress σ_b

2. **Upper Normal Stress, $\sigma_{o,u}$**

The upper normal stress distribution along the chip-solder interface for all the substrates are compressive in nature as shown in Figure 5.8. For the low thermal conductivity substrates the maximum for Epoxy Fiberglass is

-46 MPa and the maximum for Polyimide Fiberglass is -40 Mpa and they are constant over a range of .1 < δ < .9.   Both upper
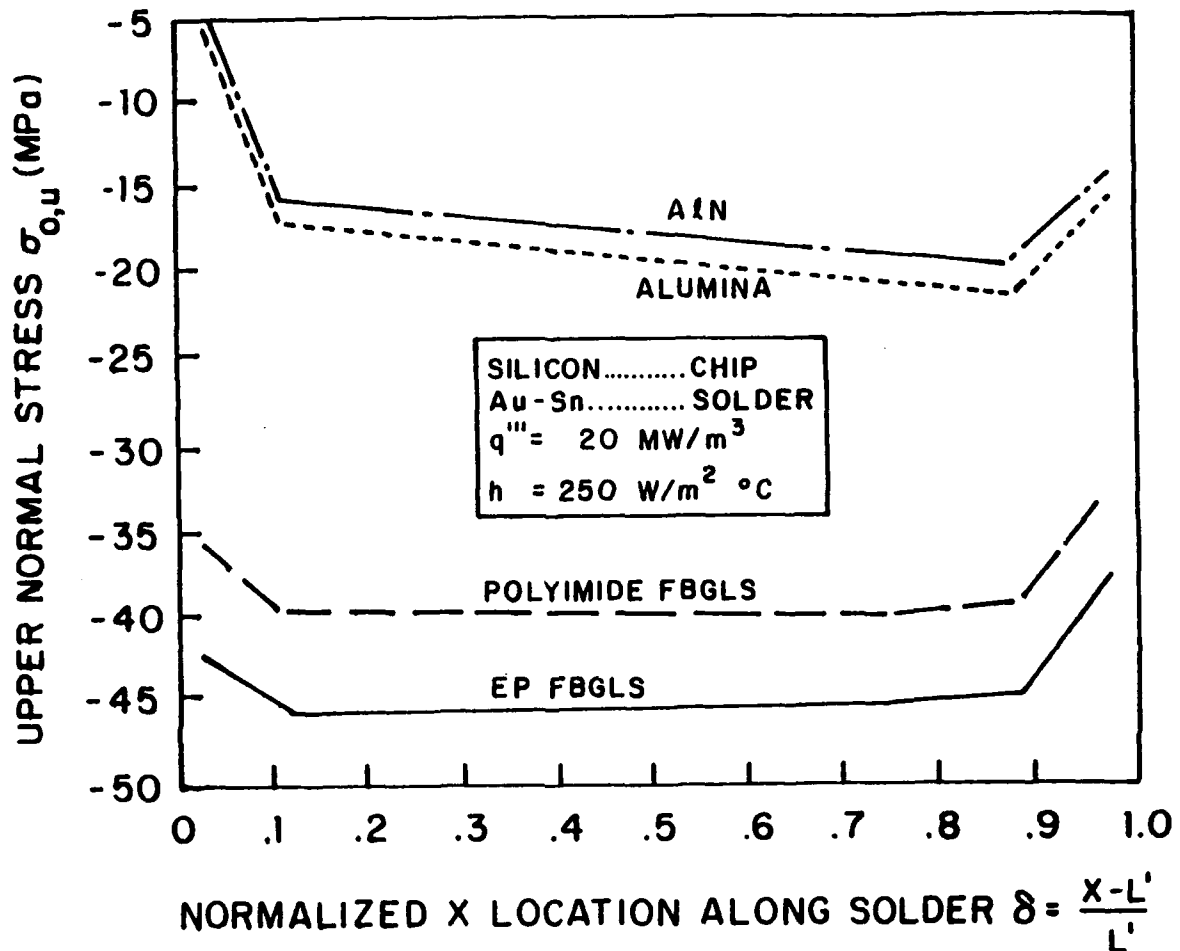
Figure 5.8 Upper normal stress $\sigma_{o,u}$

normal shear stress distributions decrease at the edges of the solder due to the fact that the stress at a free surface is zero.   The normal stress is once again the maximum stress examined for the low thermal conductivity substrates.

The high thermal conductivity substrates have increased by about 20% over the Pb-Sn material package.   There

are sharp increases at δ = .1 and a slight increase to a maximum of about -20 MPa at δ = .9.

Again we note that in contrast to the chip-solder interface, the normal stresses at the solder substrate interface are very small on the order of KPa and in addition are tensile stresses for all substrate combinations. With respect to these stresses, the advantage is obtained for the high thermal conductivity substrates (alumina and AlN) and with respect to solders, the advantage is obtained for the Pb-Sn solder.

3. Upper Bending Stress, $\sigma_{b,u}$

The upper bending stress $\sigma_{b,u}$ along the chip-solder interface is defined as the normal σ_x stress as previously mentioned. The upper bending stresses are compressive for all substrate combinations as shown in Figure 5.9. For the low thermal conductivity substrates maximums occur at δ = 0.05 and 0.95 with values of -19 MPa and -22 Mpa respectively. For the high thermal conductivity substrates a maximum occurs at δ = 0.05 at -39 Mpa. This upper bending stress is twice as large for the high thermal conductivity substrates with Au-Sn solder then Pb-Sn solder. There is a very large gradient at δ = 0.05 where the upper bending stress decreases from -39 MPa to -22 MPa, that is, about a 45% decrease. For the high thermal conductivity substrates the upper bending stress continues to decrease at a gradual rate across the remaining domain, δ = .2

70

to $\delta = .9$. With respect to these stresses, the advantage is obtained for the low thermal conductivity substrates (epoxy and polyimide fiberglasses) and with respect to solders, the advantage is obtained for the Pb-Sn solder.
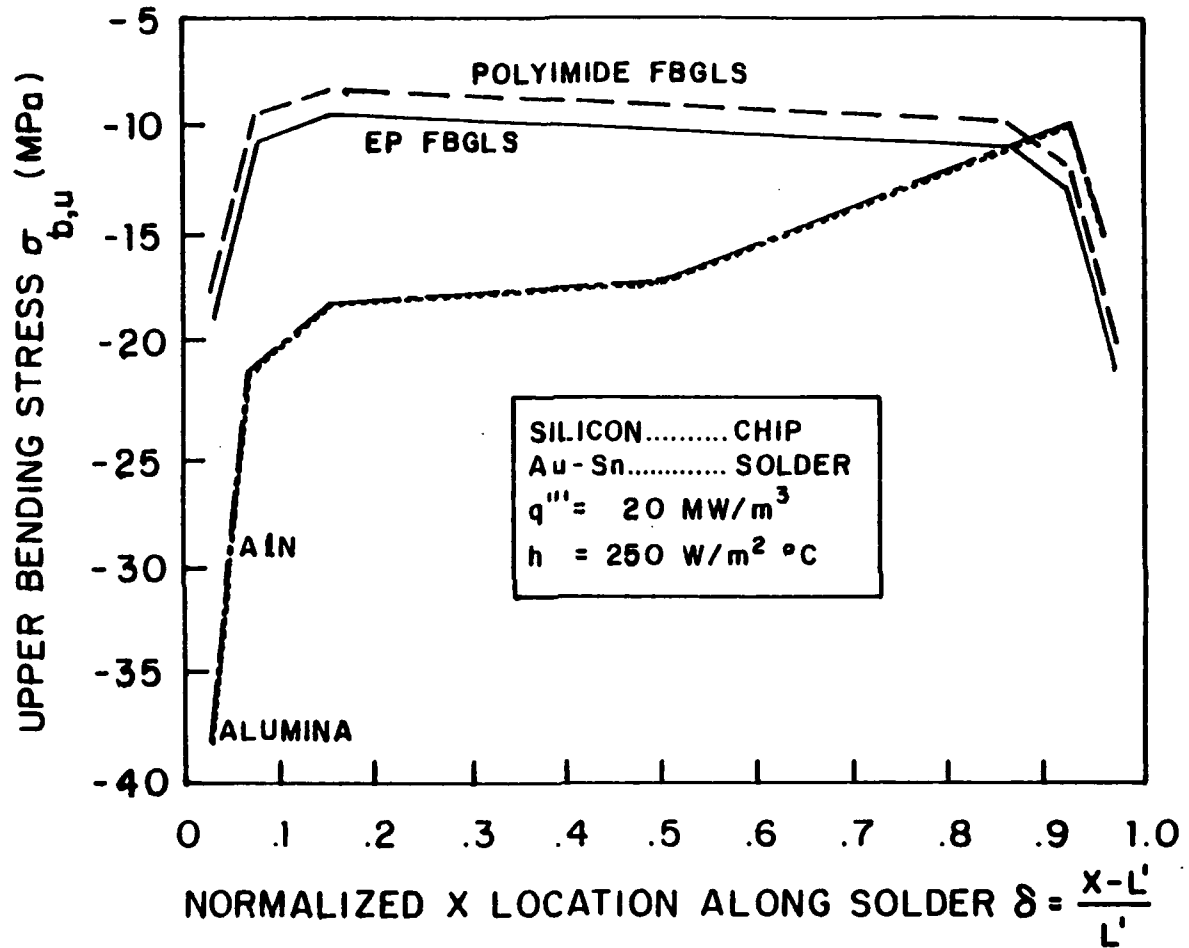
Figure 5.9 Upper Bending Stress $\sigma_{b,u}$

4. Lower Bending Stress, $\sigma_{b,l}$

The lower bending stresses are compressive for all substrate combinations as shown in Figure 5.10. For the low thermal conductivity substrates a maximum occurs at $\delta = 0.05$

71

with a value of -39 MPa and a minimum at -7 MPa at δ = 0.9.
This is an increase of 200% over the same package with Pb-Sn
solder. The lower bending stress for the high thermal
conductivity substrates remain fairly constant over a range of
.15 < δ < .8 with a value of -38 MPa and is a maximum at δ =
.95 at -49 MPa. This is an increase of about 260% over the
same package with Pb-Sn solder. The lower bending stresses
are the highest stresses presented for the high thermal
conductivity substrates. With respect to these stresses, the
advantage is obtained for the low thermal conductivity
substrates (epoxy and polyimide fiberglasses) and with respect
to solders, the advantage is obtained for the Pb-Sn solder.
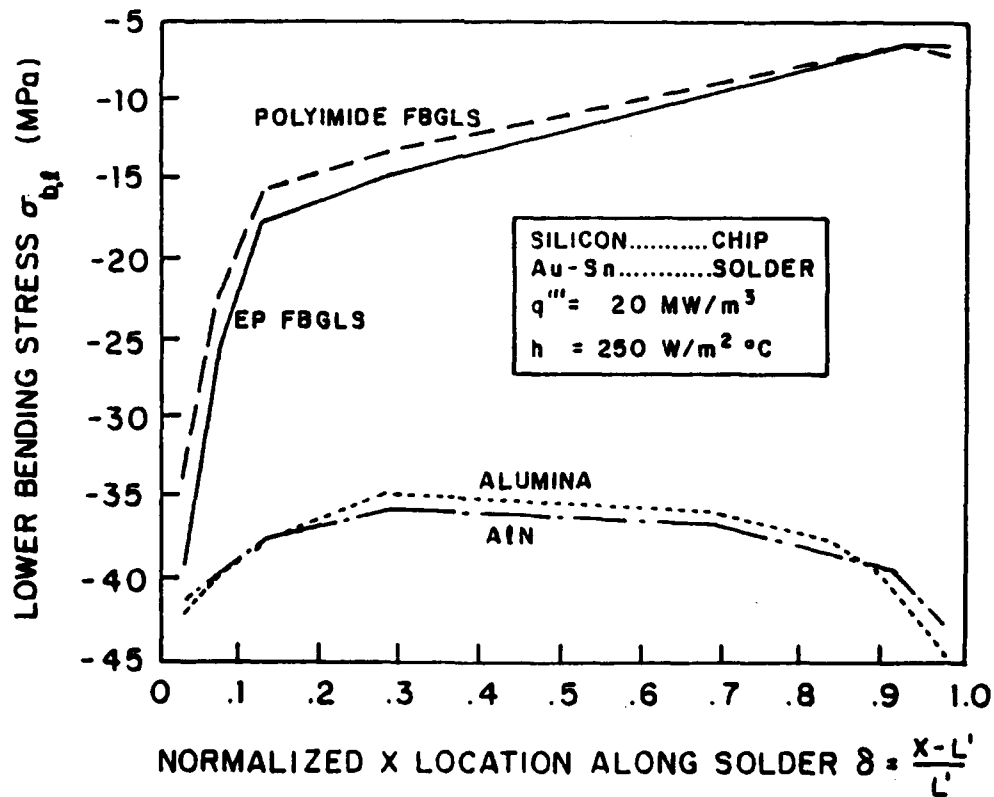
Figure 5.10   Lower bending stress $\sigma_{b,l}$

5. Upper Shear Stress τ_u

The upper shear stresses at the chip/solder interface are positive at $\delta = .05$ and negative at $\delta = .95$ for all substrate combinations as shown in Figure 5.11. For the low
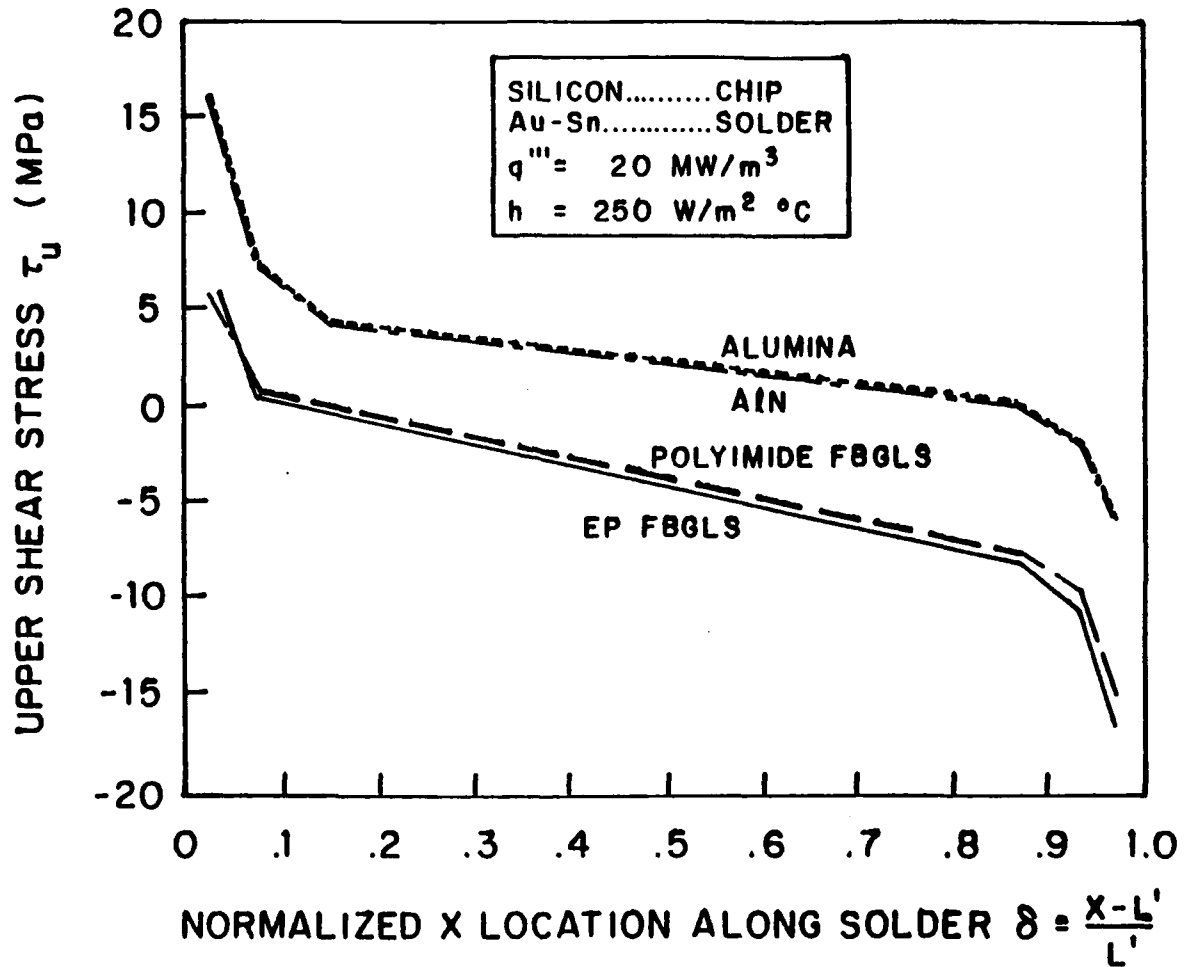
Figure 5.11 Upper shear stress τ_u

thermal conductivity substrates the maximum shear stress is negative and occurs at $\delta = .95$ with a value of -15 MPa and crosses zero stress at $\delta \approx .15$. For the high thermal conductivity substrates the maximum shear stress is positive

and occurs at δ = .05 with a value of 16 MPa and crosses zero stress at δ ≈ .8. The maximum upper shear stresses for both types of substrates show only a slight increase over the Pb-Sn solder packages. With respect to these stresses, there is no clear cut advantage for either set of substrates, nor either solder.

6. Lower Shear Stress τ_l

The lower shear stresses are opposite in sign from the upper shear stresses, in that the lower shear stresses at the solder/substrate interface are negative at δ = .05 and are positive at δ = .95 for all substrate combinations as shown in Figure 5.12. For the low thermal conductivity substrates the maximum shear stresses occur at δ = .05 with a value of -21 MPa. This represents an increase of 130% over the same package with Pb-Sn solder. The lower shear stress then decreases to -10 Mpa at δ = .1 and then slowly decreases to about zero at δ = .95. For the high thermal conductivity substrates the maximum shear stresses occur at δ = .95 with a value of 39 MPa. This represents an increase of 240% over the same package with Pb-Sn solder. At δ = .05 the lower shear stress is negative at -32 MPa which represents an increase of 110% over the same package with Pb-Sn solder. With respect to these stresses, the advantage is obtained for the low thermal conductivity substrates (epoxy and polyimide fiberglasses) and

with respect to solders, the advantage is obtained for the Pb-Sn solder.
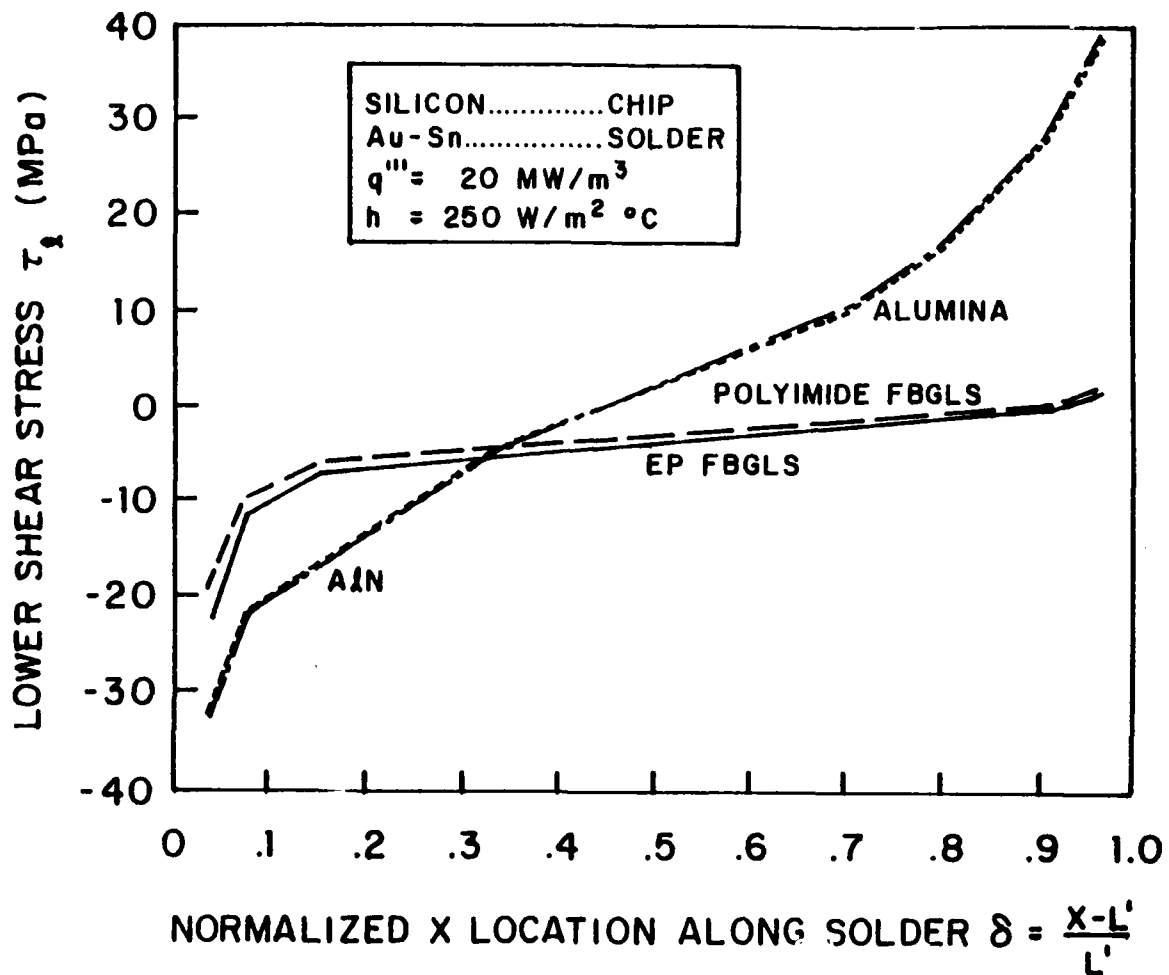
Figure 5.12 Lower Shear Stress τ_l

D. SUMMARY OF STRESS ANALYSIS

The following table represents the maximum stress : (given in MPa) for each material combination studied. Various comparisons are possible.

TABLE 5.2 MAXIMUM STRESSES

		Pb–Sn	Au–Sn
EP FBGLS	σ_b	−8	−8
	σ_o	−49	−46
	$\sigma_{b,u}$	−16	−20
	$\sigma_{b,l}$	−19.5	−39
	τ_u	−14.5	−16
	τ_l	−16	−21
POLY FBGLS	σ_b	−7.5	−7.5
	σ_o	−41	−40
	$\sigma_{b,u}$	−14	−18
	$\sigma_{b,l}$	−16.5	−34
	τ_u	−13	−14
	τ_l	−15	−20
ALUMINA	σ_b	−2.5	−3
	σ_o	−16	−20
	$\sigma_{b,u}$	−17	−38
	$\sigma_{b,l}$	−15	−45
	τ_u	11	16
	τ_l	15	40
AlN	σ_b	−2.5	−3
	σ_o	−15	−19
	$\sigma_{b,u}$	−17	−38
	$\sigma_{b,l}$	−14	−43
	τ_u	11	16
	τ_l	15	40

For the Epoxy fiberglass substrate packages there is little difference in centerline bending σ_b, normal σ_o, and upper shear τ_u stresses and only a slightly larger upper bending $\sigma_{b,u}$, and lower shear τ_l stresses for Au-Sn versus Pb-Sn solder. For this substrate the lower bending $\sigma_{b,l}$ stresses are twice as great for Au-Sn versus Pb-Sn solder. The normal stresses are the largest stresses for this substrate for both Pb-Sn and Au-Sn solders. The most significant stresses with regard to deforming the solder joint are the lower bending and lower shear. The upper normal stress is not significant because it tends to compress a solder crack rather then propagate it.

For the Polyimide fiberglass substrate packages there is little difference in centerline bending σ_b, normal σ_o, and upper shear τ_u stresses and only a slightly larger upper bending $\sigma_{b,u}$, and lower shear τ_l stresses for Au-Sn versus Pb-Sn solder. For this substrate the lower bending $\sigma_{b,l}$ stresses are twice as great for Au-Sn versus Pb-Sn solder. The normal stresses are the largest stresses for this substrate for both Pb-Sn and Au-Sn solders. The most significant stresses with regard to deforming the solder joint are the lower bending and lower shear. The upper normal stress is not significant because it tends to compress a solder crack rather then propogate it. The Polyimide fiberglass packages have stress distributions similiar to Epoxy fiberglass, but tend to be slightly lower in magnitude.

For the Alumina substrate only the centerline bending σ_b stresses are similiar for both solders. The upper normal σ_o and upper shear τ_u stresses are slightly larger for Au-Sn versus Pb-Sn solders. The upper bending $\sigma_{b,u}$ stress is 225% larger, lower bending $\sigma_{b,l}$ stress is 300% larger, and the lower shear τ_l stress is 265% larger for the Au-Sn versus Pb-Sn solder. The upper bending stress is largest for the Pb-Sn solder while the lower bending stress is largest for the Au-Sn solder. The most significant stresses with regard to deforming the solder joint are the upper bending, lower bending and lower shear.

For the AlN substrate only the centerline bending σ_b stresses are similiar for both solders. The upper normal σ_o and upper shear τ_u stresses are slightly larger for Au-Sn versus Pb-Sn solders. The upper bending $\sigma_{b,u}$ stress is 225% larger, lower bending $\sigma_{b,l}$ stress is 305% larger, and the lower shear τ_l stress is 265% larger for the Au-Sn versus Pb-Sn solder. The upper bending stress is largest for the Pb-Sn solder while the lower bending stress is largest for the Au-Sn solder. The most significant stresses with regard to deforming the solder joint are the upper bending, lower bending and lower shear. The AlN packages have stress distributions which are approximately less than 5% different from Alumina.

Based on the stress results from this investigation the following ranking of material combinations are presented based

on obtaining the lowest stresses in the package. The silicon chip is used in all packages.

1. Pb-Sn with Alumina or Aln
2. Pb-Sn with Polyimide fiberglass
3. Pb-Sn with Epoxy fiberglass
4. Au-Sn with Polyimide fiberglass
5. Au-Sn with Epoxy fiberglass
6. Au-Sn with Alumina or Aln

Bending (σ_b) and Shear (τ) stresses at the solder-substrate interface can be significant. The lower inside corner of the solder-substrate interface $(\delta = 0.0)$ is the point where failure is most likely to occur due to bending and shear stresses.

This investigator recommends the following topics for further research. Alter the thermal code for transient temperature response of the package. The result of this would be to track stress in time. In this way the changes in temperature and stress can be tracked in time after the electronic device has been turned on. Conduct a parametric study of a general tri-material package varying the materials coefficient of thermal expansion and modulus of elasticity to better understand the effect on stresses produced in the tri-material package.

APPENDIX A.

        PROGRAM HEAT
****
*   *
*   This F.E.M. program solves for the Temperature distribution in   *
* electronic packages. The governing differential equation is   *
* POISSON's equation. More specifically: *
*   *
*   *
*   When symmetry is envoked homogeneous Neumann boundary conditions *
* are used at these locations. The other boundaries are Cauchy.   *
*   *
*   *
* Listing of variables: *
*   *
* aaij   = local nodal point values of BIGA matrix   *
* ALPHA   =
* AREA   = vector of element areas   *
* bi   = triangular coordinate property of each element   *
* bbij   = contribution from Cauchy boundary to BIGA matrix   *
* BIGA   = global left hand matrix   *
* BIGF   = right hand side vector   *
* BDRYVAL = value of boundary point   *
* BLOW   = (BUP,BVERT) inverse of the absolute temp of the fluid   *
* cauchfi = contribution from Cauchy boundary to BIGF vector   *
* ci   = triangular coordinate property of each element   *
* DEL1,2,3 = difference between assumed and calc. surface temps   *
* DELMAX   = maximum of dell or del2 or del3   *
* DIVSUB   = # of rows of substrate   *
* DIVX   = # of divisions in x direction for a grid density   *
* DIVY   = # of divisions in y direction for a grid density   *
* DIVXAIR = # of columns of air in grid   *
* DIVYAIR = # of rows of air(solder) in grid   *
* ff1   = contribution of source term to BIGF vector   *
* GEN   = if equal to 1 then internal heat generation is involved *
* HLOW   = lower side heat transfer coefficient   *
* HUP   = upper side heat transfer coefficient   *
* HVERT   = right side heat transfer coefficient   *
* IMAT   = identifies what material properties go with which element*
* ICOR   = establishes correspondence between local and global coor.*
* KEL   = therm. conductivity of element   *
* KINVS   = kinematic viscosity of the fluid   *
* NBCLOW   = if = 1 ; then lower boundary is a Cauchy   *
* NBCUP   = if = 1 ; then upper boundary is a Cauchy   *
* NBCVERT = if = 1 ; then right boundary is a Cauchy   *
* NBDLEFT = if = 1 ; then left boundary is a Direchlet   *
* NBDRIT   = if = 1 ; then right boundary is a Direchlet   *
* NBDUP   = if = 1 ; then upper boundary is a Direchlet   *
* NBDLOW   = if = 1 ; then lower boundary is a Direchlet   *
* NCOL   = number of columns for grid subroutine   *
* NROW   = number of rows for grid subroutine   *
* NSUBEL   = # of substrate elements   *
* NAIREL   = # of columns of air in grid   *

80

```
* NARSOEL = # of air & solder elements                                 *
* QDOT    = volumetric heat generation of electronic device            *
* RALLOW  = Raleigh # of the fluid at the lower surface                *
* RALUP   = Raleigh # of the fluid at the upper surface                *
* RALVERT = Raleigh # of the fluid at the vertical surface             *
* RHO     = density of 4 different materials                           *
* RHOEL   = density of element                                         *
* SPHT    = specific heat of 4 different materials                     *
* SPHTEL  = specific heat of element                                   *
* TAMB    = ambient temperature                                        *
* TEMP    = solution vector of temperatures                            *
* TFLLOW  = fluid temperature at lower surface                         *
* TFLUP   = fluid temperature at upper surface                         *
.* TFLVERT = fluid temperature at vertical surface                     *
* TSLOW   = average surface temperature of lower surface               *
* TSUP    = average surface temperature of upper surface               *
-* TSVERT  = average surface temperature of vertical surface           *
* THERCON = thermal conductivity of 4 different materials              *
* X       = x position of system nodal point                          *
* XPOS    = x position of new grid density                            *
* Y       = y position of system nodal point                          *
* YPOS    = y position of new grid density                            *
***********************************************************************

        INCLUDE 'HEATCOMN.FOR'

******** ensure the proper amount of workspace is allocated ***
******** on problems with a large quantity of unknowns a ******
******** FORTRAN STOP may be encountered.  the amount of ******
******** work space allocated in RWKSP and IWKIN must be ******
******** increased
        COMMON/WORKSP/RWKSP
        REAL RWKSP (900000)
        CALL IWKIN (900000)

******** ensure the proper data files are being read **********
        OPEN(7,FILE='HEAT.OUT',STATUS='NEW')
        OPEN(8,FILE='TEST1.OUT',STATUS='NEW')
        OPEN(9,FILE='TEST2.OUT',STATUS='NEW')

*** reads given data and creates mesh
        CALL INPUT2
        CALL GRIDPLUS

***     creates biga matrix and bigf vector
        CALL HEATMAT

***     replaces Galerkin equation with direchlet bdry temperatures
***     modifies equations so that heat flux at boundaries of material
***     interfaces are equal
        CALL HEATMOD

***     solves simultaneous system of equations
        CALL LSARG(NSNP,BIGA,NSNP,BIGF,1,TEMP)

***     creates output file
 999    CALL OUTPUT

        END
```

```
      SUBROUTINE INPUT2

*****************************************************************
****  Reads in data to construct thermal grid

      INCLUDE 'HEATCOMN.FOR'
      OPEN(11,FILE='data8.DAT',STATUS='OLD')
      OPEN(21,FILE='TEST.OUT',STATUS='NEW')

      READ(11,*) NCOL1,NCOL2,NROW
      READ(11,*) (XPOS(I),I=1,NDIFX)
      READ(11,*) (YPOS(I),I=1,NDIFY)
      READ(11,*) (XINCOL(I),I=1,NDIFX-1)
      READ(11,*) (YINCRROW(I),I=1,NDIFY-1)
      READ(11,*) (THERCON(I),RHO(I),SPHT(I),I=1,NMATL)
      READ(11,*) DIVSUB,DIVXAIR,DIVYAIR,DIVXSOL
      READ(11,*) NBCLOW,NBCUP,NBCVERT,NBCSUB,TAMB
      READ(11,*) HLOW,HUP,HVERT,HSUB
      READ(11,*) GEN,QTPR
      READ(11,*) NBDUP,NBDRDEV,NBDUSUB,NBDRIT,NBDLOW
      READ(11,*) TUP,TRTDEV,TUPSUB,TRIGHT,TLOW

      END

      SUBROUTINE GRIDPLUS

*****************************************************************
****  overlays a grid on a square or rectangle with up to nine
****  different mesh densities in X and Y directions , sets up
****  geometric and material properties for the Galerkin eq.

      INCLUDE 'HEATCOMN.FOR'

C      open(21,file='test.out',status='new')
      DATA KEL,XVALUE,YVALUE      /NEL*0,0,0/
      RBMAX1 = NCOL1 + 1
      RBMAX2 = NCOL2 + 1
      RTMAX  = NROW + 1
      XCOUNT = 1
      NN     = 1
      RBMAX  = RBMAX1


*****************************************************************
****  assigns X and Y coordinates to system Global nodal points

      DO 100 I = 1,NSNP

            X(I) = XVALUE
            Y(I) = YVALUE

            IF(XVALUE.LT.XPOS(2).AND.XVALUE.GE.XPOS(1))THEN
                XINCCOL = XINCOL(1)
            ELSEIF(XVALUE.LT.XPOS(3).AND.XVALUE.GE.XPOS(2))THEN
                XINCCOL = XINCOL(2)
            ELSEIF(XVALUE.LT.XPOS(4).AND.XVALUE.GE.XPOS(3))THEN
                XINCCOL = XINCOL(3)
            ELSEIF(XVALUE.LT.XPOS(5).AND.XVALUE.GE.XPOS(4))THEN
                XINCCOL = XINCOL(4)
            ELSEIF(XVALUE.LT.XPOS(6).AND.XVALUE.GE.XPOS(5))THEN
                XINCCOL = XINCOL(5)
```

```fortran
      ELSEIF(XVALUE.LT.XPOS(9).AND.XVALUE.GE.XPOS(8))THEN
          XINCCOL = XINCOL(8)

      ELSE
        XINCCOL =  XINCOL(9)
      ENDIF

      XVALUE = XVALUE + XINCCOL

      IF(YVALUE.LT.YPOS(2).AND.YVALUE.GE.YPOS(1))THEN
          YINCROW = YINCRROW(1)
      ELSEIF(YVALUE.LT.YPOS(3).AND.YVALUE.GE.YPOS(2))THEN
          YINCROW = YINCRROW(2)
      ELSEIF(YVALUE.LT.YPOS(4).AND.YVALUE.GE.YPOS(3))THEN
          YINCROW = YINCRROW(3)
      ELSEIF(YVALUE.LT.YPOS(5).AND.YVALUE.GE.YPOS(4))THEN
          YINCROW = YINCRROW(4)
      ELSEIF(YVALUE.LT.YPOS(6).AND.YVALUE.GE.YPOS(5))THEN
          YINCROW = YINCRROW(5)
      ELSEIF(YVALUE.LT.YPOS(7).AND.YVALUE.GE.YPOS(6))THEN
          YINCROW = YINCRROW(6)

        ELSEIF(YVALUE.LT.YPOS(8).AND.YVALUE.GE.YPOS(7))THEN
           YINCROW = YINCRROW(7)
        ELSEIF(YVALUE.LT.YPOS(9).AND.YVALUE.GE.YPOS(8))THEN
           YINCROW = YINCRROW(8)
        ELSE
          YINCROW = YINCRROW(9)
        ENDIF

**** begins numbering process  of assembly after substrate
        IF(I.GT.((NCOL1+1)*(DIVSUB+1)))THEN
           RBMAX = RBMAX2
        ENDIF

        IF(XCOUNT.GE.RBMAX)THEN
           XVALUE = 0.0
           YVALUE = YVALUE + YINCROW
           XCOUNT = 0.0
        ENDIF

        XCOUNT = XCOUNT + 1
 100  CONTINUE

**************************************************************
**** creates correspondence table for Local-Global nodal points

      DO 200 IROW = 1,DIVSUB + 1
         KK = (IROW-1)*(RBMAX1)
         DO 210 ICOL = 1,NCOL1

            IEL = ((IROW-1)*(2*NCOL1))+(2*ICOL)-1
            JEL = IEL + 1
            ICOR(IEL,1) = ICOL + KK
            ICOR(IEL,2) = ICOL + NCOL1 + KK + 2
            ICOR(IEL,3) = ICOL + NCOL1 + KK + 1
            ICOR(JEL,1) = ICOL + KK
            ICOR(JEL,2) = ICOL + KK + 1
            ICOR(JEL,3) = ICOL + NCOL1 + KK + 2
```

83

```fortran
210     CONTINUE
200   CONTINUE

**** correspondence starting two rows above substrate
      KK   = (RBMAX1*(DIVSUB+1))
      IEL = (NCOL1*DIVSUB*2) + (NCOL2*2) + 1
      DO 220 IROW = 1,NROW-(DIVSUB+1)
         DO 230 ICOL = 1,NCOL2

            JEL = IEL + 1
            ICOR(IEL,1) = ICOL + KK
            ICOR(IEL,2) = ICOL + NCOL2 + KK + 2
            ICOR(IEL,3) = ICOL + NCOL2 + KK + 1
            ICOR(JEL,1) = ICOL + KK
            ICOR(JEL,2) = ICOL + KK + 1
            ICOR(JEL,3) = ICOL + NCOL2 + KK + 2
            IEL = IEL + 2

230      CONTINUE
      KK = KK + RBMAX2
220   CONTINUE


***********************************************************************
**** assigns material properties to elements

      NSUBEL   = NCOL1 * DIVSUB * 2
      NAIREL   = 2 * DIVXAIR
      NARSOEL  = 2 * DIVYAIR * NCOL2
      LCOUNT   = 1
      NCOUNT   = 1
      MCOUNT   = 1

      DO 300 I = 1,NEL-1,2
         IF(I.LT.NSUBEL)THEN
**** substrate (single material) ****
            IMAT(I)   = 1
            IMAT(I+1) = 1
**** substrate (multiple material) ****
         ELSEIF(I.GT.NSUBEL.AND.I.LT.(NARSOEL+NSUBEL))THEN
            IF(NCOUNT.LE.DIVXAIR)THEN
**** air ****
               IMAT(I)   = 2
               IMAT(I+1) = 2
            ELSEIF(NCOUNT.LE.DIVXAIR+DIVXSOL)THEN
**** solder ****
               IMAT(I)   = 3
               IMAT(I+1) = 3
**** coating/cover ****
            ELSE
               IMAT(I)   = 5
               IMAT(I+1) = 5
            ENDIF
            NCOUNT = NCOUNT + 1
            IF(NCOUNT.GT.NCOL2)THEN
               NCOUNT = 1
            ENDIF
         ELSEIF(I.GT.NARSOEL+NSUBEL.AND.
     :            I.LT.NEL-(NCOL2*2))THEN
            IF(MCOUNT.LE.NCOL2-1)THEN
```

84

```
**** device ****
             IMAT(I)   = 4
             IMAT(I+1) = 4
**** coating/cover ****
          ELSE
             IMAT(I)   = 5
             IMAT(I+1) = 5
          ENDIF
          MCOUNT = MCOUNT + 1
          IF(MCOUNT.GT.NCOL2)THEN
             MCOUNT = 1
          ENDIF
        ELSE
**** coating/cover ****
             IMAT(I)   = 5
             IMAT(I+1) = 5
          ENDIF
  300   CONTINUE

        DO 310 I = 1,NEL
          II        = IMAT(I)
          KEL(I)    = THERCON(II)
          RHOEL(I)  = RHO(II)


          SPHTEL(I) = SPHT(II)
          IF(I.GT.(NSUBEL+NARSOEL))THEN
             QDOTEL(I) = QTPR
          ENDIF
  310   CONTINUE

*****************************************************************
**** assigns boundary conditions to elements at the convective
**** (CAUCHY) boundaries.

        DO 400 I = 2,2*NCOL1,2

*** assigns Cauchy boundary to lower side of rectangle
          IF(NBCLOW.EQ.1)THEN
          NBDRY(I) = 1
          ENDIF
  400   CONTINUE

        DO 410 I = (NEL-(2*NCOL2))+1,NEL-1,2

*** assigns Cauchy boundary to upper side of rectangle
          IF(NBCUP.EQ.1)THEN
          NBDRY(I) = 2
          ENDIF
  410   CONTINUE

        DO 420 I = NSUBEL-((NCOL1-NCOL2)*2)+1,NSUBEL-1,2

*** assigns Cauchy boundary to upper tip of substrate
          IF(NBCSUB.EQ.1)THEN
          NBDRY(I) = 4
          ENDIF
  420   CONTINUE
```

85

```
         DO 430 I - NSUBEL+(NCOL2*2),NEL,NCOL2*2

*** assigns Cauchy boundary to vertical side of rectangle
         IF(NBCVERT.EQ.1)THEN
         NBDRY(I) - 3
         ENDIF
 430   CONTINUE

*************************************************************
**** assigns Direchlet boundary to system Global nodal points
****

**** assigns Direchlet boundary to lower side of substrate

       DO 500 I - 1,RBMAX1
          IF(NBDLOW.EQ.1)THEN
          NDIRECH(I) - 1
          BDRYVAL(I) - TLOW
          ENDIF
 500   CONTINUE

**** assigns Direchlet boundary to right hand side of substrate

       DO 510 I - RBMAX1*2,RBMAX1*(DIVSUB+1),RBMAX1
          IF(NBDRIT.EQ.1)THEN
          NDIRECH(I) - 1

          BDRYVAL(I) - TRIGHT
          ENDIF
 510   CONTINUE

**** assigns Direchlet boundary to upper side of device

       DO 520 I - NSNP,NSNP-NCOL2,-1
          IF(NBDUP.EQ.1)THEN
          NDIRECH(I) - 1
          BDRYVAL(I) - TUP
          ENDIF
 520   CONTINUE

**** assigns Direchlet boundary to right side of device
       III - NSNP-(RBMAX2*(NROW-DIVSUB-1))
       DO 530 I - NSNP-RBMAX2,III,-RBMAX2
          IF(NBDRDEV.EQ.1)THEN
          NDIRECH(I) - 1
          BDRYVAL(I) - TRTDEV
          ENDIF
 530   CONTINUE

**** assigns Direchlet boundary to upper side of substrate

       DO 540 I - (RBMAX1*DIVSUB)+RBMAX2,RBMAX1*(DIVSUB+1)
          IF(NBDUSUB.EQ.1)THEN
          NDIRECH(I) - 1
          BDRYVAL(I) - TUPSUB
          ENDIF
 540   CONTINUE
       END
```

```fortran
      SUBROUTINE HEATMAT

*********************************************************************
**** calculates the BIGA matrix and BIGF vector that are the
**** system of simultaneous equations to be solved;  accounts
**** for the main operator(Del^2), Cauchy boundary, and the
**** forcing function to Poisson's equation

      INCLUDE 'HEATCOMN.FOR'

      DATA BIGA,BIGF              / NDIM*0,NSNP*0 /
      DATA bb21,bb22,bb23,bb33 /0.0,0.0,0.0,0.0/
      DATA cauchf1,cauchf2,ff1 /0.0,0.0,0.0/

      DO 10  IEL = 1,NEL

            I1 = ICOR(IEL,1)
            I2 = ICOR(IEL,2)
            I3 = ICOR(IEL,3)

            B1 = Y(I2) - Y(I3)
            B2 = Y(I3) - Y(I1)
            B3 = Y(I1) - Y(I2)

            C1 = X(I3) - X(I2)
            C2 = X(I1) - X(I3)
            C3 = X(I2) - X(I1)

            AREA(IEL) = (ABS(C1*B2-C2*B1))/2.
            write(8,*) iel,area(iel)
            aa11 = KEL(IEL)*(B1**2 + C1**2)/(-4.*AREA(IEL))
            aa12 = KEL(IEL)*(B1*B2  +  C1*C2)/(-4.*AREA(IEL))
            aa13 = KEL(IEL)*(B1*B3  +  C1*C3)/(-4.*AREA(IEL))
            aa21 = KEL(IEL)*(B2*B1  +  C2*C1)/(-4.*AREA(IEL))
            aa22 = KEL(IEL)*(B2**2 + C2**2)/(-4.*AREA(IEL))
            aa23 = KEL(IEL)*(B2*B3  +  C2*C3)/(-4.*AREA(IEL))
            aa31 = KEL(IEL)*(B3*B1  +  C3*C1)/(-4.*AREA(IEL))
            aa32 = KEL(IEL)*(B3*B2  +  C3*C2)/(-4.*AREA(IEL))
            aa33 = KEL(IEL)*(B3**2 + C3**2)/(-4.*AREA(IEL))


*********************************************************************
**** calculation of Cauchy boundary to BIGA matrix and BIGF
**** vector

            IF(NBDRY(IEL).NE.0)THEN
**** boundary with local nodal points 1 - 2 on bottom side
            IF(NBDRY(IEL).EQ.1)THEN
                  bb22    = (HLOW*ABS(C3))/-3.0
                  bb21    = (HLOW*ABS(C3))/-6.0
                  cauchf1 = (TAMB*HLOW*ABS(C3))/-2.0
**** boundary with local nodal points 2 - 3 on upper side
            ELSEIF(NBDRY(IEL).EQ.2)THEN
                  bb33    = (HUP*ABS(C1))/-3.0
                  bb23    = (HUP*ABS(C1))/-6.0
                  cauchf2 = (TAMB*HUP*ABS(C1))/-2.0
**** boundary with local nodal points 2 - 3 on right side
            ELSEIF(NBDRY(IEL).EQ.3)THEN
                  bb33    = (HVERT*ABS(B1))/-3.0
                  bb23    = (HVERT*ABS(B1))/-6.0
```

```
                  cauchf2  = (TAMB*HVERT*ABS(B1))/-2.0
              ELSE
                  bb33     = (HSUB*ABS(C1))/-3.0
                  bb23     = (HSUB*ABS(C1))/-6.0
                  cauchf2  = (TAMB*HSUB*ABS(C1))/-2.0
              ENDIF
          ENDIF
```

```
*****************************************************************
**** the contribution of the Cauchy boundary is symmetric
**** bb11=bb22 bb12=bb21      bb22=bb33 bb23=bb32
```

```
          BIGA(I1,I1) = BIGA(I1,I1) + aa11 + bb22
          BIGA(I1,I2) = BIGA(I1,I2) + aa12 + bb21
          BIGA(I1,I3) = BIGA(I1,I3) + aa13
          BIGA(I2,I1) = BIGA(I2,I1) + aa21 + bb21
          BIGA(I2,I2) = BIGA(I2,I2) + aa22 + bb22 + bb33
          BIGA(I2,I3) = BIGA(I2,I3) + aa23 + bb23
          BIGA(I3,I1) = BIGA(I3,I1) + aa31
          BIGA(I3,I2) = BIGA(I3,I2) + aa32 + bb23
          BIGA(I3,I3) = BIGA(I3,I3) + aa33 + bb33

          bb22 = 0.0
          bb21 = 0.0
          bb23 = 0.0
          bb33 = 0.0
```

```
*****************************************************************
**** used for Poisson's equation (internal heat generaticn)
```

```
      IF(GEN.EQ.1.0)THEN
          IF(IMAT(IEL).EQ.4)THEN
              ff1 = -AREA(IEL)*QTPREL(IEL)/3.0
          ENDIF
      ENDIF
```

```
*****************************************************************
**** the two terms that comprise the BIGF matrix are from the
**** Cauchy boundary condition and the source term of the chip
**** a lumped approximation is used for both cases; cauchf1 is
**** for a 1-2 boundary edge cauchf2 is for a 2-3 boundary edge
```

```
          BIGF(I1) = BIGF(I1) + ff1 + cauchf1
          BIGF(I2) = BIGF(I2) + ff1 + cauchf1 + cauchf2
          BIGF(I3) = BIGF(I3) + ff1 + cauchf2

          cauchf1  = 0.0
          cauchf2  = 0.0
          ff1      = 0.0
```

```
10    CONTINUE
      END
```

```
      SUBROUTINE HEATMOD
```

```
*****************************************************************
**** modifies BIGA matrix and BIGF vector if a system Global
**** point is a Direchlet boundary ie. replaces the Galerkin eq.
```

```fortran
      INCLUDE 'HEATCOMN.FOR
**** modifies system of equations for Direchlet boundary points
      DO 10  I = 1,NSNP

          IF (NDIRECH(I) .EQ. 1)THEN
          BIGA(I,I) = 1.0

              DO 20 J = 1,I-1
                 BIGA(I,J) = 0.0
 20           CONTINUE

              DO 30 JJ = I+1,NSNP
                 BIGA(I,JJ) = 0.0
 30           CONTINUE

          BIGF(I) = BDRYVAL(I)
          ENDIF

 10   CONTINUE
      END
      SUBROUTINE OUTPUT

*********************************************************************
**** creates output file of temperature distribution and a data file
**** for graphing the temperature contours

      INCLUDE 'HEATCOMN.FOR
      OPEN(10,FILE='HEAT.DAT',STATUS='NEW')
      write(7,*) '             Temperatures through solder'
      write(7,*) '8',temp(8),'23',temp(23),'38',temp(38),'53',temp(53)
      write(7,*) '68',temp(68),'83',temp(83),'93',temp(93),
     :           '103',temp(103)
      write(7,*) '113',temp(113),'123',temp(123),'133',temp(133)

**** energy balance

      qconv = 0.0
      do 200 i =  126,134
      qconv=qconv+(hup*(((temp(I)+temp(I+1))/2)-tamb)*(X(I+1)-x(I)))

 200  continue
      do 210 i =  1,14
      qconv=qconv+(hlow*(((temp(I)+temp(I+1))/2)-tamb)*(X(I+1)-x(I)))
 210  continue
      do 220 i =  70,74
      qconv=qconv+(hsub*(((temp(I)+temp(I+1))/2)-tamb)*(X(I+1)-x(I)))
 220  continue
      do 230 i =  85,125,10
      qconv=qconv+(hvert*(((temp(I)+temp(I+10))/2)-tamb)*
     :              (y(I+10)-y(I)))
 230  continue
      qconv=qconv+(hvert*(((temp(70)+temp(85))/2)-tamb)*(y(85)-y(70)))

      WRITE(7,*)
      write(7,*) '        Heat loss to convection = ',qconv,'W/M'

      POWER = QPRT*0.0025*0.002
      WRITE(7,*) 'The power output of the device =',power,'W/M'
      END
```

```
PROGRAM FILTER

REAL X(135),Y(135),T(135),TEMPT(200),TEMPB(200)

OPEN(12,FILE='bh3.out',STATUS='OLD')
OPEN(13,FILE='bh3f.DAT',STATUS='NEW')

READ(12,*) (X(I),Y(I),T(I),I=1,135)
```

**** calculates intermediate temperatures ******

```
      TA = (T(61)-T(46))*.75 + T(46)
      TB = (T(61)+T(46))/2.0
      TC = (T(62)-T(47))*.75 + T(47)
      TD = (T(66)+T(47))/2.0
      TE = (T(63)-T(48))*.75 + T(48)
      TF = (T(63)+T(48))/2.0
      TG = (T(64)-T(49))*.75 + T(49)
      TH = (T(64)+T(49))/2.0
      TI = (T(65)-T(64))*.75 + T(64)
      TL = (T(50)-T(49))*.75 + T(49)
      TJ = (TI-TL)*.75 + TL
      TK = (TI+TL)/2.0
      TM = (T(65)-T(50))*.75 + T(50)
      TN = (T(65)+T(50))/2.0
      TO = (T(65)+T(66))/2.0
      TR = (T(51)-T(50))*.75 + T(50)
      TP = (TO-TR)*.75 + TR
      TQ = (TO+TR)/2.0
      TS = (T(65)+T(66))/2.0
      TV = (T(50)+T(51))/2.0
      TT = (TS-TV)*.75 + TV
      TU = (TS+TV)/2.0
      TW = (T(66)-T(51))*.75 + T(51)
      TX = (T(66)+T(51))/2.0
      TY = (T(67)-T(52))*.75 + T(52)
      TZ = (T(67)+T(52))/2.0

      TAA = (T(68)-T(53))*.75 + T(53)
      TAB = (T(68)+T(53))/2.0
      TAC = (T(69)-T(54))*.75 + T(54)
      TAD = (T(69)+T(54))/2.0
      TAE = (T(69)+T(70))/2.0
      TAH = (T(54)+T(55))/2.0
      TAF = (TAE-TAH)*.75 + TAH
      TAG = (TAE+TAH)/2.0
      TAI = (T(69)-T(70))*.75 + T(70)
      TAL = (T(54)-T(55))*.75 + T(54)
      TAJ = (TAI-TAL)*.75 + TAL
      TAK = (TAI+TAL)/2.0
      TAM = (T(70)-T(55))*.75 + T(55)
      TAN = (T(70)+T(55))/2.0
      TAO = (T(70)-T(71))*.75 + T(71)
```

```
        TAR = (T(55)-T(56))*.75 + T(55)
        TAP = (TAO-TAR)*.75 + TAR
        TAQ = (TAO+TAR)/2.0
        TAS = (T(71)-T(56))*.75 + T(56)
        TAT = (T(71)+T(56))/2.0
        TAU = (T(75)-T(60))*.75 + T(60)
        TAV = (T(75)+T(60))/2.0
        TAW = (T(35)-T(34))*.75 + T(34)
        TAX = (T(36)-T(35))*.75 + T(35)
        TAY = (T(36)+T(35))/2.0
        TAZ = (T(39)+T(40))/2.0

        TBA = (T(39)-T(40))*.75 + T(40)
        TBB = (T(40)-T(41))*.75 + T(41)
        TBC = (T(5)-T(4))*.75 + T(4)
        TBD = (T(6)-T(5))*.75 + T(5)
        TBE = (T(6)+T(5))/2.0
        TBF = (T(9)+T(10))/2.0
        TBG = (T(9)-T(10))*.75 + T(10)
        TBH = (T(10)-T(11))*.75 + T(11)


**** calculates average temperatures for rectangular element FEM program
**** weld.for (chip and solder)

        TEMPS1    = (T(95)+T(85)+T(96)+T(86))/4.0
        DO 100 I = 1,115
            TEMPT(I) = TEMPS1
            TEMPB(I) = TEMPS1
 100    CONTINUE

**** calculates average temperatures for rectangular element FEM program
**** weld.for (substrate)

        TEMPT(116)    = (T(61)+T(61))/2.0
        TEMPB(116)    = (TA+TC)/2.0

        TEMPT(117)    = (T(62)+T(63))/2.0
        TEMPB(117)    = (TC+TD)/2.0

        TEMPT(118)    = (T(63)+T(64))/2.0
        TEMPB(118)    = (TE+TG)/2.0

        TEMPT(119)    = (T(64)+TI)/2.0
        TEMPB(119)    = (TG+TJ)/2.0

        TEMPT(120)    = (T(65)+TI)/2.0
        TEMPB(120)    = (TJ+TM)/2.0

        TEMPT(121)    = (T(65)+TO)/2.0
        TEMPB(121)    = (TM+TP)/2.0

        TEMPT(122)    = (TO+TS)/2.0
        TEMPB(122)    = (TP+TT)/2.0

        TEMPT(123)    = (T(66)+TS)/2.0
        TEMPB(123)    = (TT+TW)/2.0

        TEMPT(124)    = (T(66)+T(67))/2.0
        TEMPB(124)    = (TW+TY)/2.0
```

```
TEMPT(125)    = (T(67)+T(68))/2.0
TEMPB(125)    = (TY+TAA)/2.0

TEMPT(126)    = (T(68)+T(69))/2.0
TEMPB(126)    = (TAA+TAC)/2.0

TEMPT(127)    = (T(69)+TAE)/2.0
TEMPB(127)    = (TAC+TAF)/2.0

TEMPT(128)    = (TAE+TAI)/2.0
TEMPB(128)    = (TAF+TAJ)/2.0

TEMPT(129)    = (T(70)+TAI)/2.0
TEMPB(129)    = (TAJ+TAM)/2.0

TEMPT(130)    = (T(70)+TAO)/2.0
TEMPB(130)    = (TAM+TAP)/2.0

TEMPT(131)    = (T(71)+TAO)/2.0
TEMPB(131)    = (TAP+TAS)/2.0

TEMPT(132)    = (T(71)+T(75))/2.0
TEMPB(132)    = (TAS+TAU)/2.0

TEMPT(133)    = (TA+TC)/2.0
TEMPB(133)    = (TB+TD)/2.0

TEMPT(134)    = (TC+TE)/2.0
TEMPB(134)    = (TD+TF)/2.0

TEMPT(135)    = (TE+TG)/2.0
TEMPB(135)    = (TF+TH)/2.0

TEMPT(136)    = (TG+TJ)/2.0
TEMPB(136)    = (TH+TK)/2.0

TEMPT(137)    = (TJ+TM)/2.0
TEMPB(137)    = (TK+TN)/2.0

TEMPT(138)    = (TM+TP)/2.0
TEMPB(138)    = (TN+TQ)/2.0

TEMPT(139)    = (TP+TT)/2.0
TEMPB(139)    = (TQ+TU)/2.0

TEMPT(140)    = (TT+TW)/2.0
TEMPB(140)    = (TU+TX)/2.0

TEMPT(141)    = (TW+TY)/2.0
TEMPB(141)    = (TX+TZ)/2.0

TEMPT(142)    = (TY+TAA)/2.0
TEMPB(142)    = (TZ+TAB)/2.0

TEMPT(143)    = (TAA+TAC)/2.0
TEMPB(143)    = (TAB+TAD)/2.0

TEMPT(144)    = (TAC+TAF)/2.0
TEMPB(144)    = (TAD+TAG)/2.0
```

```
TEMPT(145)     = (TAF+TAJ)/2.0
TEMPB(145)     = (TAG+TAK)/2.0

TEMPT(146)     = (TAJ+TAM)/2.0
TEMPB(146)     = (TAK+TAN)/2.0

TEMPT(147)     = (TAM+TAP)/2.0
TEMPB(147)     = (TAN+TAQ)/2.0

TEMPT(148)     = (TAP+TAS)/2.0
TEMPB(148)     = (TAQ+TAT)/2.0

TEMPT(149)     = (TAS+TAU)/2.0
TEMPB(149)     = (TAT+TAV)/2.0

TEMPT(150)     = (TB+TD)/2.0
TEMPB(150)     = (T(46)+T(47))/2.0

TEMPT(151)     = (TD+TF)/2.0
TEMPB(151)     = (T(47)+T(48))/2.0

TEMPT(152)     = (TF+TH)/2.0
TEMPB(152)     = (T(48)+T(49))/2.0

TEMPT(153)     = (TH+TK)/2.0
TEMPB(153)     = (TL+T(49))/2.0

TEMPT(154)     = (TK+TL)/2.0
TEMPB(154)     = (TN+T(50))/2.0

TEMPT(155)     = (TN+TQ)/2.0
TEMPB(155)     = (TR+T(50))/2.0

TEMPT(156)     = (TQ+TU)/2.0
TEMPB(156)     = (TR+TV)/2.0

TEMPT(157)     = (TU+TX)/2.0
TEMPB(157)     = (TV+T(51))/2.0

TEMPT(158)     = (TX+TZ)/2.0
TEMPB(158)     = (T(51)+T(52))/2.0

TEMPT(159)     = (TZ+TAB)/2.0
TEMPB(159)     = (T(52)+T(53))/2.0

TEMPT(160)     = (TAB+TAD)/2.0
TEMPB(160)     = (T(53)+T(54))/2.0

TEMPT(161)     = (TAD+TAG)/2.0
TEMPB(161)     = (T(54)+TAH)/2.0

TEMPT(162)     = (TAG+TAK)/2.0
TEMPB(162)     = (TAH+TAL)/2.0

TEMPT(163)     = (TAK+TAN)/2.0
TEMPB(163)     = (TAL+T(55))/2.0

TEMPT(164)     = (TAN+TAQ)/2.0
TEMPB(164)     = (TAR+T(55))/2.0
```

```
TEMPT(165)     =  (TAQ+TAT)/2.0
TEMPB(165)     =  (TAR+T(56))/2.0

TEMPT(166)     =  (TAT+TAV)/2.0
TEMPB(166)     =  (T(56)+T(60))/2.0

TEMPT(167)     =  (T(46)+T(47))/2.0
TEMPB(167)     =  (T(31)+T(32))/2.0

TEMPT(168)     =  (T(47)+T(48))/2.0
TEMPB(168)     =  (T(32)+T(33))/2.0

TEMPT(169)     =  (T(48)+T(49))/2.0
TEMPB(169)     =  (T(33)+T(34))/2.0

TEMPT(170)     =  (T(49)+TL)/2.0
TEMPB(170)     =  (T(34)+TAW)/2.0

TEMPT(171)     =  (T(50)+TL)/2.0
TEMPB(171)     =  (T(35)+TAW)/2.0

TEMPT(172)     =  (T(50)+TR)/2.0
TEMPB(172)     =  (T(35)+TAX)/2.0

TEMPT(173)     =  (TR+TV)/2.0
TEMPB(173)     =  (TAX+TAY)/2.0

TEMPT(174)     =  (T(51)+TV)/2.0
TEMPB(174)     =  (T(36)+TAY)/2.0

TEMPT(175)     =  (T(51)+T(52))/2.0
TEMPB(175)     =  (T(36)+T(37))/2.0

TEMPT(176)     =  (T(52)+T(53))/2.0
TEMPB(176)     =  (T(37)+T(38))/2.0

TEMPT(177)     =  (T(53)+T(54))/2.0
TEMPB(177)     =  (T(38)+T(39))/2.0

TEMPT(178)     =  (T(54)+TAH)/2.0
TEMPB(178)     =  (T(39)+TAZ)/2.0

TEMPT(179)     =  (TAH+TAL)/2.0
TEMPB(179)     =  (TAZ+TBA)/2.0

TEMPT(180)     =  (T(55)+TAL)/2.0
TEMPB(180)     =  (T(40)+TBA)/2.0

TEMPT(181)     =  (T(55)+TAR)/2.0
TEMPB(181)     =  (T(40)+TBB)/2.0

TEMPT(182)     =  (T(56)+TAR)/2.0
TEMPB(182)     =  (T(41)+TBB)/2.0

TEMPT(183)     =  (T(56)+T(60))/2.0
TEMPB(183)     =  (T(41)+T(45))/2.0

TEMPT(184)     =  (T(31)+T(32))/2.0
TEMPB(184)     =  (T(1)+T(2))/2.0
```

```
        TEMPT(185)      = (T(32)+T(33))/2.0
        TEMPB(185)      = (T(2)+T(3))/2.0

        TEMPT(186)      = (T(33)+T(34))/2.0
        TEMPB(186)      = (T(3)+T(4))/2.0

        TEMPT(187)      = (T(34)+TAW)/2.0
        TEMPB(187)      = (T(4)+TBC)/2.0

        TEMPT(188)      = (T(35)+TAW)/2.0
        TEMPB(188)      = (T(5)+TBC)/2.0

        TEMPT(189)      = (T(35)+TAX)/2.0
        TEMPB(189)      = (T(5)+TBD)/2.0

        TEMPT(190)      = (TAX+TAY)/2.0
        TEMPB(190)      = (TBD+TBE)/2.0

        TEMPT(191)      = (T(36)+TAY)/2.0
        TEMPB(191)      = (T(6)+TBE)/2.0

        TEMPT(192)      = (T(36)+T(37))/2.0
        TEMPB(192)      = (T(6)+T(7))/2.0

        TEMPT(193)      = (T(37)+T(38))/2.0
        TEMPB(193)      = (T(7)+T(8))/2.0

        TEMPT(194)      = (T(38)+T(39))/2.0
        TEMPB(194)      = (T(8)+T(9))/2.0

        TEMPT(195)      = (T(39)+TAZ)/2.0
        TEMPB(195)      = (T(9)+TBF)/2.0

        TEMPT(196)      = (TAZ+TBA)/2.0
        TEMPB(196)      = (TBF+TBG)/2.0

        TEMPT(197)      = (T(40)+TBA)/2.0
        TEMPB(197)      = (T(10)+TBG)/2.0

        TEMPT(198)      = (T(40)+TBB)/2.0
        TEMPB(198)      = (T(10)+TBH)/2.0

        TEMPT(199)      = (T(41)+TBB)/2.0
        TEMPB(199)      = (T(11)+TBH)/2.0

        TEMPT(200)      = (T(41)+T(45))/2.0
        TEMPB(200)      = (T(11)+T(15))/2.0

****  use if printout is desired
      DO 900 I = 1,200
          WRITE(13,*) TEMPT(I),'   ',TEMPB(I)
 900  CONTINUE

      END
```

LIST OF REFERENCES

1. Tummala, Rao R. and Rymaszewski, E.J., Microelectronics Packaging Handbook, Van Nostrand Reinhold, 1989.

2. Timoshenko, S., "Analysis of Bi-metal Thermostats", Journal of the Optical Society of America, Vol. 11, pp. 233-255, (1925).

3. Goland, M., and Reissner,E., "The Stresses in Cemented Joints", Journal of Applied Mechanics, Transactions, ASME, 11, pp. 17-27, March, (1984).

4. Suhir, E., Advances in Thermal Modeling of Electronic Components and Systems, Volume 1, Chapter 5, pp. 337-412. Hemisphere Publishing Co., (1989).

5. Incropera, F.P., and DeWitt, D.P., Introduction to Heat Transfer, John Wiley and Sons, 1990.

6. Allaire, P.E., Basics of the Finite Element Method, Wm. C. Brown Publishers, College Division, 1985.

INITIAL DISTRIBUTION LIST

No. of Copies

1. Library, Code 52   2
   Naval Postgraduate School
   Monterey, California 93943-5002

2. Department Chairman, Code ME   1
   Department of Mechanical Engineering
   Naval Postgraduate School
   Monterey, California 93943-5000

3. Naval Engineering Curricular Office, Code 34   1
   Naval Postgraduate School
   Monterey, California 93943-5000

4. Professor David Salinas, Code ME/Sa   4
   Department of Mechanical Engineering
   Naval Postgraduate School
   Monterey, California 93943-5000

5. Professor Young Kwon, Code ME/Kw   2
   Department of Mechanical Engineering
   Naval Postgraduate School
   Monterey, California 93943-5000

6. Defense Technical Information Center   2
   Cameron Station
   Alexandria, Virginia 22304-6145

7. LT Andrei Sapsai Jr.   1
   2295 South Orchard Road
   Vineland New Jersey 08360